Mapping Seismic site Effects at REgional and NAtional scales (‘SERENA’ PRIN project): *outcomes and future perspectives*

PRIN SERENA Project Working Group

a cura di:
Dario Albarello, Iolanda Gaudiosi

Collana a cura del **CentroMS**

BookMS

STRATEGIE DI MITIGAZIONE

edizioni
Consiglio Nazionale delle Ricerche

Mapping Seismic site Effects at REgional and NAtional scales ('SERENA' PRIN project): *outcomes and future perspectives*

PRIN SERENA Project Working Group

a cura di:
Dario Albarello, Iolanda Gaudiosi

Collana a cura del **CentroMS**

BookMS
STRATEGIE DI MITIGAZIONE

edizioni
Consiglio Nazionale delle Ricerche

Mapping Seismic site Effects at REgional and NAtional scales ('SERENA'PRIN project):
outcomes and future perspectives

A cura di:
Dario Albarello *(Università di Siena),* **Iolanda Gaudiosi** *(Consiglio Nazionale delle Ricerche – Istituto di Geologia Ambientale e Geoingegneria)*

PRIN SERENA PROJECT
Working Group:

Albarello Dario[1]
Alvioli Massimiliano[2]
Ariano Mario[1]
Barnaba Carla[3]
Brunelli Giulio[4]
Bucci Francesco[2]
Caielli Grazia Maria[5]
Calamita Giuseppe[6]
Cammis Lorenzo[7]
Cara Fabrizio[4]
Carfagna Nicolò[1]
Castelbarco Tommaso[4]
Catalano Stefano[7]
Cavuoto Giuseppe[8]
Cultrera Giovanna[4]
D'Agostino Alberto[7]
Davani Federica[5]
Disperati Leonardo[1]
de Franco Roberto[5]
di Fiore Vincenzo[8]
Di Giulio Giuseppe[4]
Fantozzi Pier Lorenzo[1]
Felicetta Chiara[4]
Gallipoli Maria Rosaria[6]
Gaudiosi Iolanda[5]
Hailemikael Salomon[4]
Klin Peter[3]
Lanzano Giovanni[4]
Laurenzano Giovanna[3]
Lovati Sara[4]
Marchesini Ivan[2]
Martini Guido[9]
Mendicelli Amerigo[5]
Mercuri Alessia[4]
Minarelli Luca[4]
Monte Nunzia[2]
Mori Federico[5]
Moscatelli Massimiliano[5]
Norini Gianluca[5]
Ortolano Gaetano[7]
Pacor Francesca[4]
Paolucci Enrico[10]
Peloso Alessandro[9]
Pennica Francesco[5]
Peronace Edoardo[5]
Pettenati Franco[3]
Pieruccini Pierluigi[11]
Porchia Attilio[5]
Reichenbach Paola[2]
Rusconi Davide[5]
Santangelo Michele[2]
Sgobba Sara[4]
Stabile Tony Alfredo[6]
Taverna Perla[3]
Tortorici Giuseppe[5]
Tragni Nicola[6]

[1] *Università di Siena*
[2] *Consiglio Nazionale delle Ricerche – Istituto di Ricerca per la Protezione Idrogeologica*
[3] *Istituto Nazionale di Oceanografia e di Geofisica Sperimentale*
[4] *Istituto Nazionale di Geofisica e Vulcanologia*
[5] *Consiglio Nazionale delle Ricerche – Istituto di Geologia Ambientale e Geoingegneria*
[6] *Consiglio Nazionale delle Ricerche – Istituto di Metodologie per l'Analisi Ambientale*
[7] *Università di Catania*
[8] *Consiglio Nazionale delle Ricerche – Istituto di Scienze del Patrimonio Culturale*
[9] *ENEA*
[10] *Università di Bologna*
[11] *Università di Torino*

Progetto grafico:
FF3300 S.r.l.

edizioni
Consiglio Nazionale delle Ricerche

ISBN (ed. stampa) 978-88-8080-901-2
ISBN (ed. digitale) 978-88-8080-902-9
"PRIN SERENA Project "Mapping Seismic site Effects at REgional and NAtional scales. Outcomes and future perspectives"
https://doi.org/10.32053/MAPPING_SEISMIC_SITE_EFFECTS_AT_REGIONAL_AND_NATIONAL_SCALES_SERENA

Per citare il presente testo, si raccomanda di utilizzare la seguente dicitura:

PRIN SERENA Project Working Group (2026) **Mapping Seismic site Effects at REgional and NAtional scales ('SERENA' PRIN project):** ***outcomes and future perspectives***
Cnr Edizioni, 2026.

Index

Preface

Seismic Microzonation (SM) has become a fully mature and consolidated tool for seismic risk mitigation in Italy. This evolution is largely the result of the extensive application, across urban areas, of the criteria, procedures, and investigation methodologies defined in the national Guidelines for SM studies, together with the standardized protocols for digital data archiving and cartographic representation of both acquired datasets and derived products. The virtuous collaboration among Public Institutions responsible for land-use planning and natural disaster risk management – namely the State, Regions, Municipalities and the Civil Protection authorities – together with the scientific community and the professionals entrusted with the preparation of SM studies, has enabled the acquisition of a substantial amount of new data. Over the years, this collaborative framework has also strengthened and refined the practical experience gained in the field, often in the post-emergency context following major earthquakes.

Considerable progress has been made since the publication of the "Indirizzi e criteri per la Microzonazione Sismica" volume, ICMS 2008, by the Technical Commission for Seismic Microzonation. Nevertheless, broader territorial coverage aimed at understanding and evaluating the response to seismic hazard is still lacking. In fact, focusing solely on inhabited centers or portions of them, which in practice represent only small portions of the territory, although often thoroughly investigated and characterized, is not always sufficient to ensure effective large-scale risk reduction and civil protection actions. For example, lifelines, connecting roads, and other extra-urban infrastructures are not addressed in standard SM studies, and the assessment of co-seismic instabilities continues to pose persistent challenges to the full achievement of SM objectives.

This volume, characterized by a high scientific, analytical, and methodological content, seeks to address these gaps and represents a valuable contribution toward further advancement in SM applications and in the assessment of seismic hazard and risk in general. The volume synthesizes the outcomes of the multi-year PRIN SERENA Project, which involved leading experts in seismic microzonation and seismic hazard from numerous Italian Universities and Public Research Institutions, and stands as an important reference point also at the international level. Indeed, it is the first volume entirely published in English within the BookMS series.

The initiative of producing this volume was strongly supported by the Center for Seismic Microzonation and its applications – CentroMS (https://www.centromicrozonazionesismica.it/en/), as it fully aligns with the Center's objectives and mission to promote innovative methods for the implementation of SM studies and the underlying scientific development. The many authors and editors of the present volume are, therefore, warmly thanked for their great efforts in producing this noteworthy contribution to the scientific advancement of Seismic Microzonation.

Prof. Stefano Catalano
(University of Catania, Former President of CentroMS)
Dr Marco Mancini
(CNR – IGAG, Scientific Head of CentroMS)

1. Introduction

Seismic microzonation (SM) studies aim at accounting for the effects of small scale (tens to hundreds of meters) morphostratigraphical settings on the seismic hazard. Unlike site response studies that aim at defining the local seismic hazard at the scale of a single building, SM is extensive as it covers relatively wide areas encompassing a settlement. In Italy, SM is governed by specific guidelines (SM Working Group, 2015) that have enabled the standardization of procedures and outcomes provided to local Authorities responsible for land management and emergency planning. In recent years, many SM studies have been conducted in areas of higher seismic hazard, supported by the National Department of Civil Protection and regional authorities. However, despite the fact that these studies involve thousands of municipalities, they strictly focus on urbanized areas, which cover less than 2% of the whole territory under municipal jurisdiction. This implies that most lifelines (including roads), and smaller settlements lie in areas where local hazard has not been estimated. This lack of information poses a critical challenge for emergency planning and risk management. Conversely, applying standard SM guidelines over larger areas is unfeasible due to the high costs.

The PRIN project 'SERENA' (Mapping **S**eismic site Effects at **R**egional and **N**ational Scale, 2020MMCPER) was conceived to address this gap by developing and applying new conceptual approaches to the Italian territory. The project assessment explored the feasibility of producing national or regional scale maps and of implementing new methodologies for three kinds of site effects:

i) **1D seismo-stratigraphic resonance**, responsible for the local enhancement of seismic ground shaking;
ii) **topographic amplification**, induced by the interaction of seismic waves with rugged topography;
iii) seismically induced gravitational instabilities, including **landslides and rockfalls**.

The challenge was to derive meaningful results by the full exploitation of information available over the whole study area concerning surface geology, digital elevation models (DEM) and geophysical/geotechnical data inferred from the statistical analysis of the huge amount of information provided by SM studies already available.
Despite the different scale of analysis, the studies carried out during the project share some key issues, described in the following.

First of all, geological and geomorphological information is summarized by identifying GeoMorphoStratigraphic Units (GMSU thereafter) corresponding to mappable homogenous geological and geomorphological settings characterized by means of three main elements: a range of total thickness, stratigraphic relationships with respect to other surrounding GMSUs and the prevailing lithological characteristics.

The lithological classification of each GMSU is based on a standardized classification protocol, which is expressed in terms of the **Engineering Geological Units** (EGU hereafter). In this respect, each GMSU is considered as nearly homogenous Engineering Geological Unit (EGU). In other terms, the EGU is the engineering geological counterpart of the GMSU. In some cases, possible alternative EGUs can be associated to the same GMSU.

A **'Seismically Homogenous Microzone'** (SHM) is an area where expected seismic and co-seismic effects can be considered homogeneous, since any internal heterogeneity can be considered as negligible with respect to those elative to the other SHMs. The shape and the seismostratigraphical configuration of SHMs are a primary outcome of the project. Each SHM is characterised by a stratigraphical succession of GMSUs, and the corresponding shape represents the shape of the uppermost or outcropping GMSU.

Finally, the seismic response for each SHM is defined in terms of **synthetic parameters** representative of the considered co-seismic effects. These parameterizations (amplification factors, susceptibility indices) can be implemented in more general hazard studies to evaluate the impact of site effects.

All these aspects will be examined in the following sections, in their respective application contexts, with constant reference to the general workflow shown in FIGURE 1.1.

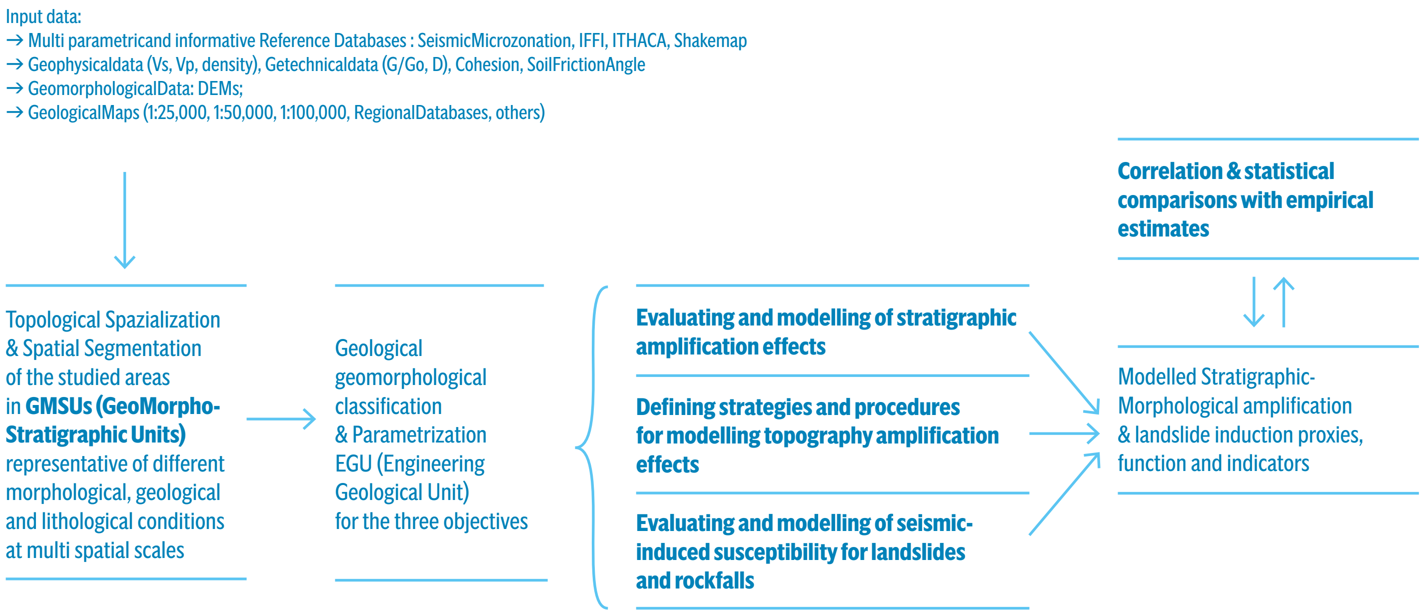

FIGURE 1.1
Synoptic workflow for evaluating seismic and co-seismic effects over large areas.

For the definition of regional scale estimates of site effects, a key point is relevant information available at the scale of interest, consistently throughout Italy. The first is the topographic data represented by the digital elevation model of Italy (DTM, Tarquini et al. 2007); the second one is the reference seismic hazard map (Stucchi et al. 2011; Meletti and Montaldo 2007). A third source of information comprises geological, lithological and geomorphological maps (and eventually databases) that are available at different scales for the whole study area (e.g., Bucci et al. 2022, 2021). The fourth source is the repository of SM studies developed by Regional Authorities within the framework of a multi-annual project supported by the National Department of Civil Protection (Albarello, 2017). With the exception of the last one, none of the considered sources of information is directly linked to site effects; thus, their exploitation for the purposes of the SERENA project required specific strategies. As an example, geological and geomorphological maps need to be re-classified in terms of discrete Units (GMSU) characterized by different engineering geological units (EGU), which in turn, must be characterized in terms of seismic and geotechnical parameters through a statistical analysis of data available. The interplay between these interpretations will be described in detail in the following.

The relative work plan of the project was articulated into seven work packages (WPs):

WP 1: Access to data and products, data management and service provision
WP2: Geological and geomorphological classification
WP3: Evaluation of stratigraphic amplification effects
WP 4: Evaluation of topographic amplification effects
WP5: Evaluation of seismic-induced slope instabilities
WP 6: Empirical testing and calibration
WP 7: Project monitoring and dissemination

Several research units included about 50 researchers from Academic structures (Universities of Siena, Catania and Torino) and Research Institutions (CNR, INGV, OGS, ENEA), were involved in these different work packages. Nevertheless, during the project, the need for continuous interaction among the WPs became evident. For instance, a strict interaction between WP2 and WP3 was mandatory since since assessing the potential impact of alternative seismostratigraphic interpretations on the seismic site response requires selecting the most significant features to be identified on the basis of geological and geomorphological evidence. Similarly, strong interaction between WP3 and WP5 was required because the seismic input including site effects was a key element for landslide susceptibility analysis.

For this reason, the presentation of results in the following sections does not strictly follow the WP structure. Instead, it focuses on six main thematic areas, presented as a dedicated section of this Volume: geological constraints for extensive mapping of seismostratigraphical configurations; 1D numerical simulation to retrieve amplification effects based on the local stratigraphy; estimate of topographic amplification effects; susceptibility to seismically induced landslides; ex post empirical testing and data storage/dissemination of project outcomes. The topic descriptions will primarily focus on methodological aspects rather than specific results, although the latter were produced for large areas and specific issues.

2. Geological constraints and engineering geological interpretation of geological units

2. Geological constraints and engineering geological interpretation of geological units

2.1 Overview

Several geological maps are available in Italy at different scales and developed for different purposes. Those of main interest in the framework of the PRIN SERENA Project are regional maps covering large areas by adopting homogenous classification criteria relative to the relevant geological outcrops. These classification criteria generally focus on stratigraphic purposes putting in evidence the respective age and formation environment, the tectonic/stratigraphic relationship between them, with no reference to their mechanical behaviour under seismic loads. To make these pieces of information useful for the project aims, these maps must be integrated and re-interpreted. The integration mainly concerns recent (Quaternary) relatively thin deposits, which are generally of scarce interest for large scale geological reconstructions, but are of main importance in site response analyses. The re-interpretation is a key aspect of the whole process.

Within the PRIN SERENA project, four main geological map scales were used to ensure a coherent multiscale geological framework:

1. **1:250,000 scale**
   Used in areas where continuous more detailed geological maps are not available:
   - → Piemonte (Piana et al. 2017);
   - → Lombardia (https://www.geoportale.regione.lombardia.it/download-pacchetti?p_p_id=dwnpackageportlet_WAR_gptdownloadportlet&p_p_lifecycle=0&p_p_state=normal&p_p_mode=view&_dwnpackageportlet_WAR_gptdownloadportlet_metadataid=r_lombar:a1cbcd90-f0dd-4af2-88ac-a9fb0ecccf3d.
2. **1:100,000 scale**
   Used as the national reference for lithological characterization:
   - → Lithological map of Italy at the 1:100,000 (Bucci et al. 2022, 2021).
3. **1:50,000**
   For the test area of Val D'Agri (Southern Italy, Carbone et al. 1991).
4. **1:10,000 scale**
   Adopted for Central Italy, where high-resolution geological maps are available from regional authorities:
   - → Tuscany (https://www.regione.toscana.it/-/banche-dati-cartografia-geologica);
   - → Umbria (https://www.regione.umbria.it/paesaggio-urbanistica/cartografia-geologica);
   - → Marche (https://www.regione.marche.it/Regione-Utile/Paesaggio-Territorio-Urbanistica/Cartografia/Repertorio/Cartageologicaregionale10000);
   - → Emilia-Romagna (https://ambiente.regione.emilia-romagna.it/it/geologia/cartografia/webgis-banchedati/cartografia-geologica).

As described hereafter, depending on the scale it was necessary to adapt the kind of analysis to the available level of detail.

First, engineering geological features of geological bodies must be inferred based on geological information generally focused on formational/evolutionary concepts. Second, since geological mapping concerns outcropping structures, the respective stratigraphic layering must be inferred, based on geomorphological proxies and the overall geological/structural characteristics of the considered areas and their reciprocal geometrical relationships.

The general strategy adopted is to provide a morphostratigraphic and lithological re-classification of geological outcrops to identify GMSUs (see also Section 1), each characterized by specific geomorphological and lithostratigraphic settings of surface and shallow subsoil as an effect of their geological history. Thus, the first step of the project focused on the definition of GMSUs, based on geological and geomorphological proxies and the statistical analysis of stratigraphic and topographic data. The main assumption behind this characterization is that both geological and geomorphological aspects must be jointly considered to infer stratigraphic successions and their engineering geological properties.

Within each GMSU, the stratigraphical organization of the included geological bodies is pointed out and reclassified in terms of prevailing engineering geological characteristics (Engineering Geological Units, EGU) and range of thickness. To this purpose, a strategy for aggregation of EGUs is adopted (see Section 2.2 and FIGURE 2.1) by all the research groups involved in the project. This ensures to make large scale geological analysis directly comparable to those from local microzonation studies.

A second main aspect of the analysis is to provide a kind of third dimension to the geological maps. Seismic resonance phenomena induced by the presence of seismic impedance contrasts in the subsoil represents the phenomenon responsible for most diffuse amplification effects of the seismic ground motion at local scale. Despite the fact that more complex effects are expected due to lateral variations of mechanical properties of the subsoil, vertical layering significantly impacts seismic response in all cases. Quantifying such 1D effects remains a main goal of any microzonation study and is also the basis for computing seismic loads to be considered in anti-seismic design of structures. Thus, different strategies have been adopted to reconstruct the 1D layering based on available geological data and to spatialize this information. The adopted strategy depends on the scale of the considered geological maps. This is an important aspect of the project, and some methodological examples will be described in the following sections. A common strategy adopted independently from the scale of analysis is the definition of a stratigraphic matrix relative to each GMSU. This matrix lists all the possible 1D stratigraphic succession (log) present in the respective GMSU, by considering outcropping geological bodies mapped in the reference geological-geomorphological model re-classified in terms of corresponding EGUs. The respective position within the log is determined by its stratigraphical position with respect to the other GMSUs. The number of EGUs within each log is limited by the range of respective thickness down to depths non exceeding 300 m.

It is worth to note that, since extensive evaluations are required which must consider a large amount of geological, geomorphological and lithological information, large use has been made of supervised numerical procedures to manage available data. This required the development of GIS-based codes which represent a main outcome of the project.

In the following, the classification scheme adopted for soil deposits is described at first. Then, the procedure adopted for providing a reference lithological map 1:100,000 for the whole Italian area is illustrated. Lastly, some examples are reported of the different procedures adopted to reconstruct engineering geological layering from available geological maps at regional scale.

2.2 Engineering geological classification of geological bodies

Italian SM studies, carried out under the national program of seismic prevention (Moscatelli et al. 2020), adopted an engineering-geological classification of the soil deposits (Amanti et al. 2020; TCSM, 2018; Cesarano et al. 2022). The main purpose of TCSM (2018) is to provide the practitioners (in charge of the SM studies) with a standardized tool for evaluating engineering-geological features of the subsoil. Each SM class is coded in TABLE 2.1. When direct geophysical/geotechnical measurements are not available, and/or when the scale of analysis is higher than 1:10,000 (i.e., when working over extensive areas), a classification based on aggregated engineering geological units may be adopted. The main assumption of this approach is that the lithological features defining each class adequately reflect, with an equivalent level of approximation, the seismo-geotechnical behaviour of the corresponding materials under seismic loading.

The resulting classification scheme is organized in three levels (orders) as reported below (FIGURE 2.1).

In the First order classification, only two main engineering-geological categories are identified: “Cover terrains” and “Geological bedrock”. The “Cover terrains” units encompass all the various types of mainly loose, incoherent, and unconsolidated shallow deposits, generally of Quaternary age. They include slope deposits, terraced and recent alluvial deposits, terraced and coastal marine deposits, Pleistocene glacial deposits, lacustrine sediments, and landslide deposits. The “Geological bedrock” units are mainly made of pre-Quaternary sedimentary, igneous, and metamorphic rocks or by very thick (>100 m) over-consolidated Early Quaternary deposits. In general, these units include lithoid and consolidated geological formations, including those weathered and fractured, classified following lithostratigraphic and structural features, and sedimentary facies (Catalano et al. 2019, Hailemikael et al. 2020). It is worth noting that geological bedrock is here defined in geological terms (i.e., by considering age and tectono-stratigraphical relationships with overlying and underlying units) with no reference to its stiffness. Thus, it does not correspond to the seismic bedrock, which instead is characterized in terms of peculiar Vs values (NHERP, 2004; CEN, 2003).

The second order classification is based on the grain size distribution. In this case, the “Cover terrains” are classified in three main classes: 1) gravel, 2) sand and silt, and 3) clay dominated. With respect to the “Geological bedrock”, three classes are identified: 1) lapideous (e.g., limestone, dolomites) and cemented clastic rocks (e.g., sandstones, conglomerates); 2) cohesive over-consolidated rocks (e.g. mudstones) and alternations of lithotypes (e.g., Flysch succession made of sandstones interbedded with mudstones and siltstones; 3) weathered and fractured rocks.

In the third order classification, the "Cover terrains" are classified into 17 EGUs, according to the Unified Soil Classification System. With respect to the "Geological bedrock", 16 EGUs have been identified starting from second order classification by considering; i) layering, and ii) presence of fractured and/or weathered horizons (Cesarano et al. 2022).

TABLE 2.1 Engineering-geological classification adopted in seismic microzonation studies by following the Italian standards relative to seismic microzonation studies (Romagnoli et al. 2022).

COVER TERRAINS		GEOLOGICAL BEDROCK	
RI	Terrains containing remains of human activity anthropic deposits	LP	Lapideous
GW	Well sorted gravels, mixed gravels and sands	GR	Grainy cemented
GP	Not sorted gravels, mixed gravels and sands	CO	Cohesive over-consolidated
GM	Silty gravels, mixed gravels, sands and silts	AL	Alternations of lithotypes
GC	Clayey gravels, mixed gravels, sands and clays	LPS	Lapideous stratified LP
SW	Well sorted sands, mixed sands and gravels	GRS	Grainy cemented stratified GR
SP	Not well sorted sands	COS	Cohesive over-consolidated stratified CO
SM	Silty sands, mixed sands and silts	ALS	Alternations of lithotypes stratified AL
SC	Clayey sands, mixed sands and clays	SFLP	Lapideous fractured/weathered LP
OL	Organic silts, low plasticity organic silty-clays	SFGR	Grainy cemented fractured/weathered GR
OH	Middle plasticity organic clays, organic silts	SFCO	Cohesive over-consolidated fractured/weathered CO
MH	Inorganic silts, fine sands, diatomic silts	SFAL	Alternations of lithotypes fractured/weathered AL
ML	Inorganic silts, fine silty-clayey sands, low plasticity clayey, silts	SFLPS	Lapideous stratified fractured/weathered LPS
CL	Middle-low plasticity inorganic clays, gravel-sandy clays,silty clays	SFGRS	Grainy cemented stratified fractured/weathered GRS
CH	High plasticity inorganic clays	SFCOS	Cohesive over-consolidated stratified fractured/weathered COS
PT	Peat and organic soils	SFALS	Alternations of lithotypes stratified fractured/weathered ALS
LC	Lithoid Cover deposit		

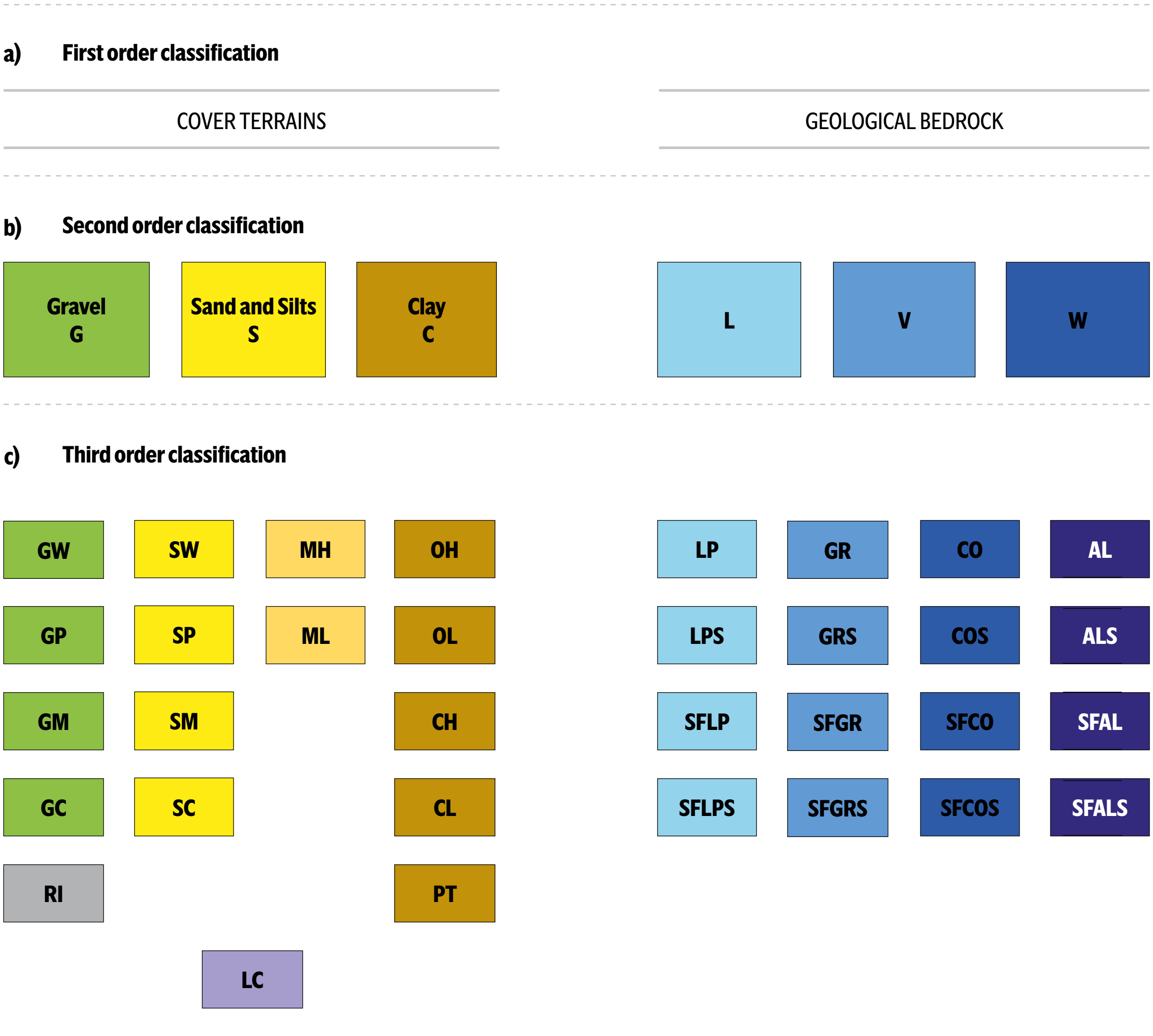

FIGURE 2.1 Schematic three-levels engineering-geological classification. Modified from Romagnoli et al. (2022).

2.3 A reference engineering geological map of Italy 1:100,000

2.3.1 Outcropping bedrocks

The engineering geological map of Italy at a scale of 1:100,000 was compiled starting from the data structure of the Lithological Map of Italy 1:100,000 (Bucci et al. 2022, 2021, FIGURE 2.2a). Throughout a further semantic reclassification, the new map integrates more detailed geological information extracted from the source dataset of the Geological Map of Italy at a scale of 1:100,000, to adequately discretize rocks and soils classes based on their physical-mechanical properties.

The adoption of the lithological map as a starting point is motivated by its comprehensive and updated characterization of the lithostratigraphic units of Italy, where expected geomechanical properties constitute the primary classification criterion. This conceptual framework ensures coherence with the original geological information while providing an analytically robust basis for deriving an engineering geological map at the same representation scale.

We first set a preliminary conversion between the input lithological classes (Bucci et al. 2022) and the EGU classes (TABLE 2.1 and FIGURE 2.1). FIGURE 2.2b illustrates a generally reasonable engineering geological classification of Italy, which has the advantage of being homogeneous on a national scale. It is worth noting that the engineering geological classification of engineering geological outcrops only partially corresponds to the three-levels classification in TABLE 2.1, since the classification follows the third order classification scheme for geological bedrock and a second order classification schema for cover terrains. Nevertheless, two major limitations affected the final product. First, the lithological class of alluvial deposits (cover terrains) was treated as homogeneous, whereas an engineering geological representation requires its differentiation into gravels, sands and clays, given their markedly different mechanical behaviour. Second, the original lithological classification did not distinguish between geological bedrock and cover terrains, a distinction that is essential in an engineering geological framework. Addressing these limitations would require renewed extraction and reinterpretation of information from the original source database.

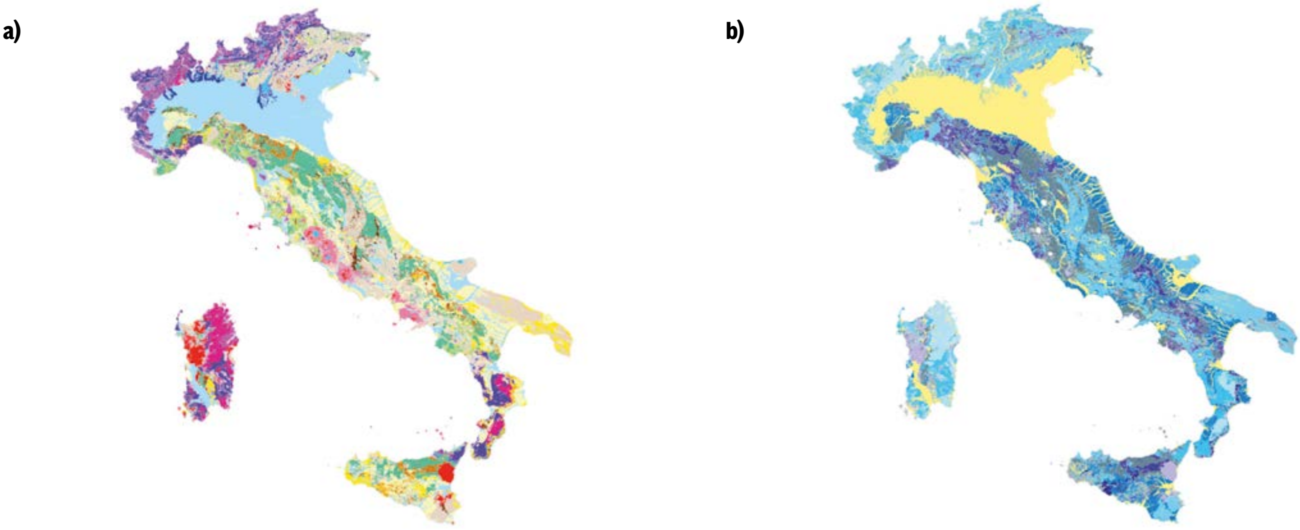

Lithological Classes

Al	Alluvial and marine deposits	Gd	Glacial drift
Ucr	Unconsolidated dastic rocks	Cm	Chaotic – mélange
Cr	Carbonate rocks	Lb	Lavas and basalts
Ssr	Siliciclastic sedimentary rocks	M	Marlstone
Sr	Schistose metamorphic rocks	E	Evaporites
Ccr	Consolidated elastic rocks	Li	Lakes and Ice
Ir	Intrusive rocks	B	Beach deposits
Nsr	Non-schistose metamorphic rocks	Mw	Mass wasting material
Pr	Pyroclastic rocks	Ad	Anthropogenic deposits
SM	Mixed sedimentary rocks		

EGU, third-order classification

ALS	Alternations of tithotypes stratified
LP	Lapideus
LPS	Lapideous stratified
SFAL	Alternations of lilhotypes fractured/weathered
SFALS	Alternations or lithotypes stratified fractured/ weathered
SFCOS	Cohesive over-consolidated stratified fractured/ weathered
SFGR	Grainy cemented fractured/weathered
SFGRS	Grainy cemented stratified fractured/weathered
SFLPS	Lapideous stratified fractured/weathered

EGU, second-order classification

G	Gravel
LC	Lithoid cover
S	Sand
C	Clay

FIGURE 2.2
a) Lithological map at 1:100,000 scale (modified from Bucci et al. 2022);
b) Preliminary engineering geological map at 1:100,000 scale, subdivided into EGUs.

To derive the final engineering geological map from the preliminary version, three sequential work phases were defined. The first phase consisted of a renewed data acquisition, including the extended legend and the lower and upper stratigraphic age attributed to each polygon of the Geological Map of Italy at 1:100,000 scale. The second phase addressed the systematic distinction between bedrock and cover terrains, a fundamental requirement within an engineering geological perspective. The third phase involved the differentiation of lithological classes characterized by internal heterogeneity, with particular attention to alluvial deposits, pyroclastics and lavas, loose clastic sediments, and cemented clastic sediments.

Throughout all phases, the original geometry of the geological features was preserved, ensuring full consistency with the source cartography and avoiding any modification of the geometric features.

The outputs of the methodological procedures described above constitute the new engineering geological map (FIGURE 2.3b). From a cartographic perspective, the implications of the adopted workflow can be effectively assessed through a comparison between the preliminary engineering geological Map (FIGURE 2.2a) and the Final engineering geological Map (FIGURE 2.3b). The most evident differences emerge in the Po Plain (Box 1 in FIGURES 2.3a and 2.3b): in the preliminary version alluvial deposits were uniformly classified as sands, whereas in the final map they are differentiated into sands, gravels and clays, reflecting their internal lithological and mechanical variability. Additional significant changes, clearly appreciable at the national scale, concern the Tavoliere delle Puglie (Box 2 in FIGURES 2.3a and 2.3b). In the preliminary map, the original unconsolidated clastic units were classified within the Cohesive, Subordinately Layered, Fractured or Altered Rocks class, SFCOS. In the final version, these units are more consistently articulated into Gravels, G, Sands, S, and the underlying clayey substrate, assigned to the Cohesive, Subordinately Layered, Fractured or Altered class. These differences, together with numerous others observable at progressively finer spatial scales, highlight the multi-scale impact of the reclassification process and its influence on the Engineering geological representation of the national territory.

Overall, the final engineering geological classification is markedly more specific and internally articulated than the preliminary version, particularly with respect to cover deposits. This refinement represents a substantial cartographic advancement and carries relevant scientific implications for the estimation of seismic amplification, especially where alluvial cover terrains are present, which host a large proportion of the national urban fabric and population.

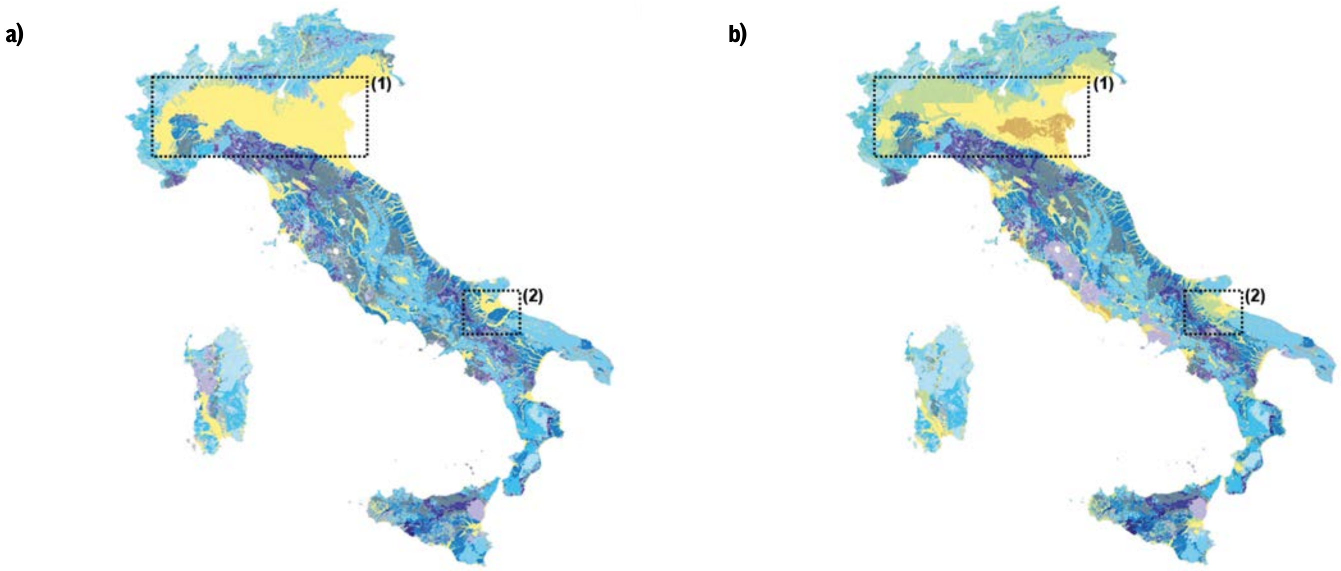

EGU, third-order classification

EGU, second-order classification

ALS	Altemations of lithotypes stratified	SFCOS	Cohesive over-consolidated stratified fractured/weathered	G	Gravel
LP	Lapideus	SFGR	Grainy cemented fractured/weathered	LC	Lithoid cover
LPS	Lapideous stratified	SFGRA	Grainy cemented stratified fractured/ weathered	S	Sand
SFAL	Altemations of lithotypes fractured/weathered	SFLPS	Lapideous stratified fractured/weathered	C	Clay
SFALS	Altemations of lithotypes stratified fractured/ weathered				

FIGURE 2.3
a) Preliminary Engineering Geological Map;
b) Final Engineering Geological Map.

2.3.2 Including shallow alluvial quaternary deposits in the reference engineering geological map

Due to the scale of the considered analysis, some important small scale lithostratigraphic elements cannot be included in the reference map described above. In particular, the presence of relatively thin quaternary deposits, which play a very important role in site response evaluations, is generally discarded. A specific procedure has been adopted to provide the reference map with this important information (Mendicelli et al. 2024).

The basic idea is that the digital elevation model may provide proxies to infer the possible presence of recent alluvial deposits. In particular, Machine Learning procedures may help develop a predictive model based on a number of morphometric parameters inferred by available digital elevation data. In particular, the following morphometric parameters were considered:

1. Height Above the Nearest Drainage (HAND);
2. Slope;
3. multiscale Topographic Position Index (mTPI);
4. Tangential Curvature (tcurv);
5. Profile Curvature (pcurve);
6. Topographic wetness index (TWI)

as well as the following categorical parameter: lithological categories.

Thus, the lithological map at 1:100,000 scale described in the previous section was reclassified into a map with three categories: 1) Alluvial Holocene deposits; 2) Pleistocene terrace deposits; 3) geological bedrock units.

As usual when Machine Learning algorithms are used, a learning phase is necessary. This was planned where the optimal combination of these predictive parameters is considered. In particular, the learning phase took advantage by the detailed geological maps provided by Central Italy regions (1:10,000 maps from Tuscany, Marche, Umbria, Emilia-Romagna) and Calabria (1:25,000) relative to outcropping formations including most of recent alluvial deposits. The machine learning algorithm considered was the Light Gradient-Boosting Machine which results in an effective and less time-consuming process with respect to other procedures.

When applied to a test area in the Marche Region (from Macerata to Falconara Marittima), the model achieved a global performance index equal to 0.87. The prediction accuracy is more satisfactory for Holocene alluviums, whereas a lower performance index is obtained for Pleistocene alluvial terraces.

Having defined the parameters of the machine-learning model, the next step has been the integration of the obtained results in the 1:100,000 Lithological Map, encoded into engineering geological Units.

Based on proximity criteria and using a Python procedure that considers the engineering geological class of closest outcrops reported in the map at 1:100,000 scale described in the previous section, an engineering geological class equal to G, S or C was re-assigned to each starting polygon. In this way, a new reference map has been built where the estimated alluvial cover terrains are reported (FIGURE 2.4).

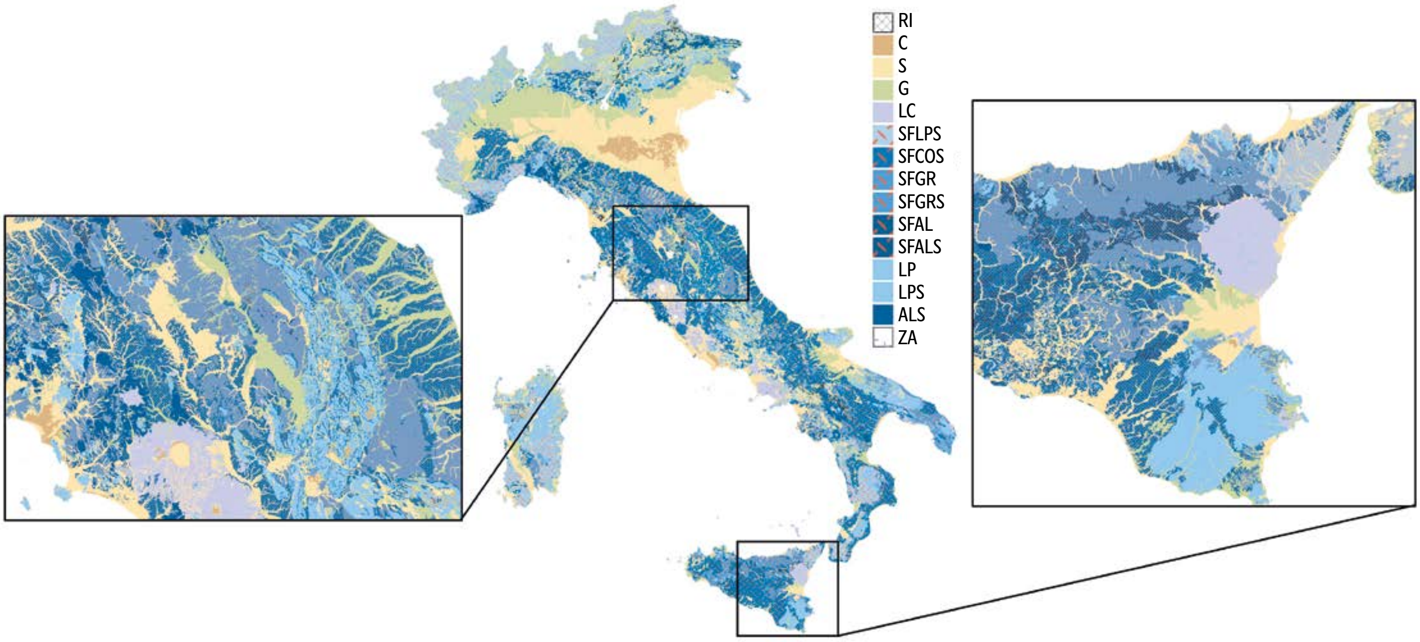

FIGURE 2.4
Reference engineering geological map of Italy 1:100,000 inclusive of alluvial cover terrains.

The main differences with the map of FIGURE 2.3 concern alluvial cover terrains and in particular areas where most of classes are grouped into: sand dominated (S), gravel dominated (G) and clay dominated (C) deposits.

It is worth noting that, also in this case, the engineering geological classification of engineering geological outcrops only partially corresponds to the three-levels classification in TABLE 2.1, since the classification follows the third order classification scheme for geological bedrock soil deposits and a second order classification schema for cover soil deposits.

2.4 Retrieving Engineering Geological Units (EGUs) from 1:10,000 geological maps

Beyond the 1:100,000 lithological map of Italy, some of the Italian Regions are covered by 1:10,000 scale Geological and Geomorphological maps (Section 2.1). These are important high-resolution geological databases of great importance for the project. However, a limitation of these data is that they have been made in different time span, adopting slightly different criteria both for geological data interpretation and data storage. Such heterogeneity is highlighted by the frequent poor lateral continuity from Region to Region. To cope with this problem, at first the maps from each Region have been analysed separately.

The Regional maps (and respective classification criteria within the legend) has been analysed to identify the relevant GMSUs based on a careful expert analysis of the specific geological/geomorphological context. For each GMSU, a set of EGUs has been identified, together with their relative stratigraphic position. Finally, the prevailing engineering geological classes has been attributed to each EGUs. One example of outcomes provided by this approach is reported in TABLE 2.2 relative to the Tuscany Region.

GMSU	BEDROCK-COVER TERRAINS	GEOMORPHOLOGICAL POSITION	OUTCROP DESCRIPTION AND AGE	LITHOTYPES	THICKNESS RANGE FOR LITHOTYPES
11 12	Cover	Valleys and slopes	Gravelly, sandy and clayey alluvial, slope, coastal and glacial deposits (Quaternary)	G, S, C	50–100
			Gravelly, sandy and clayey alluvial, slope, coastal and glacial deposits (Quaternary)	G, S, C	<50
20	Bedrock	Slopes	Volcanics, pyroclastics and lavas (Quaternary)	L, S, V, W	10–100
30		Basins	Continental sandstones, conglomerates and clays of the tectonic basins (Early-Middle Pliocene)	V W	3–150 3–50
41		Basins	Marine, coastal and continental sandstones, conglomerates and clays of the tectonic basins (Early-Middle Pliocene)	V W	3–300 3–300
42		Basins	Marine, coastal and continental sandstones, conglomerates and clays of the tectonic basins (Late Messinian)	V W	3–50 3–100
43		Basins	Marine, coastal and continental sandstones, conglomerates and clays of the tectonic basins (Messinian)	V W	3–50 3–100
44		Basins	Marine, coastal and continental sandstones, conglomerates and clays of the tectonic basins (Middle Miocene)	V W	3–50 3–100
45		Basins	Clayey lacustrine deposits of the tectonic basins (Early-Middle Miocene)	W L	3–50 3–300
50		Ridges	Deep sea mainly mixed limestones and claystones of the Ligurian, Subligurian and Epiligurian Units (Createaceous-Early Miocene)	V W	3–150 3–150
60		Ridges	Foreland arenaceous dominated successions of the Tuscan Units (Oligocene-Miocene)	V W L	3–300 3–300 3–300
70		Ridges	Limestone dominated successions of the Tuscan Units (Triassic-Eocene)	V W	3–300 3–300
80		Ridges	Metamorphic complex of the Tuscan Units and Paleozoic Basement (Paleozoic to Eocene)	L, V, W	300

TABLE 2.2
The Geological-Geomorphological Units model of the Tuscany Region including the classification of its GMSUs defined based on their stratigraphical and geomorphological positions. GMSUs 11 and 12 are not arranged in stratigraphic since they represent alternative outcrop. The information encompasses the primary geological characteristics of each GMSU, the total thickness ranges, the lithotype (EGUs classification is based on the second order classification of Figure 2.1), its potential stratigraphic sequence (in the numerical order in the first columns from the shallower to the deeper), and the corresponding thicknesses. Modified after Pieruccini et al. (2024).

2.5 Assessing Engineering Geological stratigraphic logs

As shortly outlined above, the inference of the local engineering geological stratigraphic successions based on geological maps requires different approach according to the type and scale of available reference maps: 1) Regions where no stratigraphic reconstructions can be provided due to the lack of reliable geological maps; and 2) areas where relevant GMSUs can be assessed. In the latter case, according to the available geological maps two different approach can be applied: 1) when the reference map is at 1:100,000 scale and 2) when the available maps are at 1:10,000 scale. In the following four examples are provided relative to these different conditions.

2.5.1 Archetypal Engineering Geological logs

This approach based on geological maps at 1:100,000 scale. In this approach, a set of possible stratigraphic combinations of EGUs has been built by a preliminary permutation of all the possible the possible combinations present in the Italian area. Then, the configurations are extracted which respect the condition that EGU belonging to cover terrains always overly those of geological bedrock. In all cases, the bottom of each of these archetypal logs corresponds to a bedrock EGU.

Possible ranges of thicknesses relative to each EGU have been considered in the range 5-95 m binned at 10m (two layers 5 m and 95 m of thickness were also considered).
A hybrid second/third level for EGUs classification (see FIGURE 2.1) has been considered (TABLE 2.3). More details are given in FIGURE 3.4 and in Section 3.3.1.

TABLE 2.3
List of EGUs classification considered in the stochastic modelling and combined to construct archetypal engineering geological logs.

COVER TERRAIN	ALTERED BEDROCK	BEDROCK
S	W	AL
G		CO
C		GR
LC		LP
		L

As a whole, four kinds of logs were considered:

1. Cover terrain, Altered bedrock, Bedrock;
2. Cover terrain, Bedrock;
3. Altered bedrock, 1-2 Bedrock units;
4. 2 Cover terrain units, 1 Altered bedrock, 1 Bedrock;
5. 2 Cover terrain units, Bedrock.

21.135 archetypal seismo-stratigraphic logs were defined and re-organized by grouping all the configurations showing the same outcrop. In this way, a set of possible seismostratigraphic configurations is associated with each outcrop of the reference engineering geological map. This implies that those configurations are considered as representative for each outcrop which is assumed as internally uniform. In this view, the outcrops of the reference engineering geological map represent the large-scale equivalent of the seismically homogeneous microzone (SHM) considered in SM studies.

2.5.2 Engineering Geological logs from the 1:100,000 reference map

An automatic extraction and spatialization of representative engineering geological logs has been defined through the application of a modified version of a custom Python script already applied in a pilot study by D'Agostino et al. (2025). This semi-automated methodology was designed to turn the GMSU map into spatially distributed logs of overlying GMSUs (and the corresponding EGUs). The procedure automatically reconstructs stratigraphic logs from geological raster data by combining a pixel-based search with user-defined stratigraphic rules. It produces a raster output in which each pixel is assigned to a unique integer ID representing a full sequence GMSUs and a corresponding engineering geological unit. Optional QGIS-based supervised fitting offers more controlled reconstructions. The output is then automatically converted into a polygon map, by merging adjacent pixels with same column ID. Contours of the GMSU polygons in the original map do not necessarily coincide with those of SHM in the resulting map.

The required core inputs are a raster geothematic map categorized by an attribute "POS" encoding the relative vertical order of outcropping units, from the shallowest unit to the deepest one, and a raster thickness map of outcropping units, carrying a "THI" value for each pixel. A shapefile version of the geothematic map can also be used to supervise the reconstruction in QGIS. Users can also employ the "POS" to merge units or split a unit into sub-units, which makes the procedure adaptable to complex geological settings such as thrusting or inverted stratigraphy. The method is scale-independent in principle, but its detail depends strongly on the resolution and scale of the input map. Larger-scale, high-resolution maps support more detailed stratigraphic interpretations, while smaller-scale maps are better suited to broader regional overviews.

The main algorithm, coded in Python, employs a square sliding window whose size depends on the Global Maximum Search Radius, or GMSR. The window is centered on each pixel, the outcropping unit at the center becomes the first element of the stratigraphic column, and adjacent units with progressively deeper "pos" values are appended until a Column Interruption Criterion (CIC) rule is met (see FIGURE 2.5). Each reconstructed column is associated with a confidence value that decreases as the search has to expand farther from the central pixel. In practice, confidence is inversely related to the radius needed to satisfy the stopping criterion, so shorter searches imply more reliable reconstructions.

To make the computation efficient, the scripts use dynamic binary masks implemented through optimized array-based Python libraries such as NumPy and SciPy. Columns that share the same sequence of units and thicknesses receive the same progressive integer ID, so identical stratigraphic patterns are spatially mapped consistently across the study area.

The CIC determines when the construction of a log must stop. Five criteria are available: a) minimum cumulative thickness, b) first substrate reached, c) second substrate type 1, d) second substrate type 2, and e) fitting to a predefined validated column type. The thickness-based criterion (a) stops when the

FIGURE 2.5
Schematic representation of the procedure inputs and main algorithm. (a) Input raster geothematic map reclassified by geometric position of outcropping units ('pos' attribute); (b) Input raster thickness map showing estimated thickness of outcropping units per pixel ('thi' attribute); (c) Automated pixel-wise stratigraphic column construction and spatialization. Step 4 shows how the procedure skips the unit with 'pos' = 3 because the current lowermost unit already has a deeper position value (pos = 5). From D'Agostino et al. (2025).

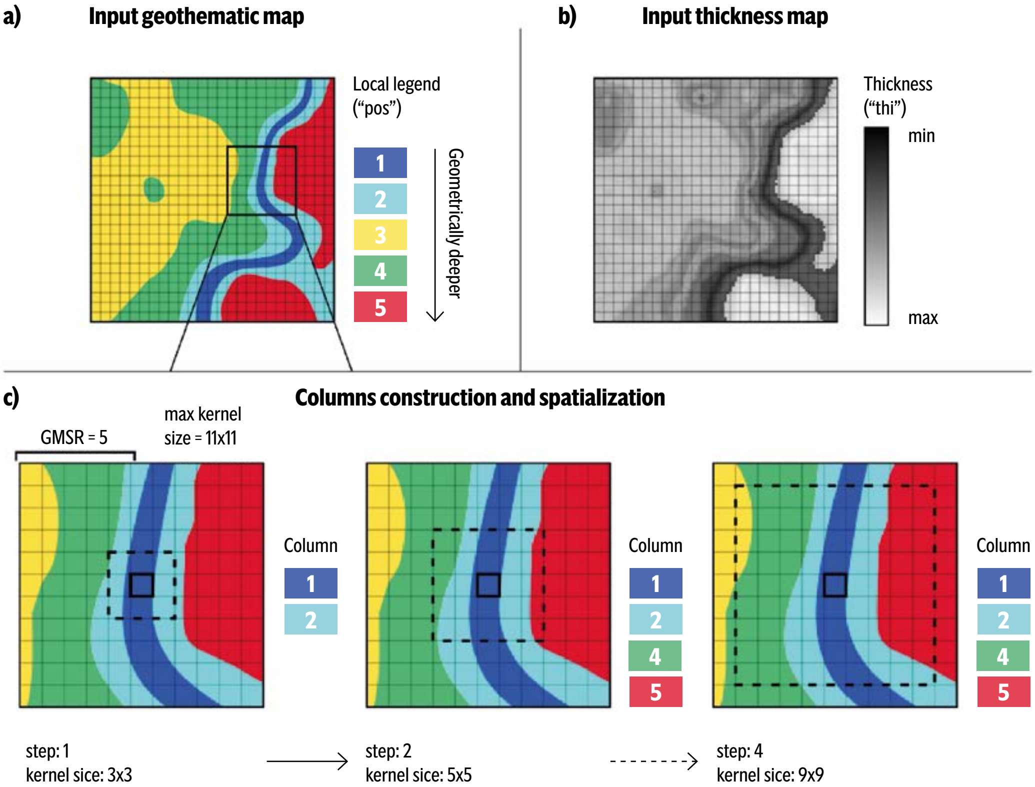

cumulative thickness reaches a chosen threshold. The first substrate-based criteria (b) stop when a unit defined by the user as substrate is reached, while the "second substrate" variants (c, d) add extra flexibility when the outcropping unit is already a substrate.

The fitting criterion (e) is the most constrained option: the algorithm only returns a column if it exactly matches one valid pre-established stratigraphic column. If no criterion is satisfied before the search radius is exhausted, the algorithm still returns the built column but assigns it zero confidence. The pre-definition of valid stratigraphic columns is achieved by means of a dedicated supervised QGIS workflow, which allows reconstructing stratigraphic columns step by step from a polygon shapefile. At each step, the script checks polygon neighbors, prefers those in a deeper "pos" position, and combines their thicknesses into a cumulative value (**FIGURE 2.6**). If no direct lower neighbor is found, the script expands the search to a user-defined surrounding area and continues with the same logic. Each iteration adds a new layer, updates total thickness, and builds a progressively more complete stratigraphic sequence that can then feed the main raster-based spatialization algorithm.

FIGURE 2.6
Supervised QGIS workflow for column definition. (A) Layer search logic when the unit under examination lacks immediate neighbors in lower geometric positions ("pos"); examples show stratigraphic column construction starting from a pos = 3 unit through (B) Step 1 (initial outcrop layer with immediately deeper unit) and (C) Step 2 (adding deeper neighbor layers and cumulating thickness). From D'Agostino et al. (2025).

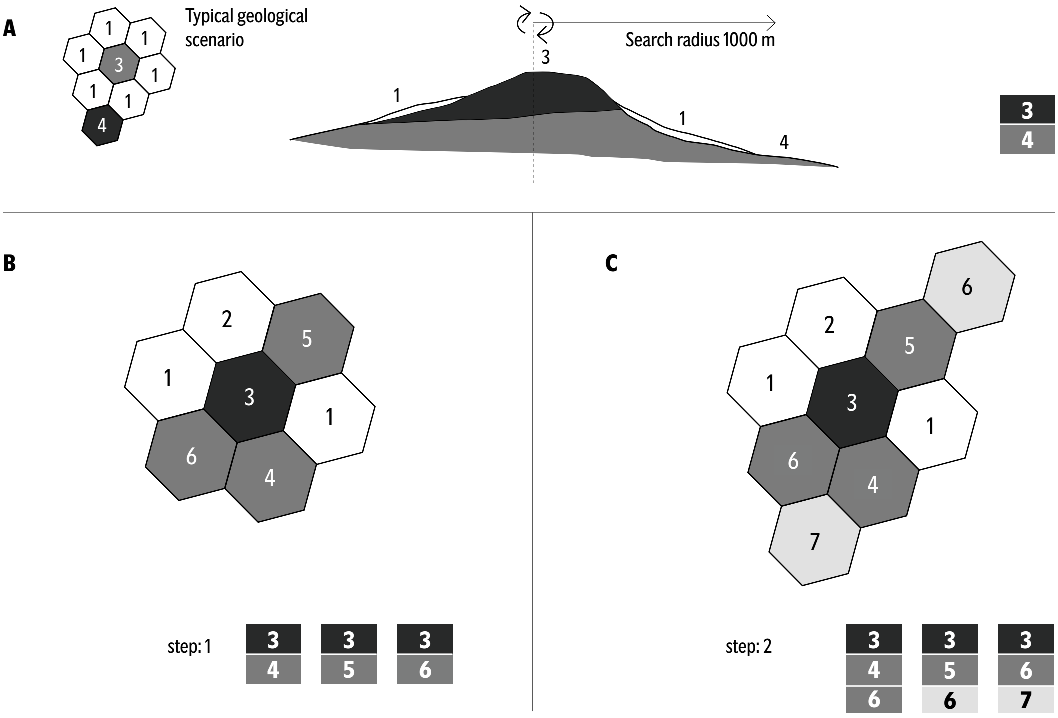

2.5.3 Engineering geological logs from the 1:10,000 geological maps

In this approach, the available geological maps, due to the detail of the scale, show the largest diversity and complexity of the represented outcropping geological units. At first, units in the map were reclassified in terms of Cover Terrains (mostly Quaternary deposits generated by recent surface processes and local geomorphological factors) or Geological Bedrock (pre-Quaternary) and and grouped in terms of as GMSU made of combinations of possible lithostratigraphical successions of layers of different thickness range and engineering geological characteristics (Logs). Thus, the GMSUs assume the characteristics of a large-scale SHM assumed as homogeneous in terms of expected seismic response. A semi-automatic method has been developed to assign a Log to each outcrop by considering a buffer within 500 m distance from the boundaries of the considered outcrop. This distance is a value obtained by assuming an average dip of the contacts between the overlapping GMSUs by 30° and the need to reach a depth of approximately 300 m below the surface. With this constraint, an Arcpy™ script was created in the ArcGIS Pro™ platform to perform the spatial analysis of the GMSUs of Tuscany Region.

The example in FIGURE 2.7 refers to one of the GMSUs of Tuscany region and helps understand how the Arcpy™ script works. The outcropping areas of the different GMSUs are registered in the spatial database as "georeferenced polygonal layers" having reference planimetric cartographic coordinates, which therefore allow the analysis of the different spatial relationships between the polygons representing the areas, using common spatial criteria analysis techniques available in GIS Platforms.

The mapped GMSUs, therefore, differ each other according to a defined stacking order from the most superficial to the deepest, and a procedure consisting of several steps may be applied. The first step consists in selecting individually (one by one) the polygons belonging to each GMSUs, starting from the outcropping one (GMSU 10 or GMSU 11) towards the deepest one (GMSU 80). The selection allows to create a "temporary layer" relating to the single selected area (FIGURE 2.7b). The second step creates a 500 m wide buffer area around the single selected area (FIGURE 2.7c). Based on the extension of this buffer area, we select all the other areas belonging to other deeper GMSUs: that is, if we are analysing a polygon belonging to the Unit 11, based on the stacking order, the polygon of the other underlaying GMSUs (GMSUs 12, 20, 30) can be selected.

The GMSU and lithotype of the selected polygons (to easily identify them in FIGURE 2.7d they are indicated with underlined labels), are processed for their extraction, sorted according to the stacking order and grouped based on their unique value.

Once all the polygons belonging to a GMSU have been found, the process is restarted with the areas belonging to the other GMSU, excluding from the analysis the already processed polygons belonging to the last upper analysed GMSU.

FIGURE 2.7
The example refers to a detailed area in the GMSU map of Tuscany. The first step consists in selecting any outcrops from the GMSUs map (Frame A) belonging to the upper litho-morpho-tectonics and creating a temporary layer (GMSU 11 in Frame B). The third step creates a 500 m wide buffer area around any temporary layer polygon and selects all other outcrops within this buffer area (Frame C). The GMSU and lithotype for the selected polygons (to easily identify them in frame D they are indicated with underlined labels) are processed for their extraction, sorted according to the stacking order, and grouped by their unique value. In this example, the Logs are composed of the upper horizon composed of three units (GMSU 11 with lithotype G; GMSU 12 with lithotype S; GMSU 12 with lithotype G) superimposed on the lower horizon composed of GMSU 30 with lithotype V superimposed again on the lower horizon GMSU 41 with lithotype V. From Pieruccini et al. (2024).

Data relative to the selected outcrops are processed in order to extract the respective GMSU and lithotype ordered, from the upper most to lowermost (TABLE 2.3). The *Log* relative to the considered outcrop (now considered as a single outcrop) is built down a depth of 300 m (TABLE 2.4).

In each new selection step of spatial analysis for the different GMSUs' group of units, the procedure excludes the GMSUs already processed from the analysis; therefore, the analysis proceeds from the upper to the lower units, from GMSU 11 to GMSU 80. As a whole, 4230 typologies of outcrops have been finally identified, each with a specific stratigraphic configuration and distributed throughout the whole study area territory. Approximately 63% of the generated outcrops are characterized by Cover

Terrains (GMSU 11 and GMSU 12), while the remaining portion correspond to outcropping Geological Bedrock.
This approach has been tentatively applied also to regiones where less detailed geological maps were available, such as the cases of Piemonte and Lombardia.

TABLE 2.4
Table summarizing the actual GMSUs selected around a polygon belonging to GMSU 11 of the example in Figure 2.7b.

GMSU	EGU-group	Type of outcropping (coverage terrains, CT or bedrock, B)	Thickness
11	G	CT	50-100
12	C	CT	3-50
12	G	CT	3-50
12	S	CT	3-50
30	L	B	3-50
30	V	B	3-50
30	W	B	3-50
41	V	B	3-300
41	W	B	3-300
42	W	B	3-100
43	V	B	3-100
50	L	B	3-200
50	V	B	3-200
50	W	B	3-200
80	L	B	300
80	V	B	300

TABLE 2.5
Actual occurrences of Logs resulting from the buffer selection around a polygon belonging to the GMSU 11 relative to the example in Figure 2.7. For each layer, the number identifies the units in Table 2.2 and the letter, the possible corresponding lithotypes.

Log n° 1	*Log* n° 2	*Log* n° 3	*Log* n° 4	*Log* n° 5	*Log* n° 6	*Log* n° 7	*Log* n° 8	*Log* n° 9	*Log* n° 10
11	12	11	12	11	12	11	12	11	12
		30L/ 30V/30W	30L/ 30V/30W	30L/ 30V/30W	30L/ 30V/30W	30L/ 30V/30W	30L/ 30V/30W	30L/ 30V/30W	30L/ 30V/30W
				41V/41W	41V/41W	41V/41W	41V/41W	41V/41W	41V/41W
						50L/ 50V/ 50/W	50L/ 50V/ 50/W	50L/ 50V/ 50/W	50L/ 50V/ 50/W
								80L/80V	80L/80V

3. Estimate of 1D seismo-stratigraphic amplification factors

3. Estimate of 1D seismo-stratigraphic amplification factors

3.1 Overview

The engineering geological logs defined in the previous sections, have been considered to simulate expected 1D seismic response under the seismic load. In order to provide outcomes compatible with those of the standard SM studies, stratigraphic amplification effects are estimated by considering synthetic Amplification Factors defined as follows:

Eq. 3.1) $$AF_{T_1,T_2} = \int_{T_1}^{T_2} \frac{SA_{out}(T)}{SA_{inp}(T)}\, dt$$

where SA_{out} and SA_{inp} represent the ordinates of the response spectra at the surface and at the reference seismic bedrock, respectively; T is the structure's natural vibration period. Four intervals where considered: PGA (T_1=T_2=0), 0.1s–0.5s, 0.4s–0.8s and 0.7s–1.1s. It is worth to note that, since amplification effects are computed by considering a parameterization inferred using indirect information and statistical considerations, estimated values are affected by significant uncertainty which has been carefully evaluated and considered in the final hazard estimate.

In order to retrieve AF values and the impact of uncertainty affecting the parameterization of the relevant engineering geological logs, the numerical code NC92soil (Acunzo et al. 2024) has been applied, a Python-based code running on the Windows operating system. The code supports multiple analysis modes for the input seismo-mechanical models: single-profile, virtual alternations, batch profiles, stochastic analysis, stochastic permutation analysis, GUI-driven runs, and Excel + GUI workflows. NC92-Soil runs on a single thread, and no parallel architecture is currently available. For this reason, if high-performance computing resources are not accessible, the full set of logs must be divided into subsets, and the program must be launched multiple times-once for each seismic spectrum and for each subset of columns.

To run NC92-Soil, several input parameters are required, including the seismic input and the mechanical parameters that describe the soil behaviour.

NC92-Soil accepts both time histories and response spectra via **Random Vibration Theory (RVT)** for equivalent-linear analyses. In this approach, time-domain inputs (such as sets of acceleration time histories) are not required. Instead, a single Fourier Amplitude Spectrum (FAS) or a single response spectrum must be specified. RVT develops a Fourier spectrum that is compatible with the response spectrum. Transfer functions are then applied to propagate the spectrum through the soil column, thus obtaining peak values and spectral accelerations.

A key feature of the NC92-Soil is the possibility to apply a Monte-Carlo approach to evaluate the impact of uncertainty affecting input data on computed AF values and other relevant parameters (e.g., the depth of the seismic bedrock). In this way expected values relative to each dimension of interest are computed along with the relevant uncertainty.

Because of the extensive numerical modeling, RVT was used since it is particularly efficient when a large number of simulations are required for probabilistic risk assessment.

For what concerns the seismic and mechanical parameters to be defined, Romagnoli et al. (2022) and Gaudiosi et al. (2023) carried out a statistical analysis on the database of shear-wave velocity information and G/G_0 and D curves collected over the last ten years in Italy in the Seismic Microzonation studies. They modelled, for each cover unit and bedrock unit, the variability of Vs with depth and the nonlinear behavior, as well as the possible correlation between consecutive layers, categorizing the materials into groups.

Seismic responses were modelled by using, as input, the response spectra provided by the Italian Seismic Hazard Map (https://esse1-gis.mi.ingv.it/) for reference soil conditions (flat morphology and outcropping rigid rock with Vs > 800 m/s). In particular, values relative to an exceedance probability of 10% in 50y have been considered.

An important element considered in the SERENA project was the attempt to account for possible sources of uncertainty affecting outcomes based on the use of ill-defined information relative to input information retrieved from indirect data relative to engineering geological logs and mechanical parameters. This was achieved by a Monte-Carlo approach where the relevant parameters were randomly varied within the range of possible values inferred from the geological and statistical constraints. In general, tens of runs were performed for each log, and the relevant outcomes have been considered to assess the probability distribution of possible AF values. In the assumption that a log-normal distribution characterizes this uncertainty relative to these values, average and standard deviations inferred from the simulation outcomes have been considered as representative of each engineering geological log.

3.2 Vs profiles and geotechnical parameterizations of the EGU considered in the simulations

The macrogroup concept proposed by Romagnoli et al. (2022) was specifically employed to categorise and group together soil and rock samples that exhibited comparable mechanical features. Materials have been categorized into different lithotypes based on the statistical comparison between intra and inter group variability of experimental Vs value relative to each lithotype.

TABLE 3.1
Parameters used to describe the mechanical and dynamic behaviour of the relevant lithotype variability as a function of depth H (in m). For each lithotype the following information is reported: unit weight, median Vs as function of depth, standard deviation of the Vs values in natural logarithms. From Pieruccini et al. (2024).

Group name	Unit weight [KN/m³]	From [m]	To [m]	Vs(h) law [m/s]	Sigma logn
C (CL, CH, OL, OH, PT)	19.4	0	28	189.00*H^0.187	0.441
C (CL, CH, OL, OH, PT)	19.4	28	150	189.00*H^0.187	0.441
C (CL, CH, OL, OH, PT)	19.4	150		189.00*H^0.187	0.441
S (SW, SP, SM, SC)	19.3	0	28	190.00*H^0.267	0.436
S (SW, SP, SM, SC)	19.3	28	150	190.00*H^0.267	0.436
S (SW, SP, SM, SC)	19.3	150		190.00*H^0.267	0.436
G (GW, GP, GC, GM)	19.8	0	28	217.00*H^0.301	0.433
G (GW, GP, GC, GM)	19.8	28		217.00*H^0.301	0.433
L (LP, LPS, SFLP, SFLPS, LC)	20.5	0	20	257.00*H^0.398	0.477
L (LP, LPS, SFLP, SFLPS, LC)	20.5	20	100	257.00*H^0.398	0.477
L (LP, LPS, SFLP, SFLPS, LC)	20.5	100		257.00*H^0.398	0.477
V (GR, GRS, ALS, AL, CO)	21.1	0	20	183*H^0.407	0.411
V (GR, GRS, ALS, AL, CO)	21.1	20	100	183*H^0.407	0.411
V (GR, GRS, ALS, AL, CO)	21.1	100		183*H^0.407	0.411
W (COS, SFGRS, SFGR, SFAL, SFCO)	21.0	0	20	170*H^0.358	0.41
W (COS, SFGRS, SFGR, SFAL, SFCO)	21.0	20	100	170*H^0.358	0.41
W (COS, SFGRS, SFGR, SFAL, SFCO)	21.0	100		170*H^0.358	0.41

The mechanical parametrization of the layers to be modelled was also based on a previous study: the dataset provided by Gaudiosi et al. (2023). The authors integrated the complete collection of geotechnical data obtained from seismic microzonation studies conducted in Italy and established a repository in which each curve was linked to the corresponding engineering geological units examined in the seismic microzonation research. However, to ensure consistency with the lithotypes defined in the prior study of Romagnoli et al. (2022), the curves used for the simulations in this study were re-calculated and used for the purpose of the dynamic parametrization. These curves were obtained by computing the new parameters for the laws that describe the non-linear soil behaviour of the two cover units: “S” and “C”.

It has to be underlined that the dataset examined by Gaudiosi et al. (2023) demonstrates a lack of knowledge for the deepest layers: the depth of investigation of the dataset is limited to about 40 m corresponding to a mean confining effective pressure σ' > 180-200 kPa. To overcome this problem, a depth-dependent model from the soil behaviour established in Eastern North America (denoted as EPRI, 1993) was used to retrieve the G/G_0 and D values. The average G/G_0 and D curves of the EPRI model are available in the depth range of 0 - 305 m. In this study, the variability of the G/G_0 and D curves for "S" and "C" in the depth range 0 - 40 m, 40 - 150 m and 150 - 300 m was compared with the ones denoted as EPRI. As depicted in **FIGURE 3.1**, the G/G_0 and D curves for S and C and their relative range of ± sigma were observed to lie within the EPRI curve, while considering a depth interval ranging from 15 to 150 meters for "C" and from 0 to 86 meters for "S". Beyond this range, EPRI curves for 500-1000 feet (152 – 305 m) were adopted in this study.

For "G", the results obtained from Rollins et al. (1998) (average interval) were adopted, for the depth interval ranging from 0 to 150 meters, and Rollins et al. (2020), for the depth interval ranging from 150 to 300 meters. Darendeli, (2001) was used for describing the variability in this case. The use of a source of literature is due to the characteristics of the archive used for the parametrization for "S" and "C": specimens for coarse soils contain finer levels, which may induce misinterpretations of the non-linear soil behaviour for gravels. Thus, in the latter case, the chosen G/G_0 and D curves are those provided by the correlation given for a uniformity coefficient (Cu) of 10, and a confining pressure value of 600 kPa.

As shown in **FIGURE 3.1e** and **3.1f**, the G/G_0 and D curves for "G" becomes more linear (shifted to the right) as the depth (and thus the confining pressure) increased. For a given confining pressure, the G/G_0 curve for gravel results offset slightly to the left of the corresponding curve for "S" defined in this study. For similar conditions, the D curves for G do not show the same shifting than those for "S": the trend is inverted. This likely reflects the potential variations in the soil behaviour, which may be due to higher fines contents or soil plasticity captured by the seismic microzonation dataset (blue curve in **FIGURE 3.1f** extracted by the archive published in Gaudiosi et al. (2023). The initial archive also exhibits a deficiency in laboratory analyses conducted on geological bedrock units with the fewest available samples. In this study, a fixed averaged damping value was employed for range of depth [0 - 20 m); [20 - 100m); [100 m - ∞), which was determined using a commonly used heuristic formula: D_0 (%) = [10/(2*Vs)]*100 (Parolai et al. 2022). Darendeli (2001) was used for describing the variability in these cases. Specifically, all the G/G_0 and D curves presented in **TABLE 3.2** were used.
The article published by Pieruccini et al. (2024) describes more in detail in the Appendix the framework in which these parameters were defined, while the excel files used in input in NC92Soil is available in Gaudiosi, 2024.

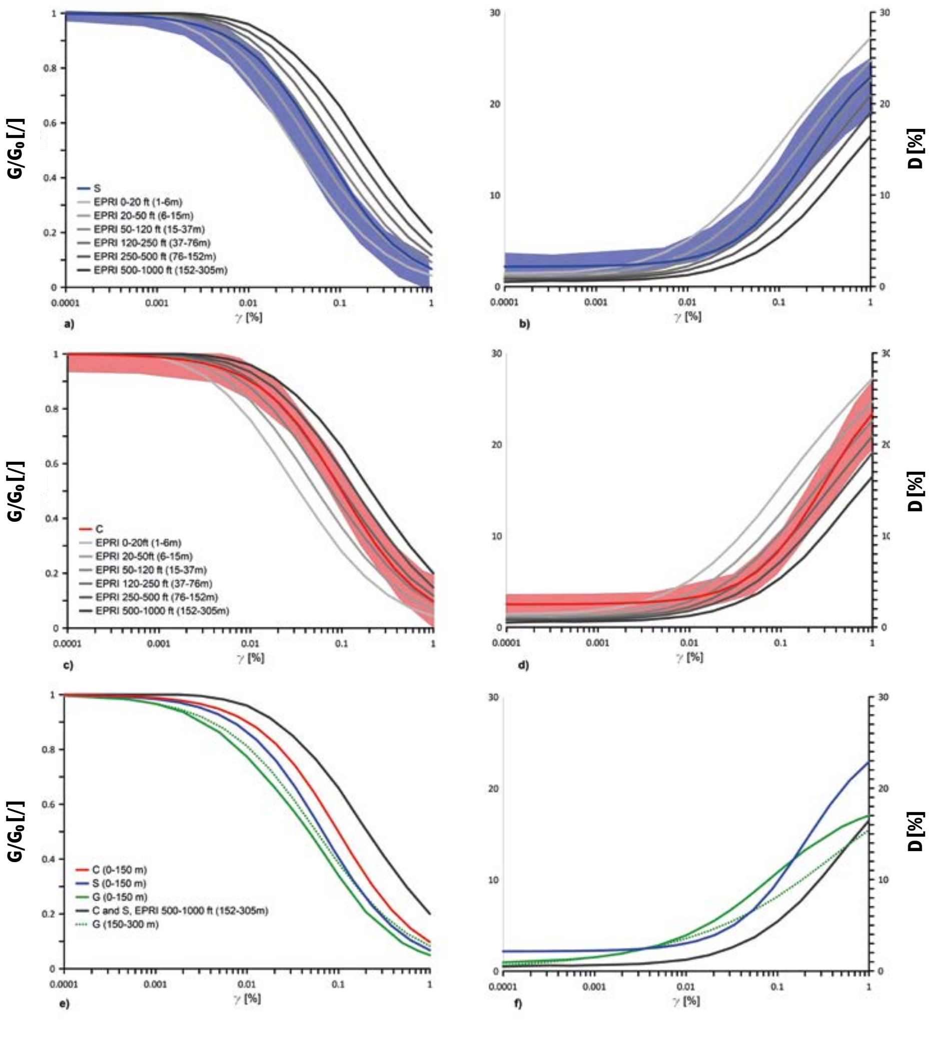

FIGURE 3.1
G_0 and D curves used in this study. a) and b), c) and b) subplots refer to sands "S" and clays "C" compared with EPRI curves, respectively. e) and f) subplots refer to the sands, clays and gravels non-linear behaviours used in this study and analysed with respect to the confining pressure values increasing. From Pieruccini et al. (2024).

Lithotype	Unit weight (kN/m³)	Vs (H)	σlogVs	G/G₀ and D curves	Standard deviations of G/G₀ and D curves	Inter-layer correlation	Depth range
C	19.4	189*H^0.187	0.441	1	0.09764*exp(-0.4429*G) - 0.07291 *exp(-75.58*G); 2.416*exp(0.02*D) -1.819*exp(-0.1347*D)	1 - 0.131*exp(-0.069*H+0.277)	0-28m
					0.09764*exp(-0.4429*G) - 0.07291*exp(-75.58*G); 2.416*exp(0.02*D) -1.819*exp(-0.1347*D)	0.976	28-150m
				2	Darendeli, 2001		150-300m
S	19.3	190*H^0.267	0.436	3	-1.17*exp(2.247*G) + 1.23*exp(2.199*G); 2.361*exp(0.0209*D) -1.788*exp(-0.1425*D)	1 - 0.131*exp(-0.069*H+0.277)	0-28m
					-1.17*exp(2.247*G) + 1.23*exp(2.199*G); 2.361*exp(0.0209*D) -1.788*exp(-0.1425*D);	0.976	28-150m
				2	Darendeli, 2001		150-300m
G	19.8	217*H^0.301	0.433	4	Darendeli, 2001	1 - 0.131*exp(-0.069*H+0.277)	
					Darendeli, 2001	0.976	0-28m
				5	Darendeli, 2001	0.976	28-150 m
							150-300 m
L	20.5	257*H^0.398	0.477	D_0=cost (1 %)	Darendeli, 2001	1 - 0.211*exp(-0.130*H+0.311)	0-20m
				D_0=cost (0.5 %)	Darendeli, 2001	0.98	20-100m
				D_0=cost (0.3 %)	Darendeli, 2001	0.98	100–300m
V	21.1	183*H^0.407	0.411	D_0=cost (1 %)		1 - 0.211*exp(-0.130*H+0.311)	0-20 m
				D_0=cost (0.5%)	Darendeli, 2001	0.98	20-100m
				D_0=cost (0.3 %)		0.98	100-300m
W	21.0	170*H^0.358	0.410	D_0=cost (1 %)	Darendeli, 2001	1 - 0.211*exp(-0.130*H+0.311)	0-20m
				D_0=cost (0.5%)	Darendeli, 2001	0.98	20-100m
				D_0=cost (0.3 %)	Darendeli, 2001	0.98	100-300m

TABLE 3.2
Parameters used in this task to describe the mechanical and dynamic behaviour of the relevant lithotype variability as a function of depth H (in m). For each lithotype the following information is reported: unit weight (and relative reference), median Vs as function of depth, standard deviation of the Vs values in natural logarithms, reference relative to G/G_0 and damping curves (1-3: this study, modified after Gaudiosi et al. (2023); 2: EPRI 93 (500-1000ft); 4: Rollins et al. (1998); 5: Rollins et al. 2020), G/G_0 and damping curves; inter-layer correlation between Vs values in subsequent layers (see, range of depths for the considered parametrization. Unit weights were computed from Gaudiosi et al. (2023).

3.3 Numerical simulations

Different modalities have been adopted to compute AF values depending on the amount of data available on purpose. In all cases, the numerical procedure requires the following steps (FIGURE 3.2):

Step 1: seismic input definition.
Step 2: definition of the soil behaviour.
Step 3: definition of the SHMs/GMSUs to be simulated, both in terms of seismo-stratigraphies and polygons.
Step 4: numerical modelling.
Step 5: attribution of AF to one or more SHMs based on the properly level of reference hazard.

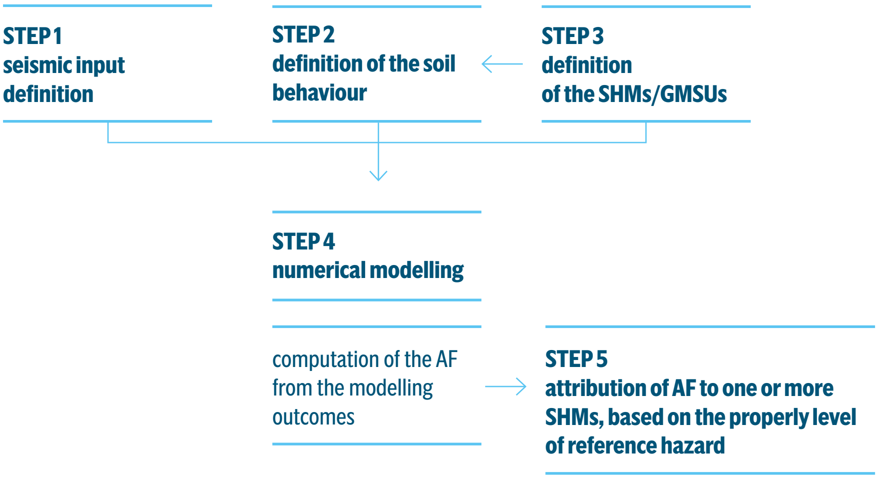

FIGURE 3.2
Overall workflow of the procedures adopted in the PRIN SERENA Project.

Due to the different amount of information available, different modalities have been considered for numerical simulations. The areas where these have been applied are shown in FIGURE 3.3.

In the following, some representative examples are presented relative to each procedure.

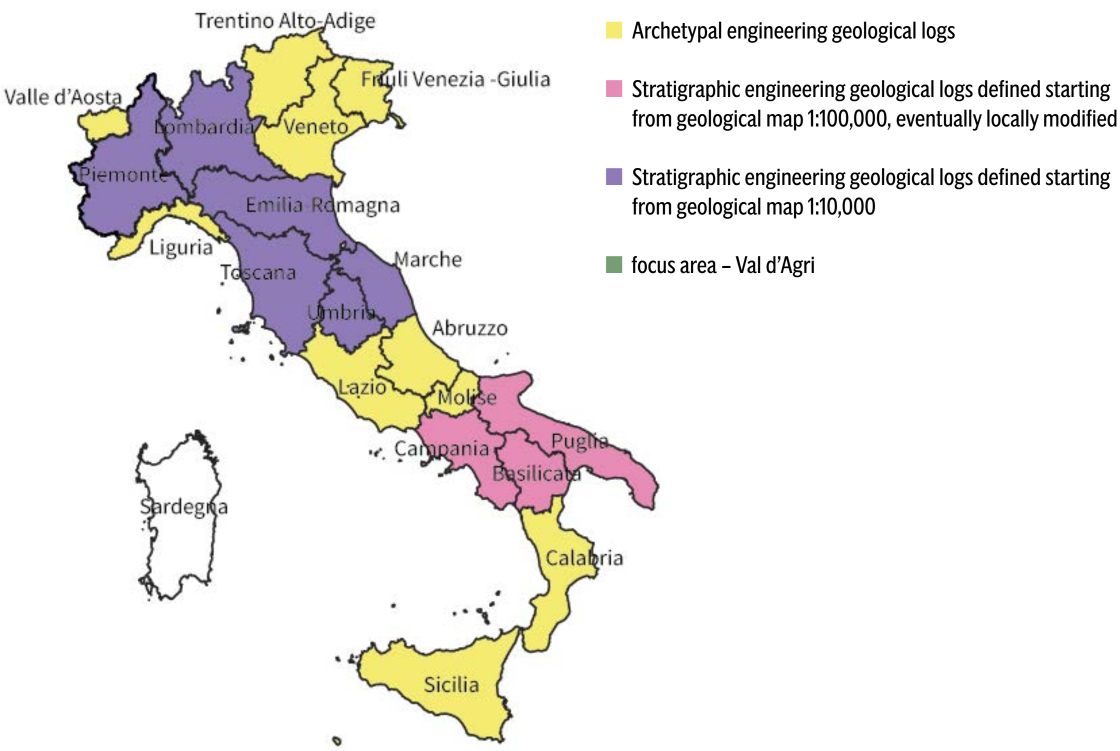

FIGURE 3.3
Overview of the different procedures considered to estimate 1D amplification factors.

3.3.1 Using archetypal engineering geological logs

In these simulations, the Vs profile relative to each EGU have been inferred the statistical parameterization provided by Romagnoli et al. (2022). To this purpose, each EGU was characterized by considering the second/third order classification of FIGURE 3.4.

FIGURE 3.4
EGUs classification schema considered in the stochastic modelling with archetypal engineering geological logs.

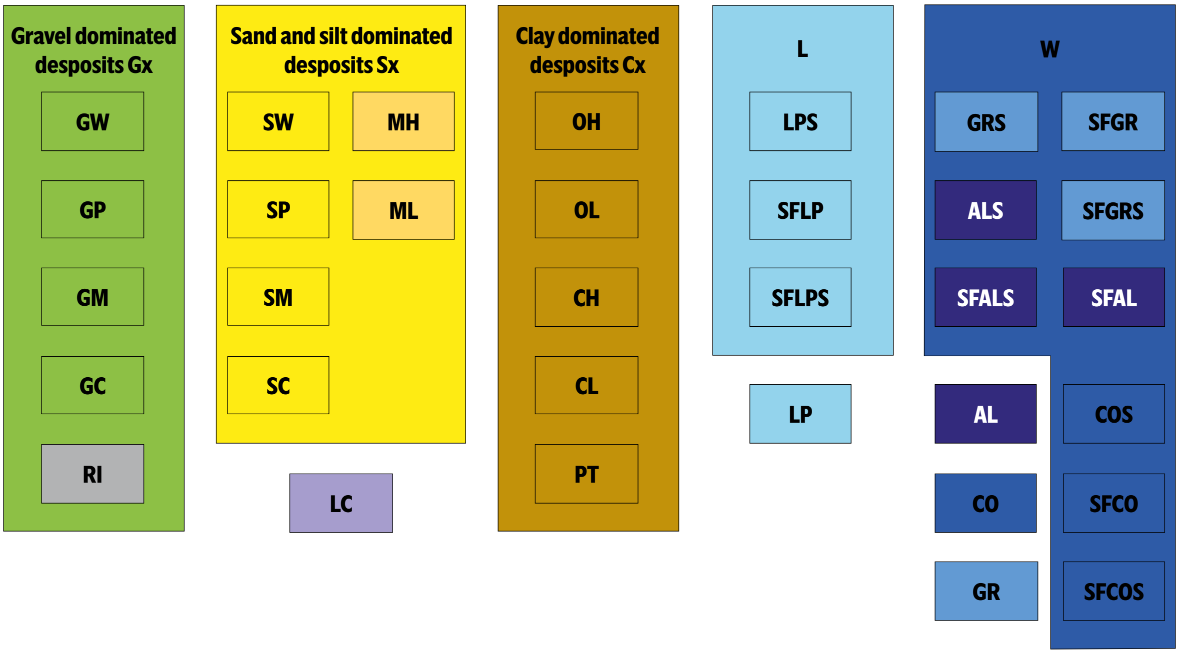

In this case, the acronyms G, S, and C used in **TABLE 3.1** and **FIGURE 2.1** have been replaced by Gx, Sx, and Cx, respectively. This notation is introduced solely to indicate that all curves and parameters used for bedrock units in the simulations were recalculated after separating the LC EGU from L and after treating LP, AL, CO, and GR as distinct classes.

A set of 53 seismic inputs (Response spectra) selected from national hazard modeling were chosen as seismic inputs by considering the different hazard levels over the whole Italian area. Since a random vibration theory (RVT) approach to the equivalent linear response analyses was used, the response spectrum compatible with the reference hazard was propagated as seismic input.

The definition of these seismic inputs was based on a procedure that evaluated the variability of the uniform-hazard spectra within the seismogenic sources, by computing the mean squared deviations between the spectral accelerations of the selected response spectrum and those of the reference spectrum over a given period range, according to the following equation:

Eq. 3.2) $$D_{rms} = \frac{1}{N}\sqrt{\sum_{i=1}^{N}\left(\frac{SA_0(T_i)}{PGA_0} - \frac{SA_s(T_i)}{PGA_s}\right)^2}$$

N is the total number of period values considered; $SA_0(Ti)$ and PGA_0 denote, respectively, the spectral acceleration at period Ti and at 0 s of the reference spectrum with Drms=0, 0.2, 0.4, and so on; whereas $SA_s(T_i)$ and PGA_s represent the spectral acceleration at period T_i and at 0 s of the spectrum being analysed.

For each seismogenetic sources, a number of spectra ranging from 1 to 5 was chosen for each region for a total number of 53 seismic input spectra.

FIGURE 3.5 shows the five selected reference motions used in these analyses among the MPS04 spectra available for Puglia region.

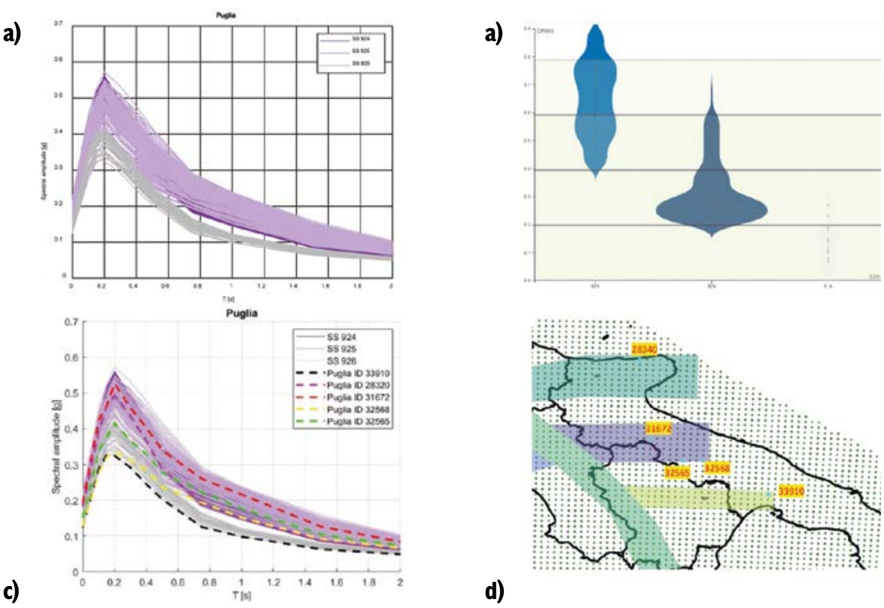

FIGURE 3.5
a) Seismic response spectra for all grid nodes within the Puglia region, as reported in the INGV MPS04 dataset and the Esse1 web-GIS.
b) Violin plots of the DRMS values, grouped according to the corresponding seismogenic sources.
c) Selected response spectra for the Puglia region.
d) Spatial distribution of the seismogenetic sources and the corresponding INGV MPS04 grid nodes from which the selected response spectra were selected.

For each archetypal log, 100 numerical simulations were performed by considering the possible variability of the Vs profile, shear modulus decay and damping curves.

For each of these columns, 100 stochastic realizations of the shear wave velocity parameters and non-linear properties were obtained. Each of the stochastic simulations was carried out with a different response spectrum, appropriately selected to respect the seismic hazard levels of the entire national territory.

For the definition of the resulting amplification factors (AF) to be used for the mapping, an experimental method was applied based on the study of the functional shapes of the individual trends of the amplification factors as a function of the geological-technical units outcropping and the thicknesses of the first outcropping layer.

The simulations carried out in this case were obtained accessing to the ICSC high-performance computing infrastructure of INFN under the PNRR HPC initiative, a multi-institutional effort involving 37 research entities and universities and 14 companies. ICSC is a distributed HPC facility funded by the Italian National Recovery and Resilience Plan, with investments supporting multiple strategic thematic spokes. The activities of this paragraph fall under Spoke 5, dedicated to disaster mitigation.

A Python wrapper was developed to orchestrate NC92-Soil runs in parallel, controlling the number of concurrent GUI instances according to available CPU cores, minimizing RAM footprint by isolating and closing processes after each run, and saving outputs into spectrum-specific folders.

As a whole, about 113 million of simulations were run varying layer thicknesses, stiffness, and decay/damping curves within their uncertainty ranges to capture parameter variability.

These simulations allowed us to visualize the influence of the soil thickness and engineering-geological properties on the Amplification Factors for each level of seismic hazard.

The main results obtained may be detailed and discussed with reference to different case studies. Results are showed here as an example from a seismic input motion with the ID 35893 (one of the seismic inputs of the Basilicata region, in Southern Italy) while a typical output may be downloaded in Gaudiosi et al. (2026).

FIGURE 3.6 plots the three AFs in the three ranges of period as a function of the soil thickness and of the engineering geological properties. Plots are retrieved from a seismic input motion with the ID 35893 (one of the seismic inputs chosen for Basilicata region and discussed in the following paragraph).

Amplification in the first range of periods: [0.1–0.5 s], decreases for units S and C as thickness increases, while unit G shows a plateau. Bedrock units show the opposite trend, except for CO, which displays an inverse behaviour.

Amplification in the intermediate and last range of periods: [0.4 – 0.8s] and [0.7-1.1 s], decreases for units S and C as thickness increases starting for a threshold value of thickness (respectively 30 m for the intermediate and 40-50 for the last range of periods). Bedrock units show plateau, although AL showed increasing values of AF as thickness increases.

FIGURE 3.7 reports for [0.1–0.5 s] all the AF available (not only the median like in FIGURE 3.6). From this graph it should be clear that, once the numerical modelling is carried out, the procedure may assign amplification factors (AFs) in the three period ranges based on two key pieces of information: the type of outcropping unit and the thickness of the first outcropping layer. AF may represent either the median or any percentile of the distribution

If other information on seismostratigraphies are available, these results may be used as lookup charts accessed through four input parameters: reference seismic hazard, the type of outcropping EGU, the type of EGU of the second layer, and the thickness of the second layer.

FIGURE 3.6
Median AFs in three ranges of periods of interest as a function of the geological-technical unit and of the thickness.

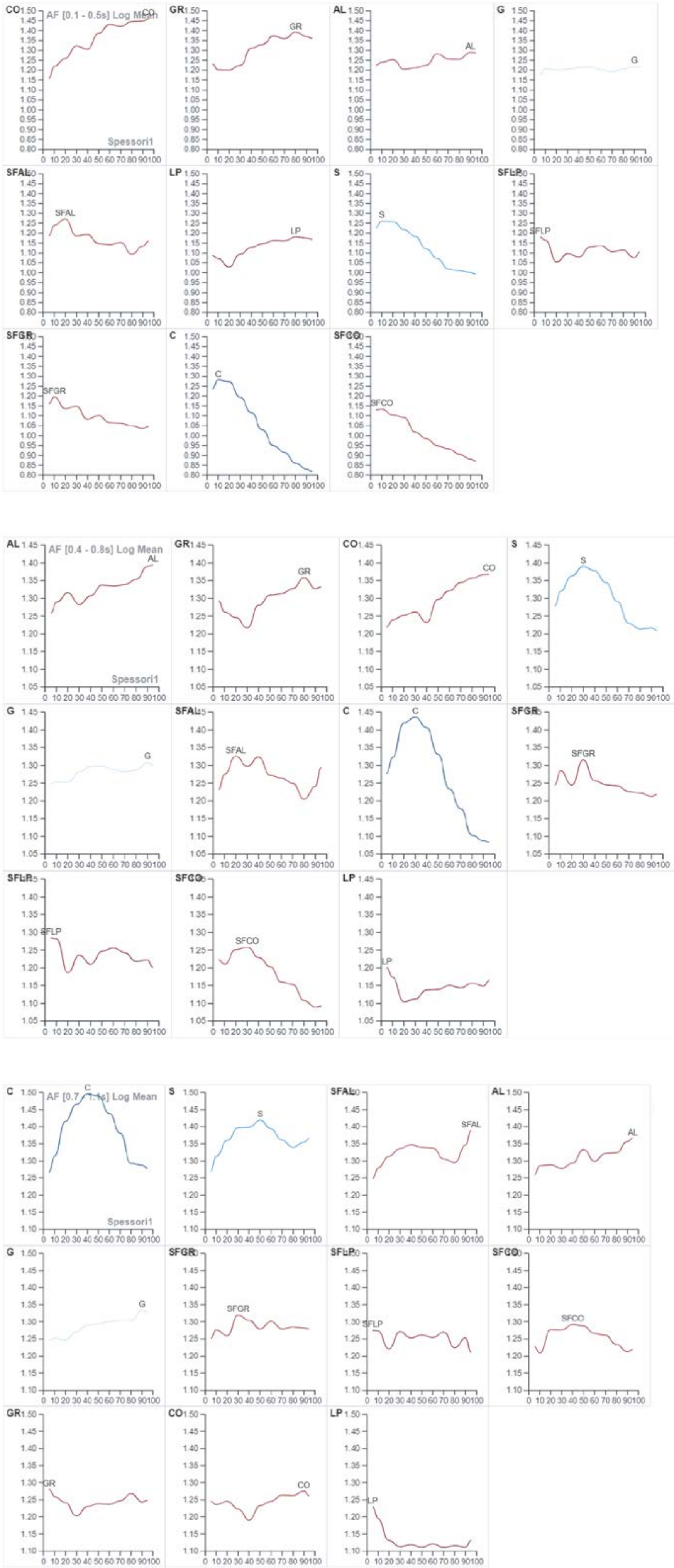

AF [0.1 - 0.5s]

AF [0.4 - 0.8s]

AF [0.7 - 1.1s]

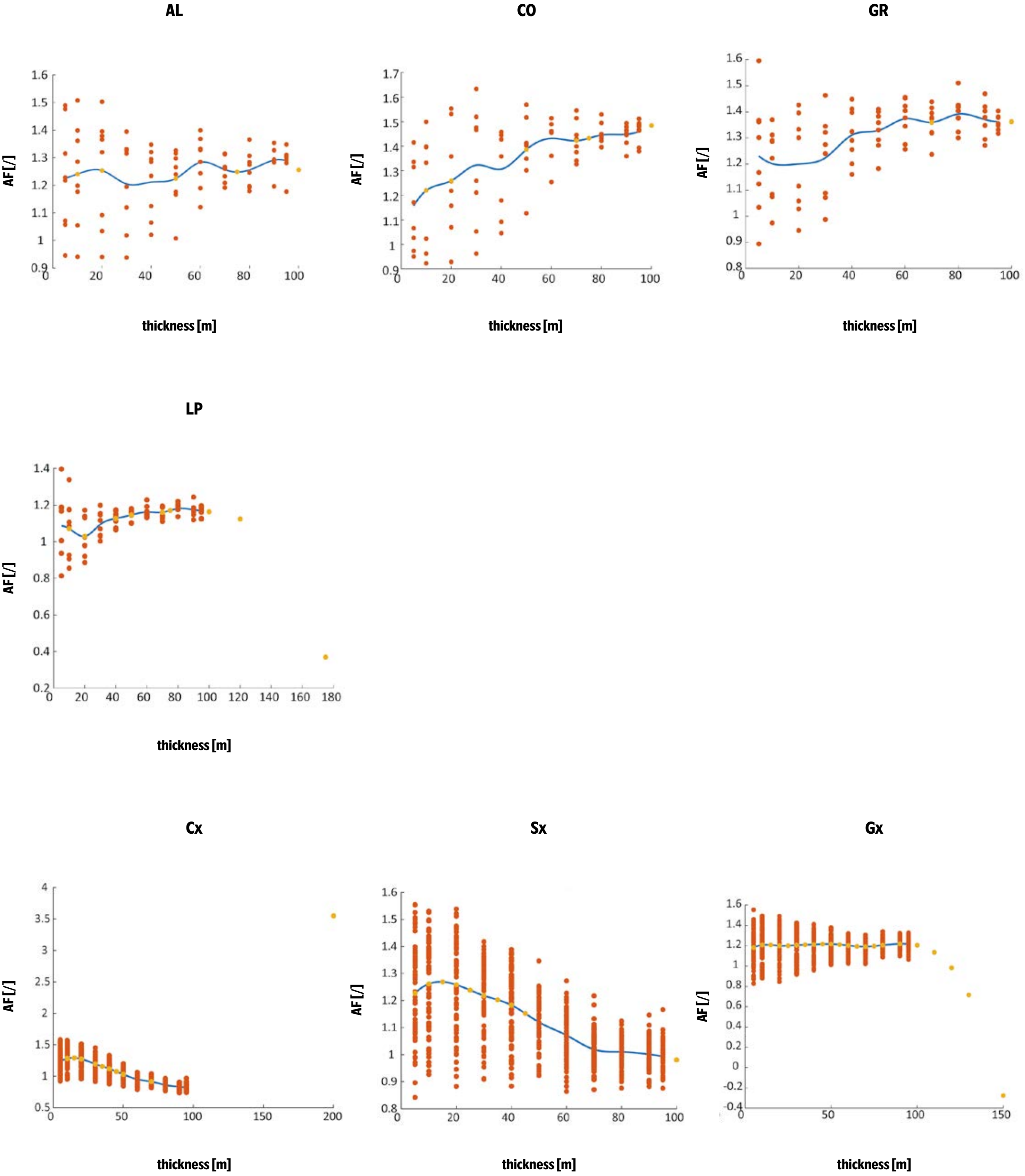

FIGURE 3.7
Values of AF1 as a function of the outcropping unit and thickness of the first layer.

3.3.2 Numerical simulations of engineering geological logs from the 1:100,000 map

The same numerical approach described above has been adopted for the logs inferred from the 1:100.1000 map. In this case, however, the third order classification has been considered for EGU in the study areas (Basilicata, Puglia and Campania).

As an example, the map of re-classified lithological map of Basilicata is reported (**FIGURE 3.8**). In general, to each EGU four classes of thickness ranges were considered: class 0 (0-10 m), class 1 (10-40 m), class 2 (40-70 m), and class 3 (70-100 m). A maximum depth 100m was considered for each engineering geological log.

In **TABLE 3.7** the engineering geological logs relative to the Basilicata region are listed.

<table>
<tr><th>Log ID</th><th>Units</th><th>Units</th><th>Thickness class</th><th>ID</th><th>Units</th><th>Units</th><th>Units</th><th>Thickness class</th><th>ID</th><th>Units</th><th>Units</th><th>Units</th><th>THI class</th></tr>
<tr><td>1</td><td>SX</td><td>CO</td><td>1|3</td><td>26</td><td>LC</td><td>CO</td><td></td><td>1|3</td><td>51</td><td>GX</td><td>LP</td><td></td><td>2|3</td></tr>
<tr><td>2</td><td>GX</td><td>CO</td><td>1|3</td><td>27</td><td>GX</td><td>AL</td><td>GR</td><td>1|1|3</td><td>52</td><td>GX</td><td>LP</td><td></td><td>0|3</td></tr>
<tr><td>3</td><td>W</td><td>CO</td><td>1|2</td><td>28</td><td>W</td><td>AL</td><td></td><td>1|3</td><td>53</td><td>GX</td><td>SX</td><td>LP</td><td>0|1|3</td></tr>
<tr><td>4</td><td>GX</td><td>GR</td><td>1|3</td><td>29</td><td>GX</td><td>LP</td><td></td><td>1|3</td><td>54</td><td>GX</td><td>SX</td><td>CO</td><td>0|1|3</td></tr>
<tr><td>5</td><td>GR</td><td></td><td>3</td><td>30</td><td>SX</td><td>CO</td><td></td><td>1|2</td><td>55</td><td>LC</td><td>LP</td><td></td><td>1|3</td></tr>
<tr><td>6</td><td>SX</td><td>GR</td><td>1|3</td><td>31</td><td>W</td><td>CO</td><td>GR</td><td>1|1|3</td><td>56</td><td>SX</td><td></td><td></td><td>1</td></tr>
<tr><td>7</td><td>SX</td><td>AL</td><td>1|3</td><td>32</td><td>SX</td><td>AL</td><td>GR</td><td>1|1|3</td><td>57</td><td>GX</td><td>SX</td><td></td><td>0|1</td></tr>
<tr><td>8</td><td>GX</td><td>AL</td><td>1|3</td><td>33</td><td>W</td><td>CO</td><td>AL</td><td>1|1|3</td><td>58</td><td>GX</td><td></td><td></td><td>1</td></tr>
<tr><td>9</td><td>W</td><td>AL</td><td>1|2</td><td>34</td><td>GX</td><td>CO</td><td></td><td>1|2</td><td>59</td><td>GX</td><td></td><td></td><td>2</td></tr>
<tr><td>10</td><td>AL</td><td></td><td>3</td><td>35</td><td>CX</td><td>LP</td><td></td><td>1|3</td><td>60</td><td>GX</td><td>CX</td><td>GR</td><td>0|1|3</td></tr>
<tr><td>11</td><td>W</td><td>GR</td><td>1|2</td><td>36</td><td>LC</td><td>LP</td><td></td><td>2|3</td><td>61</td><td>GX</td><td>GR</td><td></td><td>0|3</td></tr>
<tr><td>12</td><td>CX</td><td>CO</td><td>1|3</td><td>37</td><td>W</td><td>LP</td><td></td><td>1|3</td><td>62</td><td>SX</td><td>GX</td><td>CO</td><td>1|1|3</td></tr>
<tr><td>13</td><td>LC</td><td>GR</td><td>2|3</td><td>38</td><td>GX</td><td>AL</td><td>LP</td><td>1|1|3</td><td>63</td><td>GX</td><td>SX</td><td>AL</td><td>0|1|3</td></tr>
<tr><td>14</td><td>LC</td><td>AL</td><td>2|3</td><td>39</td><td>W</td><td>CO</td><td>LP</td><td>1|1|3</td><td>64</td><td>SX</td><td>GR</td><td></td><td>3|3</td></tr>
<tr><td>15</td><td>SX</td><td>GR</td><td>2|3</td><td>40</td><td>SX</td><td>LP</td><td></td><td>1|3</td><td>65</td><td>GX</td><td>SX</td><td>GR</td><td>0|1|3</td></tr>
<tr><td>16</td><td>SX</td><td>AL</td><td>2|3</td><td>41</td><td>W</td><td>CO</td><td></td><td>1|3</td><td>66</td><td>GX</td><td>AL</td><td></td><td>0|3</td></tr>
<tr><td>17</td><td>SX</td><td>CO</td><td>2|3</td><td>42</td><td>W</td><td>CO</td><td>AL</td><td>1|1|1</td><td>67</td><td>W</td><td>LP</td><td></td><td>1|2</td></tr>
<tr><td>18</td><td>LC</td><td>AL</td><td>1|3</td><td>43</td><td>GX</td><td>CO</td><td></td><td>3|3</td><td>68</td><td>GX</td><td>SX</td><td>LP</td><td>1|1|3</td></tr>
<tr><td>19</td><td>LC</td><td>GR</td><td>1|3</td><td>44</td><td>GX</td><td>LP</td><td></td><td>3|3</td><td>69</td><td>SX</td><td>LP</td><td></td><td>3|3</td></tr>
<tr><td>20</td><td>W</td><td>GR</td><td>1|3</td><td>45</td><td>GX</td><td>GR</td><td></td><td>3|3</td><td>70</td><td>GX</td><td>AL</td><td></td><td>3|3</td></tr>
<tr><td>21</td><td>LP</td><td></td><td>3</td><td>46</td><td>GX</td><td>CO</td><td></td><td>2|3</td><td>71</td><td>GX</td><td>SX</td><td>GR</td><td>1|1|3</td></tr>
<tr><td>22</td><td>GX</td><td>GR</td><td>2|3</td><td>47</td><td>GX</td><td>W</td><td>CO</td><td>0|1|2</td><td></td><td></td><td></td><td></td><td></td></tr>
<tr><td>23</td><td>GX</td><td>AL</td><td>2|3</td><td>48</td><td>GX</td><td>W</td><td>AL</td><td>0|1|2</td><td></td><td></td><td></td><td></td><td></td></tr>
<tr><td>24</td><td>CX</td><td>AL</td><td>1|3</td><td>49</td><td>GX</td><td>W</td><td>GR</td><td>0|1|2</td><td></td><td></td><td></td><td></td><td></td></tr>
<tr><td>25</td><td>CX</td><td>GR</td><td>1|3</td><td>50</td><td>GX</td><td>CX</td><td>AL</td><td>0|1|3</td><td></td><td></td><td></td><td></td><td></td></tr>
</table>

TABLE 3.7 Overview of the distinct Engineering Geological logs relative to the Basilicata area; THI class (Thickness Class). Categorical variable indicating subsurface thickness: 0 = 10 m; 1 = 10–40 m; 2 = 40–70 m; 3 = 70–100 m.

This approach, preferring ranges over exact values, was adopted to account for the greater uncertainty inherent the extensive estimates. Representing thickness as a range allows for a more flexible interpretation of possible stratigraphic columns and, additionally, reduces the number of combinations of unique logs that would otherwise result from the use of precise thickness values. Differently from the other applications, a hybrid classification of EGUs was adopted. In particular, four classes were considered for cover units (CX, GX, SX, LC), three relative to the unaltered geological bedrock (AL, GR, LP) and four for altered/fractured one (SFAL, SFCO, SFGR, SFLP). Additionally, weathered substrate units received a dedicated treatment during columns construction: any altered/fractured substrate unit (i.e., SFAL, SFCO, SFGR, or SFLP) was split into two components: a weathered (W) portion and an underlying unaltered substrate, corresponding respectively to AL, CO, GR, or LP. The W component was assigned a fixed thickness class (class 1: 10-40 m), while the thickness class of the unaltered portion was derived by subtracting the W thickness from the total thickness originally assigned to the altered/fractured unit. Moreover, the thickness partition was implemented as a dynamic process. Specifically, if altered/fractured units appeared during the construction of stratigraphic columns in non-outcropping (i.e., subsurface) positions and the cumulative thickness of the column under construction exceeds a determined threshold, the W (weathered) component is reduced accordingly, resulting in a thicker preserved substrate layer. The purpose of this rule is to prevent the unrealistic occurrence of highly weathered material at depth, thereby producing geologically more plausible stratigraphies.

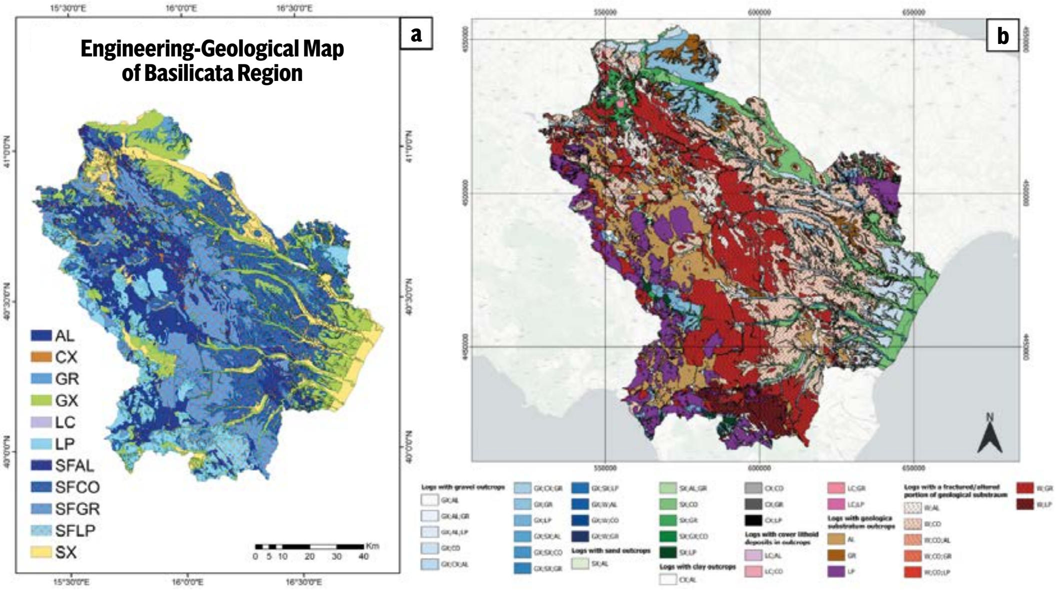

FIGURE 3.8
(a) Engineering-geological map of Basilicata region used as input in the automatic procedure for the identification of SHMs. (b) Output of the automatic procedure, displaying the identified stratigraphic columns spatialized into SHMs.

Outcomes relative to numerical simulations relative to the Basilicata region are reported in **FIGURE 3.9**. They are retrieved by considering as input motion one response spectrum defined with the same procedure indicated in 3.3.1.

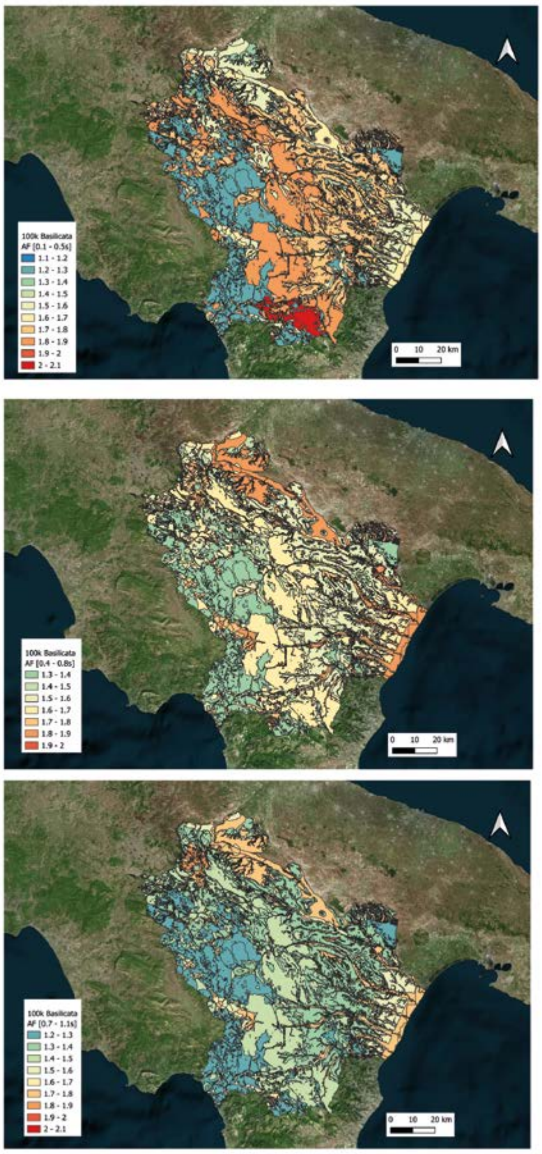

FIGURE 3.9
Median AF values obtained for the Basilicata region.

The same approach has been also applied to a relatively small area (Val D'Agri) where more detailed information was available relative to the local engineering geological logs and the S-wave velocity ranges can be narrowed to account for geophysical measurements extracted from the available seismic microzonation studies.

In this case, the analysis was carried out using the spectrum with the minimum spectral acceleration values for the Val d'Agri area. FIGURE 3.10 summarizes the rationale underlying the selection of the input motion. In this case, the response spectrum with the minimum values of spectral acceleration was chosen (ID 34778).

FIGURE 3.10 Research of the response spectrum with minimum Spectral Acceleration values for the Val d'Agri area (grey area). In Figure also the main seismo-genetic sources are reported.

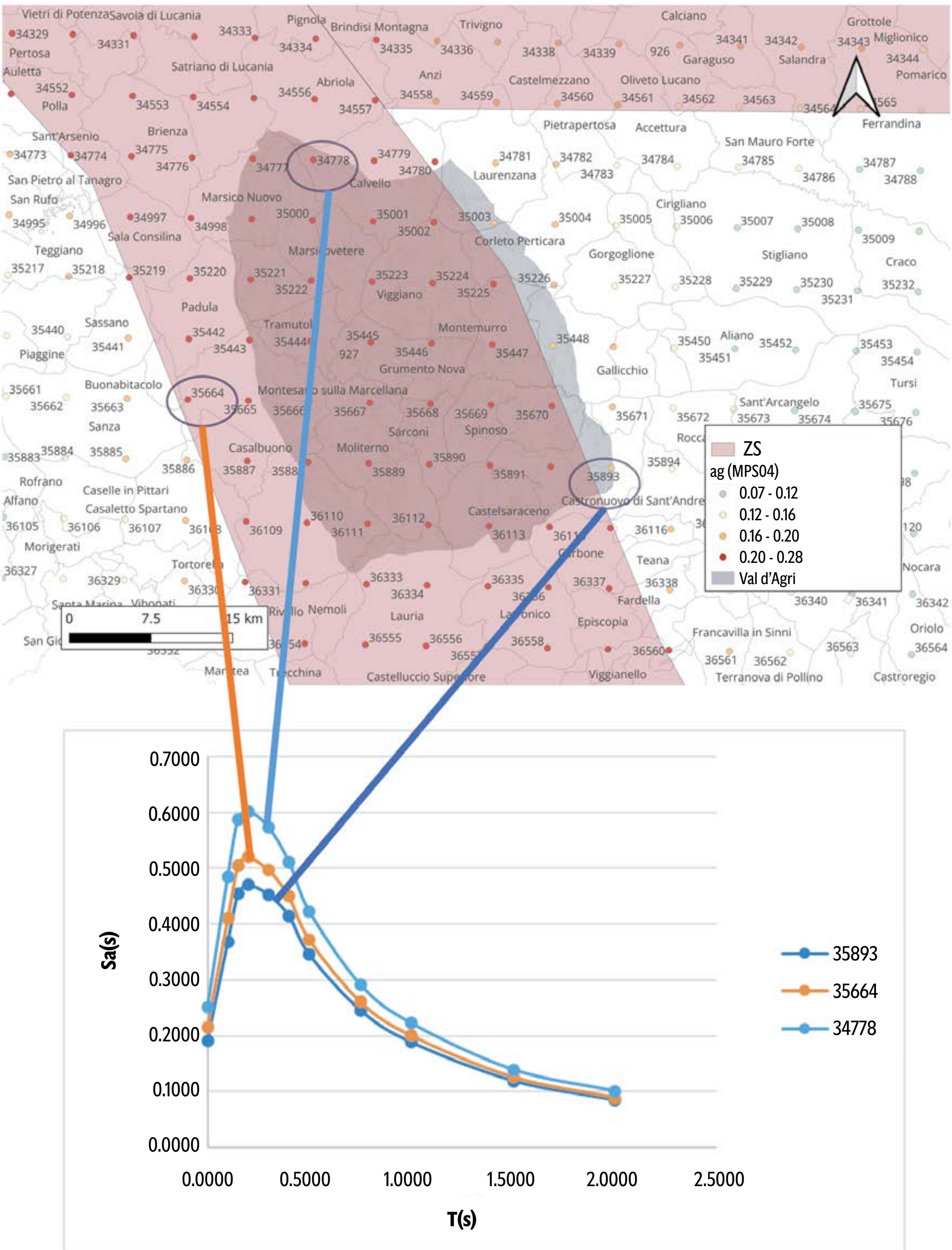

Results are plotted in FIGURE 3.11. They showed AF values with an increasing trend in the short period range. Conversely, a reduced variability was retrieved when higher periods are mapped.

Parts of the Val d'Agri territory showed significant amplifications over all ranges of periods (FIGURE 3.11) as expected due to the softness of the soils which fill the basin. Simulations also confirmed two different behaviours of the geological substratum.

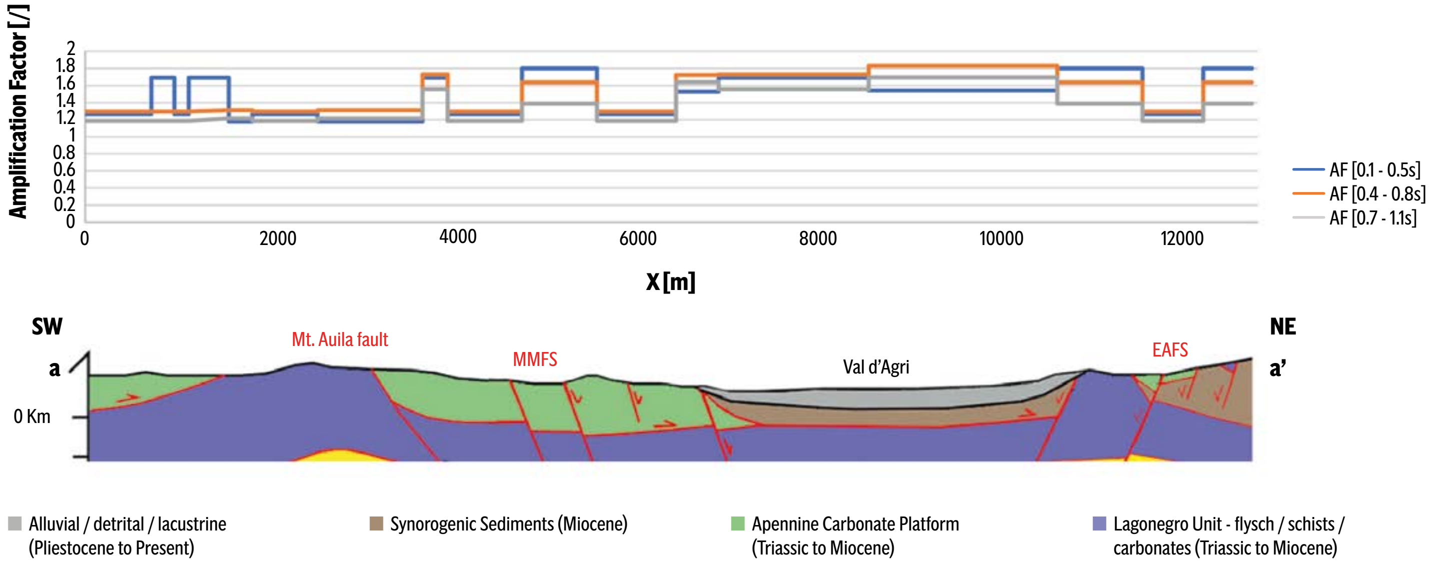

FIGURE 3.11
AFs along a cross-section crossing the Val d'Agri area.

3.3.3 Numerical simulations of engineering geological logs from the 1:10,000 maps

Hundreds random stratigraphical sequences constrained by the available information described in paragraph 2.5.3 have been considered.

Given the large number of stratigraphic profiles reconstructed for each Italian region as well as the corresponding number of 1D simulations required to estimate the seismic amplification factors of interest, simulating each individual stratigraphic model was computationally unsustainable. To reduce the computational cost relative to each region, a k-means clustering procedure was applied to the response spectra derived from the Italian Seismic Hazard Map, with the number of clusters defined as the number of seismic hazard bands observed within each region.

For recurrent profiles (frequency greater than 50 occurrences within the region), the 1D seismic response was evaluated only using as input motion the representative spectra associated with cluster centroids. The obtained results (e.g., in terms of seismic amplification factors) were then assigned to the original profiles based on their corresponding hazard cluster. This strategy allowed a significant reduction in the number of simulations while maintaining a consistent representation of spatial variability of the results.

Variability range of Vs values and non-linear soil properties used in this case study have been discussed in paragraph 3.2.

The median AF value obtained relative to each outcrop for the period range 0.1-0.5s (the most important for most common buildings) is mapped in **FIGURE 3.12** along with the respective standard deviation (in natural logarithm).

In **FIGURE 3.13**, the distribution of the median AFs relative to the considered GMSUs is presented in the form of a box-plot diagram. The three boxes for each GMSU represent the distributions of values obtained relative to the three ranges of periods considered (0.1-0.5s, 0.4-0.8s, 0.7-1.1s respectively). The plot in **FIGURE 3.12**, puts in evidence that significantly different AF values have been obtained for the considered GMSUs. This outcome is far from being obvious, due to the large variability ranges attributed to the GMSUs relative to each outcrop. This outcome is of primary importance, since demonstrates that the geological data provided by the detailed geological maps at regional scale may be very informative about the expected seismic response at the considered sites in the lack of more detailed investigations. However, important trends can be observed in the distribution of AFs values for the different GMSUs. The CTs show notable differences between GMSU 11 (the thicker alluvial deposits of the major floodplains), GMSU 12 (the shallower alluvial and slope deposits), and GMSU 20 (the Quaternary volcanics).

Amplification effects reduce with increasing the vibration period considered, except in the case of the GMSU 11 (**FIGURE 3.12a**), which is representative of the thick cover terrains of the major alluvial plains. In this case, as expected, de-amplification effects are revealed at smaller vibration periods, with a median AF value below 1. Actually, the de-amplification effects in the short period range when thick sedimentary basins exist have been experimentally documented in the case of the Kik-Net network (Paolucci et al. 2021).

The higher AF values of GMSU 12 (**FIGURE 3.12b**) and their distribution suggest the importance of the thickness of CTs scattered along the slopes and minor floodplains of the landscape. GMSU 20 (**FIGURE 3.12c**) presents lower AF values perhaps in relation to the presence of thick massive lava flows, typical of the

Monte Amiata area. A similar notable range of AF values can be observed for Mio-Pliocene continental and marine deposits of tectonic basins, consisting mostly of thick clayey, sandy, and conglomeratic facies (FIGURE 3.12d). Only GMSU 45 (FIGURE 3.12e) shows higher amplification factors, although these are shallow Miocene lacustrine clay deposits occurring in only 21 km2. Other important trends can be observed for GMSU 50 and 60 (FIGURE 3.12f) whose AF values are higher than GMSU 70 and 80 (FIGURE 3.12g) probably due to greater lithological heterogeneity.

More surprising could be considered the large amplifications where the geological bedrock outcrops. However, one must consider Vs data relative to these formations Romagnoli et al. (2022) indicate the general presence of weathering and alteration processes where these relatively old formations outcrop. This is responsible for a rapid increase of rigidity in the shallowest part of the velocity profile, which generates sharp shallow seismic impedance contrasts responsible for energy trapping and resonance of upgoing seismic waves and, ultimately, of amplification effects. This suggests that the assumption of a potential correspondence between engineering and geological bedrock (e.g., Falcone et al. 2021) is generally unreliable.

A major factor responsible for variations in the estimated AF is the estimated depth of the engineering bedrock. Most of GMSUs exhibit a weak linear correlation between amplification factors and depths of the engineering bedrock. This correlation tends to be negative when accounting for deep sedimentary covers (GMSU 11), owing to the greater variability in engineering bedrock depth (30-150m). This trend is also evident in other GMSUs, although less pronounced due to a narrower range of the relative depths of the engineering bedrock. Specifically, units characterized by shallow sedimentary covers or composed only of geological bedrock typically exhibit an engineering bedrock confined to depths ranging from 20 to 50 meters. In some cases, AF within this depth range also demonstrate a positive linear correlation. As expected, within each GMSU a significant correlation is also found between median AFs and the harmonic average of the Vs values above the engineering bedrock. This relation, which is found to be almost always slightly negative, has been recognized in all the range of periods and for all the GMSUs analyzed. The only unit that deviates from this trend is unit GMSU 11, where a distinct positive correlation between AF and the harmonic average of Vs values to the engineering bedrock is observed.

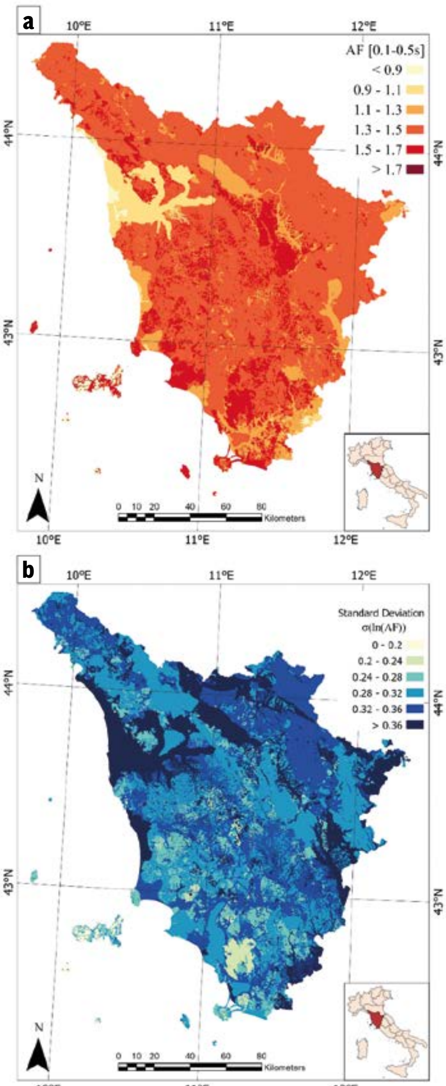

FIGURE 3.12
Outcome of the numerical simulations for each outcrop considered, relative to the period range 0.1-0,5s. a) Median AF values; b) standard deviation of AF values in natural logarithms.

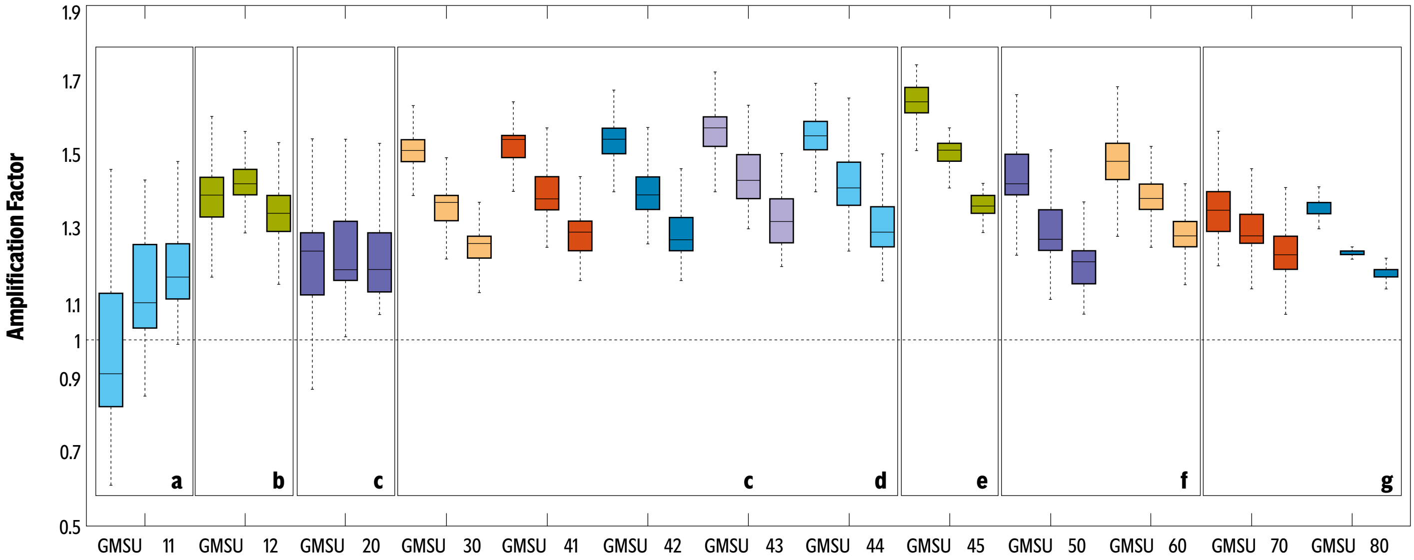

FIGURE 3.13
The distribution of median amplification factors for approximately 80,000 outcrops analysed in the Tuscany region is depicted. Different colours discretize the various GMSUs. The three coloured boxes for each GMSU represent the distributions of amplification factors across three range of period [0.1-0.5s], [0.4-0.8s], [0.7-1.1s]. Boxes labelled from (a) to (g) highlight differences in the median amplification factors relative to the considered GMSUs. Modified after Pieruccini et al. (2024).

3.4 From AF map to PGA map

A pilot study has been also performed to evaluate the impact on the seismic hazard evaluations of the 1D site amplification estimates discussed above. A key aspect concerns the implementation of these outcomes including relevant uncertainty into probabilistic seismic hazard estimates relative to standard subsoil conditions. A new approach has been developed on purpose, which coherently accounts for the inherent probabilistic character of reference hazard estimates and of uncertain amplification effects inferred from geological maps at regional scale (Albarello et al. 2025).

An estimate of seismic ground motion S_s at any *s-th* site is defined as a combination of ground motion at the reference subsoil conditions S_r and a seismostratigraphical amplification factor (A_s) such that S_s. In PSH, S_r is a random variable characterized by a probability distribution representative of information (and lack of information) about the seismogenic process and long-range propagation of seismic energy from the seismic sources. Due to uncertainty affecting the local seismic response, A_s can be also considered a random variable with a probability distribution representative of uncertainty affecting relevant parameters (the velocity profile of seismic waves, depth of the seismic bedrock, etc.). By considering the natural logarithms, by the definition of average μ and variance σ^2 of a sum of random variables, InS_s will be characterized by an expectation given by

Eq. 3.3) $$\mu(lnS_s) = \mu(lnA_s) + \mu(lnS_r)$$

and variance

Eq. 3.4) $$\sigma^2(lnS_s) = \sigma^2(lnA_s) + \sigma^2(lnS_r) + 2cov(lnA_s, lnS_r)$$

where *cov* represents the covariance of the considered random variable.

In case both the random variables A_s and S_r are characterized by a log-normal probability distribution, S_s will also be a log-normal variable fully parameterized in terms of $\mu(InS_s)$ and $\mu(InS_s)$. In particular, the $S_s\,(\alpha)$ value characterized by the exceedance probability α can be computed as:

Eq. 3.5) $$InS_s(\alpha) = \mu(lnA_s) + \mu(lnS_r) + k\sqrt{\sigma^2(lnA_s) + \sigma^2(lnS_r) + 2cov(lnA_s, lnS_r)}$$

where k and where $\mathbb{N}^{-1}(\alpha)$ is the standardized normal probability distribution (e.g., k=1.28 when α=0.1).

The assumption that S_r is a log-normal variable is widely accepted and experimentally supported (e.g., Li and Assimaki 2010; Aimar et al. 2020; Paolucci et al. 2021). The hypothesis that A_s is also log-normal has been tested in Albarello and Paolucci (2024) for a site in central Italy and has been replicated by considering PSH estimates relative to PGA for the whole Italian territory and made available by Meletti and Montaldo (2007).

Under the hypothesis that these quantiles correspond to a log-normal probability distribution, the expectation $\mu(lnS_r)$ corresponds to $S_r(\alpha)$ with $\alpha = 0.5$ (50% exceedance probability in 50 years). The standard deviation can be computed as:

Eq. 3.6) $$\sigma(lnS_r) = 1.28[lnS_r(\alpha_1) - lnS_r(\alpha_0)]$$

where $\alpha_0 = 0.5$ and $\alpha_1 = 0.1$. These values have been computed for PSH estimates at 16853 grid points covering the whole Italian territory. Based on these values, the full set of percentiles has been computed in the hypothesis that the hazard curve is the expression of the log normal variate, with parameters $\mu(lnS_r)$ and $\sigma(lnS_r)$. It can be shown (see Albarello et al. 2025) that the covariance term is negligible (possibly due to the level of expected ground shaking in the considered areas. Based on the results obtained in Northern-Central Italy the hazard level relative to and exceedance probability of 10% in 50 years in terms of PGA values has been computed for the Regions of Tuscany, Umbria, Marche, Emilia-Romagna, Piemonte and Lombardia (FIGURE 3.14).

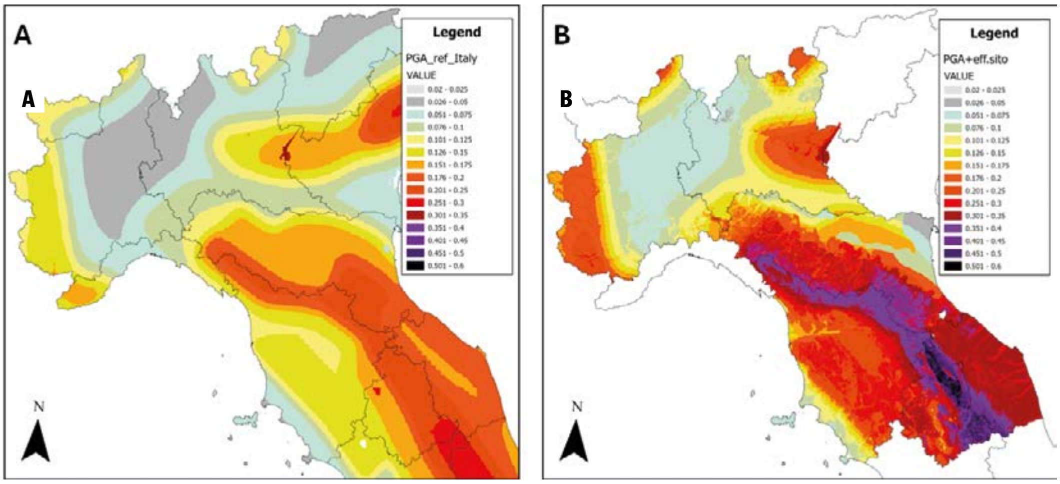

FIGURE 3.14
Figure 3.14 Impact of amplification effects estimated at regional scale on the seismic hazard values relative to an exceedance probability of 10% in 50y in PGA (fraction of g). A: hazard map relative to reference soil conditions; B: hazard map including 1D amplification affects.

4. Testing large scale estimates of 1D stratigraphic amplification effects

4.1 Empirical testing of Amplification factor (AF)

4.1.1 Data collection, standardization and spatialization
4.1.2 Site-to-site residual (δS2S)
4.1.3 Generalized Inversion Technique (GIT)
4.1.4 Standard Spectral Ratio (SSR)
4.1.5 Comparison among empirical estimates
4.1.6 Effectiveness of 1D hypotheses in δS2S data
4.1.7 Spatialization of AF and correlations between site indicators
4.1.8 Comparison between empirical and numerical estimates

4.2 Comparison between geognostic-data-derived estimates and modelling-based estimates: the Brescia test site

4. Testing large scale estimates of 1D stratigraphic amplification effects

4.1 Empirical testing of Amplification factor (AF)

Methods such as the Standard Spectral Ratio (SSR; Borcherdt, 1970), the Generalized Inversion Technique (GIT; Andrews, 1986; Castro et al. 1990), and site-to-site residual analyses (δS2S; e.g., Rodriguez-Marek et al. 2011; Luzi et al. 2014; Lanzano et al. 2025) are commonly used to calculate experimental amplification estimates.

These estimates have highlighted significant variability in site response, particularly in tectonically complex regions such as Italy. Several case studies (e.g., Gallipoli et al. 2011; Strollo et al. 2012; Laurenzano et al. 2019; Panzera et al. 2021; Priolo et al. 2020) document that amplification factors are strongly influenced by the depth, and bedrock seismic velocity, as well as by basin geometry, and buried/outcropped morphology. At the European scale, studies based on GIT (e.g., Bindi et al. 2023) further confirm the substantial variability of empirical site amplification when close estimates are compared.

As part of the PRIN SERENA project, empirical verification and calibration of the numerical ground-motion amplification maps were also undertaken. This involved the use of in-depth geological, geophysical, and seismological information. The main objectives of this study can be summarized as follows: (1) evaluation of the reliability of Amplification Factors (AF; see Section 3.1 for definition) derived from numerical modeling, through comparison with empirical estimates; (2) study of correlations between site indicators and the areal extrapolation of amplification values deduced at sites where data from seismic stations are available.

For this purpose, a database of experimental site-specific amplification estimates, previously computed or generated with new analyses, was created and stored in a GIS architecture, together with the numerical estimates from 1D simulations. The database includes more than 1900 sites both at national scale (permanent and temporary seismic networks) and for selected areas (Central Italy, North-East Italy, Basilicata region, Ferrara). We compared experimental estimates from different techniques to assess their consistency and their congruence with estimates generated by regional or national 1D simulation-based amplification models.

Moreover, to bridge the gap between point-based station data and areal coverage, we investigated the statistical correlation between different site proxies at national level.

Regarding the second aim of these activities, different strategies to compute the spatial extrapolation of amplification between instrumented sites were also explored through the use of reliable and robust proxies. Traditional interpolation techniques, such as Ordinary Kriging, rely solely on spatial proximity and may not adequately capture geological similarity. Therefore, alternative approaches were considered, including clustering techniques applied to Horizontal-to-Vertical Spectral Ratio (HVSR) curves and weak-motion amplification curves, as well as principal component analysis. These methods allow to identify sites characterized by similar dynamic behavior and to improve areal generalization.

4.1.1 Data collection, standardization and spatialization

Within the framework of the PRIN-SERENA project, a comprehensive database of experimental site-specific amplification estimates, obtained using different empirical methods, was compiled to assess both their mutual consistency and their agreement with empirical estimates from a regional or national 1D simulation-based amplification model. A more comprehensive description of these analyses can be found in Hailemikael et al. (2026), while an overview of the results is presented in this and the following sub-sections.

Leveraging data from permanent and temporary seismic networks, this extensive data collection covers more than 1000 sites (FIGURE 4.1), encompassing both the national scale and selected regional areas (including Central Italy, North-East Italy, the Basilicata region, and the Ferrara area).

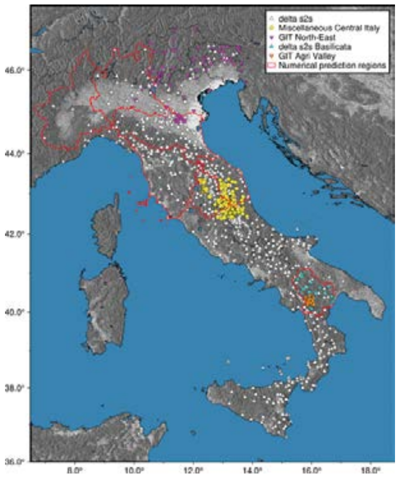

FIGURE 4.1
Distribution of sites across the Italian territory for which empirical ground-motion amplification estimates are available, distinguished by estimation method.

The empirical site response was parameterized using period-dependent Amplification Factors (AF) (Section 3.1; eq. 3.1). The period bands considered for averaging ground motions are: 0.1 – 0.5 s (AF_1), 0.4 – 0.8 s (AF_2) and 0.7 – 1.1 s (AF_3). Three distinct empirical approaches were used to compute AFs, as described below:

1: GIT_FAS and GIT_RS: amplification functions derived from the Generalized Inversion Technique (GIT) applied to input motion, computed from spectrum-compatible accelerograms (Uniform Hazard Spectrum) in terms of (a) Fourier spectrum (GIT_FAS) or (b) Response spectrum (GIT_RS). From Priolo et al. (2020).

2: δS2S: estimates based on the repeatable site-to-site terms of a reference Ground Motion Model (GMM) in SA, such as ITA10 (Bindi et al. 2011) or ITA18 for the EC8-A class (ITACA Archive, Felicetta et al. 2023).

3: SSR: both Sa^{in} and Sa^{out} were computed from recordings at the reference station and at the target one (Priolo et al. 2020).

The peak amplification factors (FA_PGA and FA_PGV for the peak acceleration and velocity, respectively) were evaluated from the residuals, defined as the logarithmic difference between observations and GMM predictions (ITA10 or ITA18).

TABLE 4.1
Empirical datasets collected within the activities of the PRIN-SERENA project.

TABLE 4.1 summarizes the datasets analyzed within the project, while FIGURE 4.1 shows the spatial distribution of sites across the Italian territory for which empirical ground-motion amplification estimates are available.

Region	AF_PGx	AFx	Reference
Italy	δs2s_ITA18	δs2s_ITA18	Lanzano et al. (2024)
North-East Italy	δs2s_ITA10	GIT_FAS	Klin et al. (2021)
Central Italy	δs2s_ITA10	GIT_RS	Priolo et al. (2020)
Central Italy (Amatrice, Capitignano and Montereale, Norcia)	-	SSR	Cara et al. (2019); Felicetta et al. (2021); Luzi et al. (2019)
Central Italy	-	δs2s_SEA21	Sgobba et al. (2024)
Central Italy (Arquata-Montegallo, Perugia, Bevagna, Spoleto, Umbertide)	δs2s_ITA10	GIT_FAS	Priolo et al. (2020); Laurenzano et al. (2019)
Basilicata	δs2s_ITA18	δs2s_ITA18	PRIN-SERENA project
Val D'Agri	δs2s_ITA10	GIT_FAS	PRIN-SERENA project
Ferrara	δs2s_ITA10	GIT_FAS	Priolo et al. (2012); Barnaba et al. (2014)

The empirical AF dataset was collected, verified, and structured within a dedicated spatial data infrastructure that publishes Open Geospatial Consortium web services (FIGURE 4.2). Analysis was then performed using open-source Python libraries within a Jupyterlab environment.
The infrastructure was deployed following the "three-tier" architectural model: Storage, Application and Presentation layers. The storage layer (geodatabase) is deployed using postgresql relational database management system (RDBMS) and stored spatial data are managed by the "postgis" extension.

The application layer, that reads spatial data from postgresql/postgis, transforms that data into usable web services. A single "HTTPS" endpoint (Presentation layer) is provisioned to grant authorized end-users access to the most current data, enabling them to utilize the most appropriate tool for their requirements. Upstream data homogenization is critical for defining consistent data structures, and the geodatabase retains the comprehensive historical evolution of the project's data. Interoperability is successfully maintained through the adoption of established standards, specifically OGC WFS and OGC WCS, implemented at the Application layer level. In the data ingestion phase, infrastructure operators employ an "ETL" (i.e. Extract, Transform, Load) methodology. A significant drawback observed in this process is the ongoing dependence on legacy data formats (e.g. ESRI Shapefile format), which lack the efficiency and compatibility required by contemporary cloud-native data management systems.

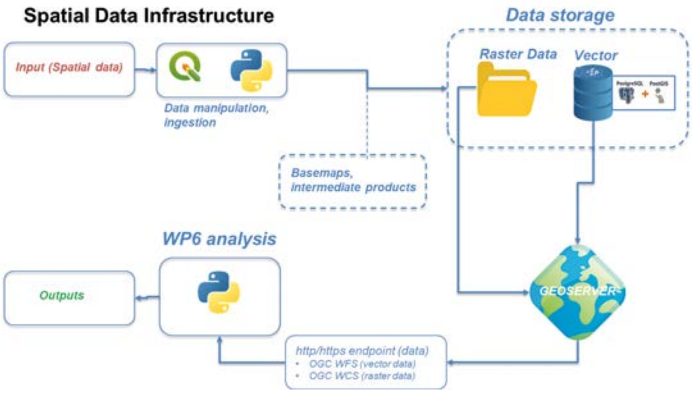

FIGURE 4.2
Spatial data infrastructure logical scheme used to share and archive seismological data for internal use only.

4.1.2 Site-to-site residual (δS2S)

The δS2S approach isolates the repeatable, systematic deviations of recorded ground motions from the median predictions of a non-ergodic ground motion model (GMM) developed for the target region (Lanzano et al. 2025). This method was primarily used to derive empirical estimates at the national scale for over 900 accelerometric and velocimetric stations, and it was applied to a wide range of parameters including PGA, PGV, spectral ordinates of acceleration response (ITA18, Lanzano et al. 2019) and Fourier spectra (Lanzano et al. 2022). To ensure a direct and standardized comparison with the 1D numerical simulations developed within the project, the empirical residuals were calculated with respect to the engineering-bedrock condition of the national building norms (Vs,30 = 800 m/s) and are thereinafter indicated as δS2S800.

This specific engineering-bedrock condition was achieved by applying the empirical correction function specifically developed during the project. This step was necessary because systematic differences were observed among the empirical estimates, primarily due to the reference ground motion for generic rock conditions.

4.1.3 Generalized Inversion Technique (GIT)

The Generalized Inversion Technique (GIT) is a well established method utilized to separate source, path, and site contributions from recorded ground motion spectra (Andrews 1986; Castro et al. 1990; Oth et al. 2011; Klin et al. 2018; Shible et al. 2022, among others). Within our database, the amplification functions derived from GIT were calculated either in terms of Fourier Amplitude Spectrum (FAS) or Acceleration Response Spectrum and then combined with seismic hazard compatible Sa ordinates to compute the final period-dependent AFs. These estimates are available for regional studies performed in Central and North-East Italy as well as for the Basilicata region in Southern Italy.

4.1.4 Standard Spectral Ratio (SSR)

The Standard Spectral Ratio (SSR) method is a traditional, widely employed empirical technique that directly evaluates site effects by computing the spectral ratio between the ground motion recorded at a target site and the motion recorded simultaneously at a nearby reference station (Borcherdt 1970). The reference station is generally selected on an outcropping bedrock site assumed to be free of significant topographic or stratigraphic amplification effects. In this case, AFs were directly calculated from the recorded ground motions. These estimates are available for a limited number of sites in Central Italy.

4.1.5 Comparison among empirical estimates

We compared the empirical estimates by using several goodness-of-fit metrics (Spearman's rank correlation coefficient τ, chi squared score and Kolmogorov-Smirnov test) to assess their reliability (Hailemikael et al. 2026). Such a quantitative framework allowed us to confirm the high correlation between site-amplification estimates from different methods ($\tau \geq 0.9$) and the lack of any significant statistical difference between sets of empirical measures, confirming their robustness in measuring the relative amplification levels between sites. In Central Italy, where systematic deviations between estimates from different methodologies were observed, these stem primarily due to the choice of the reference ground motion and can be corrected for by scaling the estimates to a common reference ground-motion level (FIGURE 4.3; Lanzano et al. 2025).

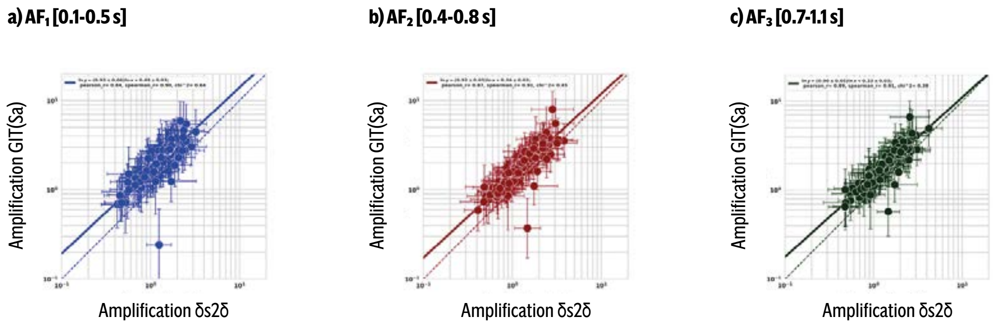

FIGURE 4.2
Figure 4.3 Scatter plots of site amplification estimates obtained from δS2S800 (in abscissa) versus those obtained from GIT (in ordinates) for Central Italy; a) short- (AF_1 in blue), b) intermediate- (AF_2 in red) and c) long-period intervals (AF_3 in green). In the scatter plots, the linear fit of log amplification values (solid line) and 1:1 line is also shown.

4.1.6 Effectiveness of 1D hypotheses in δS2S data

This subsection provides a summary of the results of the comparison of transfer functions from numerical and empirical site response analyses at recording sites, to verify their possible 1D behaviour in seismic response. More details will be available in Castelbarco et al. (2025).

Specifically, we analyze the stations in the ITalian ACcelerometric Archive database (ITACA, Felicetta et al. 2023), having a reliable estimate of $\delta S2S_{800}$ and available Vs profile (characterized by any type of geophysical survey, i.e. Down-Hole, MASW, etc.) down to the depth of the engineering bedrock (Vs=800m/s), selected as input for one-dimensional numerical analyses. The selection led to a set of 168 accelerometer stations, as shown in FIGURE 4.4. Most of them are located along the Central Apennines, which is the most densely monitored area in Italy. Class B is the most characterized subsoil category, according to the seismic design standards in Italy (NTC, 2018), although there is a non-negligible number of sites in categories C and E. Class A is poorly represented (only one site), due to the difficulties of performing geophysical tests for rock sites. As far as empirical estimates are concerned, we took advantage of the $\delta S2S_{800}$ estimates for 916 recording stations in ITACA, already discussed in Section 4.1.2 and provided by Lanzano et al. (2025).

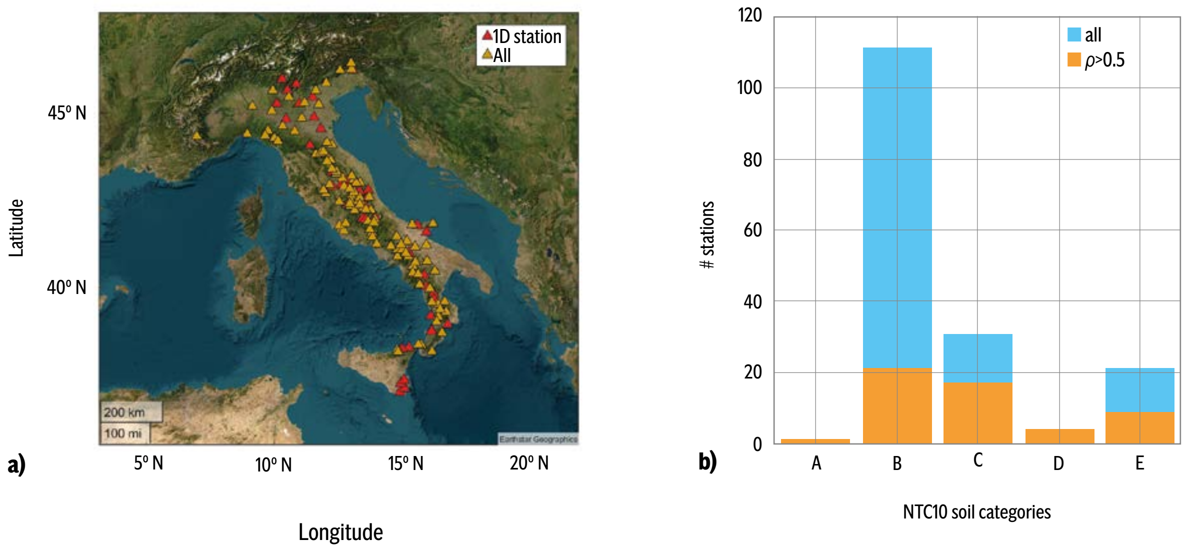

FIGURE 4.4
(a) map of the recording stations where an experimental Vs profile is available selected for 1D numerical modelling; (b) frequency distribution of the selected stations according to the NTC18 soil categories (NTC, 2018).

One-dimensional numerical analyses of local seismic response utilize the STRATA code (Kottke and Rathje, 2009; Kottke and Rathje, 2013), with a linear elastic ground deformation model. The linearity assumption is justified because the empirical amplifications, primarily from low-to-medium magnitude earthquakes recordings (up to 200 km distance), predominantly represent the site effects in the linear elastic regime. The Vs profile is introduced deterministically, without considering uncertainties of Vs values, layers thickness and bedrock depth, and the initial damping D_0 is inversely dependent on the VS values. Since the analysis is linear, the comparison among the empirical and numerical transfer functions is independent of the seismic input.

FIGURE 4.5 shows the results of two illustrative recording stations: FERS station (IV network, managed by INGV), located in the city of Ferrara in the Po River plain; AQK station (IT network, managed by the DPC), installed in L'Aquila in the Central Apennines. FERS site shows a good correspondence, both in shape and amplitude, between the empirical and numerical transfer function, having two amplification peaks at 0.6 Hz and around 2.5 Hz. In the case of the AQK station, the empirical transfer functions are very different, as the numerical amplification function does not capture the sharp peak at 0.6 Hz. In this case, the available depth of investigation of the Vs profile (see https://itaca.mi.ingv.it/ItacaNet_40/#/station/IT/AQK) is not sufficient for numerical modelling, as it stops at a depth of about 50 m and is unable to capture the deeper impedance contrast responsible for the low-frequency peak (see also Di Giulio et al. 2014).

To identify sites with a 1D empirical response, we calculate the Spearman correlation coefficient (ρ) to measure the shape similarity between the empirical and 1D numerical transfer curves, as already explored in the study by Pilz and Cotton (2019) in Japan. Using a threshold of ρ=0.5, we defined 52 stations (approximately 31% of the analysed stations) as showing clear 1D behavior in seismic response. The spatial and frequency distribution of these stations is also shown in **FIGURE 4.4A-b**. Many of the stations in category B were discarded in this analysis, yet retained a significant number of stations from categories C and D showing 1D behaviour (**FIGURE 4.4b**).

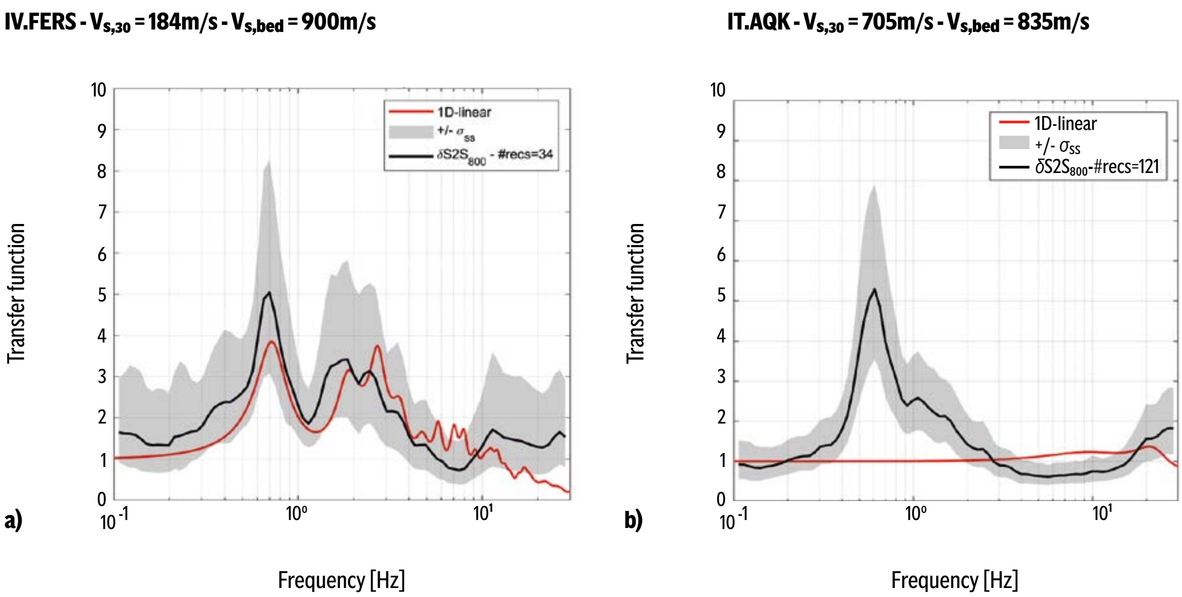

FIGURE 4.5
Comparison between empirical and numerical transfer functions at (a) IV.FERS and (b) IT.AQK stations.

4.1.7 Spatialization of AF and correlations between site indicators

To bridge the gap between point-based station data and areal coverage, we investigated the statistical correlation between different site proxies at national level. Within this context, a critical issue concerns the possibility to compare amplification estimates at accelerometric and velocimetric sites with wide areas evaluations made available by the numerical simulations described in the previous sections. To make this comparison more effective, spatial extrapolation of amplification effects estimated at the instrumented sites may be of help.

The basic assumption is that amplification functions, which are derived from earthquake recordings at a limited number of seismic stations can reasonably be considered representative of surrounding areas with similar geological characteristics. We then explored different strategies to compute the spatial extrapolation of amplification between instrumented sites using reliable and robust proxies.

Within the framework of amplification factor spatialization, an advanced methodology has been implemented to model the spatial variability of site response for the target area of Central Italy, as detailed in the work of Sgobba et al. (2024).
This approach focuses on the spatial modeling of empirical site-to-site amplification terms (δS2S), which are extracted from the residuals of a reference ground motion model specifically calibrated for Central Italy on reference rock condition (see Section 6.2.1). The application of this advanced geostatistical framework allows us to overcome the limitation of stationary spatial models such as Ordinary Kriging (OK), whose approach relies solely on the spatial distance between observations. To leverage the dense sampling and rich geological data available in Central Italy, Universal Kriging (UK) was introduced. This non-stationary technique constrains the prediction of amplification factors using known physical quantities distributed across the territory (deterministic trends called "drifts"), such

as lithostratigraphic characteristics and Vs_{30} maps. To support this, an ad-hoc Vs_{30} map was generated by integrating two primary sources: the national map by Mori et al. (2020), which has high-resolution but is statistically biased toward values typical of EC8-class B and lacks representative variability and the Wald and Allen (2007) topographic slope relationship. The resulting hybrid map provides a continuous and more representative predictor across the entire study area. Analysis reveals that the statistical dependence of δS2S terms on Vs_{30} is highly frequency-dependent: while the correlation is weak at high frequencies (PGA), it becomes significant (approximately -0.6) at intermediate and long periods (T > 0.3s). This confirms that long-period ground response is more closely linked to the deeper properties of the velocity profile. The UK model, incorporating geographic coordinates and the reconstructed Vs_{30} map, was validated through Leave-One-Out Cross-Validation (LOO-CV). It proved to be the most accurate model for minimizing Mean Square Error (MSE) also in comparison with the stationary model, demonstrating the effectiveness of integrating regional geological trends into the spatialization process.

The final maps, reconstructed across several spectral ordinates, successfully capture spatial non-stationarities and exhibit realistic patterns (FIGURE 4.6).
This provides a practice-oriented tool for generating robust empirical site amplification maps, significantly reducing uncertainty in unsampled areas. Despite these advantages, approximately 7% of testing stations showed sub-optimal predictions. This is likely due to the lack of crucial proxies, such as fundamental frequency (f_0) or engineering bedrock depth (H800); their absence from regional trend models remains a constraint for further refining predictions. Finally, the statistical biases in the inferred Vs_{30} maps, specifically the underestimation of real variability compared to direct on-site measurements, are reflected in the final amplification products and represent a key area for future improvement.

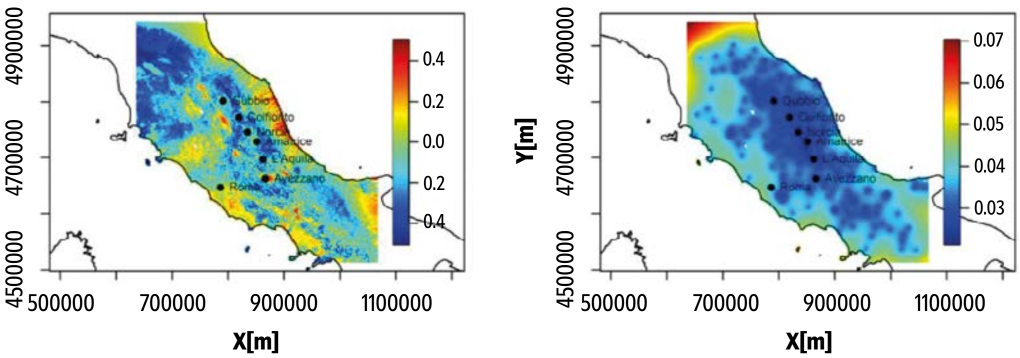

FIGURE 4.6 Maps (projected coordinate system UTM zone N32) of the best δS2S model predictions (on the left) and associated variance (on the right) for SA(1s). The prediction grid of the maps is built within the bounding box of the data locations. From Sgobba et al. (2024).

To spatially extrapolate spectral amplification curves from a limited set of sites, a methodology combining clustering, correlation analysis, and Voronoi tessellation was applied to the lower Sarca Valley (north of Lake Garda, Italy). We briefly outline the results here; further details can be found in Laurenzano et al. (2023).

Spectral amplification curves were first computed at 19 temporary seismic stations using the Generalized Inversion Technique (GIT; see Section 4.1.3). The results (FIGURE 4.7a) showed strong low-frequency amplification in the central part of the valley, where sediment thickness is greatest, moderate amplification along the valley margins, and negligible amplification at bedrock sites. To extend these results over a denser grid, ambient seismic noise measurements were used (FIGURE 4.7b).

The approach relies on the assumption that NHV (Noise Horizontal-to-Vertical) curves, although not direct amplification functions, can serve as reliable proxies. A k-means clustering procedure was independently applied to both GIT and NHV curves, showing a strong correspondence between clusters (FIGURE 4.7c) which validated the use of NHV as a proxy. Three clusters were identified, representing low-amplification bedrock sites, high-amplification central valley sites, and intermediate marginal zones. Subsequently, NHV curves from 110 additional noise-only sites were compared with those of the seismic stations through a correlation analysis.

The similarity between curves was quantified using the Pearson correlation coefficient combined with a goodness-of-fit metric. For each noise-only site, a similarity coefficient was computed (FIGURE 4.8a), and the site was assigned to the seismic station – and corresponding cluster – with the highest similarity (FIGURES 4.8B-c). In this way, the amplification curve associated with the matched cluster was assigned to each site. Finally, a Voronoi tessellation was applied to generate continuous areal zones, each associated with the centroid amplification curve of its cluster. The resulting zonation map defines three homogeneous areas characterized by distinct amplification factors, providing a high-resolution representation of local site effects suitable for seismic hazard and risk assessment. The same approach is currently being applied in the Ferrara area, where data come from a number of seismological stations installed in the area and a large set of ambient noise measurements, allowing for the extension of amplification curves across the region.

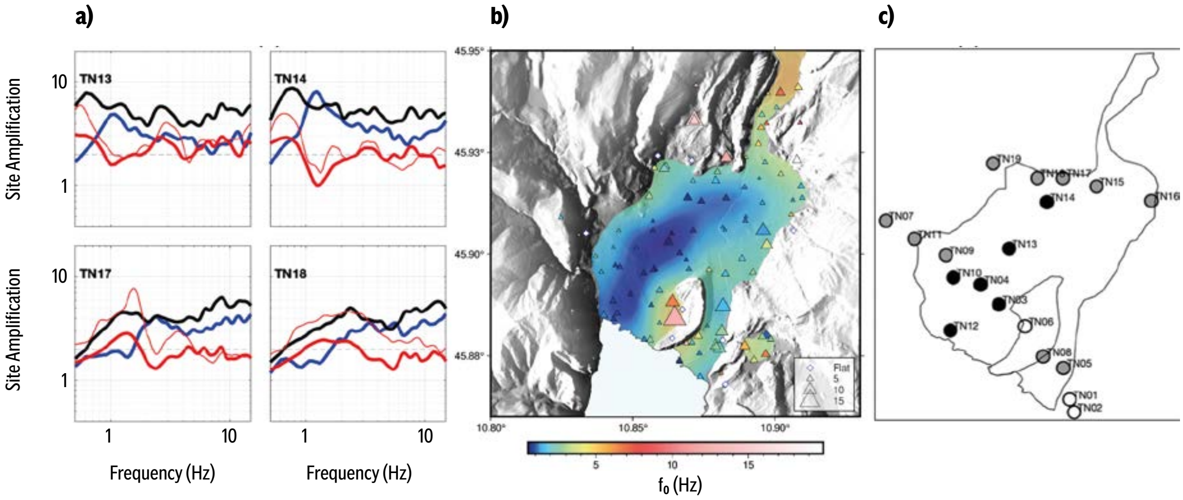

FIGURE 4.7
Site response curves for 4 of the 19 stations. Black and blue lines: GIT amplification curves for the horizontal and the vertical components, respectively), red lines: H/V ratios from earthquake recordings (thick line) and seismic noise (thin line).
(b) Map of resonance frequencies (f_0) from NHV.
(c) Spatial distribution of the 19 sites and their respective clusters obtained from GIT and NHV curves.
From Laurenzano et al. (2023).

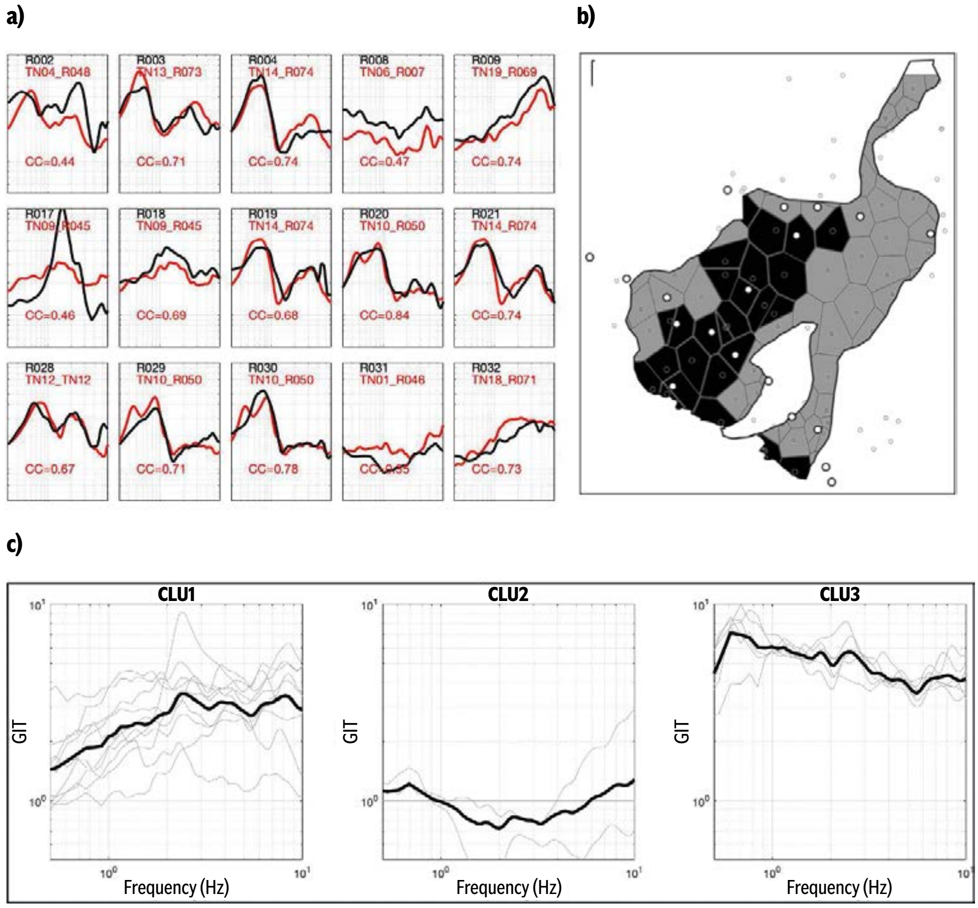

FIGURE 4.8
For each NHV curve at the noise-recording sites (black), the best-correlated NHV curve from the seismometric network (red), corresponding to the maximum CC value, is shown.
(b) Spatial extent of the clusters obtained at the 19 sites.
(c) GIT curves for each cluster: individual site curves are shown in thin gray, and cluster centroids in thick black.
From Laurenzano et al. (2023).

4.1.8 Comparison between empirical and numerical estimates

Given the robustness of site- amplification estimates obtained from empirical methods, we compared these estimates with amplification ones based on 1D numerical simulations to better understand how well simplified approaches can describe the observed data. The considered simulation-based data were calculated at different spatial scales: regional and local. In this section, the reference empirical estimates are those derived from the residual analysis, namely δS2S800 (Section 6.1.1), due to their availability at the national scale.

A preliminary comparison has been performed by considering the AF estimates provided by Falcone et al. (2021) based on the Vs_{30} values estimated by Mori et al. (2020) from morphometric proxies. It is worth noting that these estimates were not obtained in the conceptual frame of the project and do not account for the geological constraints discussed in Section 3.3.

The comparison developed within the SERENA project (Section 3) for show a lack of correlation relative to AF1 and a weak one for AF2 and AF3. Moreover, the estimates by Falcone et al. (2021) have a limited range of values that fails to capture the full variability of empirical estimates (**FIGURE 4.9**; Hailemikael et al. 2026).

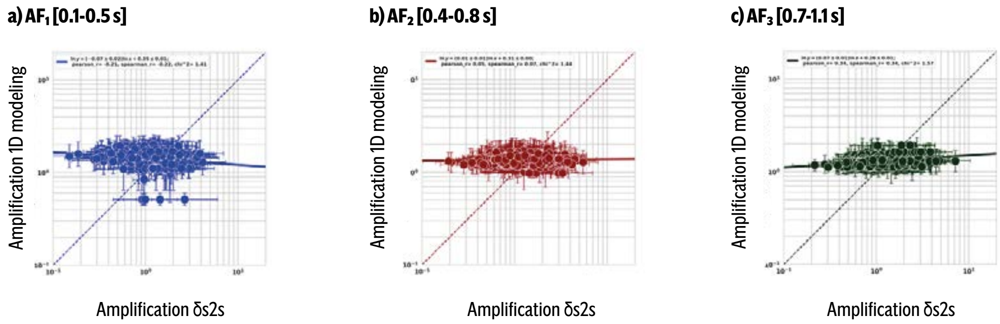

FIGURE 4.9
Scatter plot of site amplification estimates from δS2S800 method (in abscissa; Lanzano et al. 2025) versus those obtained from 1D simulations (Falcone et al. 2021), calculated for a) AF1 (blue), b) AF2 (red) and d) AF3 (green). The linear fit of log amplification values (solid line) and 1:1 line are also shown.

The residual analysis, based on the difference between the logarithm of empirical δS2S800 and AF values from Falcone et al. (2021) revealed three main scenarios for the discrepancy between estimates:

1) Satisfactory agreement (30–35% of sites): A core group of sites showed satisfactory agreement, with residuals grouped around zero.

2) Overestimation of 1D numerical simulations by Falcone et al. (2021) (65% for short periods, decreasing to 34% for long periods): The largest fraction of sites showed negative residuals. This indicates that Falcone et al. estimates overestimated the empirical ones. These sites are predominantly stiff soils and rock, distributed geographically along the Apennine belt and the Tyrrhenian side of the peninsula.

3) Underestimation of 1D numerical simulations by Falcone et al. (2021) (5% for short periods, increasing up to 16% for long periods): A smaller but critical group of sites showed significant positive residuals, implying that Falcone et al. estimates underestimated the empirical estimates. These sites are typically soft soils located in the central/eastern side of the peninsula and eastern Sicily, often within deep sedimentary basins (e.g., the Po Plain, the Fucino basin, and the Adriatic foredeep).

This critical underestimation underscores the possible intrinsic limitations of the Falcone et al. (2021) estimates in capturing complex effects (2D/3D resonances, surface waves generated at basin edges, topographical focusing effects, etc.).
A detailed comparison between empirical and numerical estimates was carried out at the regional level, exploiting the results from 1D numerical models developed within the SERENA project (Section 3) for about 860 sites in specific target regions, namely Tuscany, Marche, Umbria, Piedmont and Lombardy. The regional analyses confirmed the trends observed at the national scale. The normalized residual spatial distribution is driven by local geology: large positive residuals were observed for soft sites in the Po Plain, especially at long periods, and negative residuals for stiff and rock sites in the Apennines and Tuscany (FIGURE 4.10, right panels). Extreme values of normalized residuals correspond to the upper and lower tail of δS2S800 distribution, which has a much wider range than that of 1D simulation-based estimates (FIGURE 4.10, left panels). Analysis of the normalized residual as a function of the geological site classification (Bucci et al. 2022), further confirmed that 1D simulation-based data underestimate the empirical site amplification for soft sites (CX, GX and SX distributions within green boxes in FIGURE 4.10d), whereas site classes corresponding to stiff and rock sites have median residuals equal or lower than zero (ALS, LP, LPS, SFLPS distributions FIGURE 4.10d).

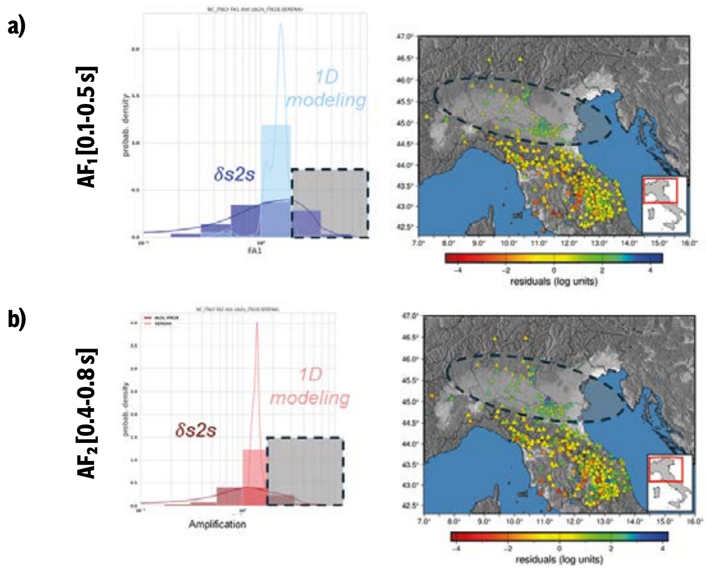

FIGURE 4.10
Spatial distribution of residuals (right column) between site amplification estimates from δS2S800 method and 1D simulations for AF1 (a), AF2 (b) and AF3 (c).
Empirical and 1D simulation-based amplification distributions are also shown (left column).
The geographical area where large positive normalized residuals are observed and the corresponding values of the amplification estimates are highlighted by the dashed gray areas.
Distribution of normalized residuals as a function

of the geological site classification (Bucci et al. 2022) is shown in the bottom panel (d); the classes corresponding to soft sediments are included in the green boxes. The dotted red line corresponds to normalized residuals of zero.

c)

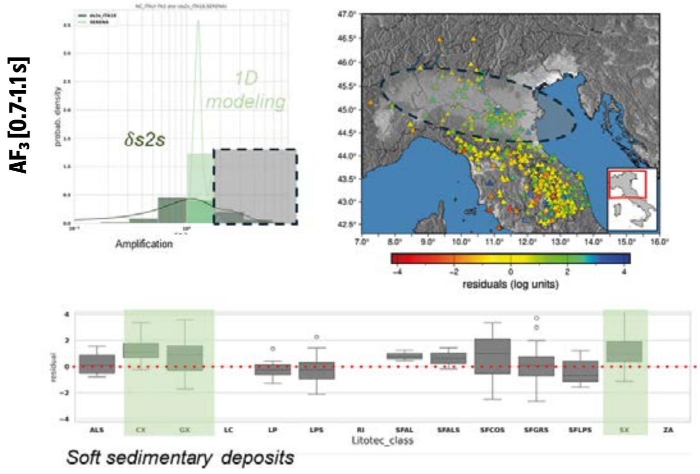

d)

While in the Section 4.1.6 we verified that, out of 168 national wide sites with available Vs profile, the site transfer functions of approximately one-third can be reproduced with 1D linear elastic numerical model, in the following paragraph we evaluate the capability of numerical models to accurately reproduce the site amplification function in different geological conditions. The aim is to define the limits of applicability of 1D modelling, determining at what depth or geological complexity the convergence between numerical predictions and experimental evidence fails, thus providing critical insights for future large-scale seismic hazard strategies.

The comparison was carried out for 21 sites located in the Val d'Agri area (southern Apennines), encompassing a wide range of geological conditions: from high-velocity carbonate outcrops (rock sites) to shallow alluvial covers and deep intermontane basins (>200 m). The analysis of a relatively small network of sites within a small area minimizes the variability introduced by source and path effects, directly testing the reliability of 1D numerical models against empirical data (Gallipoli et al. 2026).

Specifically, we compare: i) experimental AFs in the three period bands of engineering interest, estimated by a non-parametric single-step GIT approach (GIT; see Section 4.1.3), by using a dataset of approximately 2,000 waveforms recorded between 2016 and 2018 and corresponding to about one hundred local and regional events, ensuring good azimuthal coverage for each station (FIGURE 4.11a); ii) 1D stochastic and semi-stochastic numerical models (based on the NC92soil/PYSRA engine; Acunzo et al. 2024) used for national-scale mapping; iii) 1D deterministic models incorporating site-specific lithostratigraphic data.

The simulations were carried out using representations of subsurface conditions at each station, defined through expert geological assessment. The stratigraphies incorporated the relative proportions of cover lithotypes, the depth to the geological bedrock, the Vs range for each lithotype, and their associated physical and mechanical properties for each site (FIGURE 4.11b).

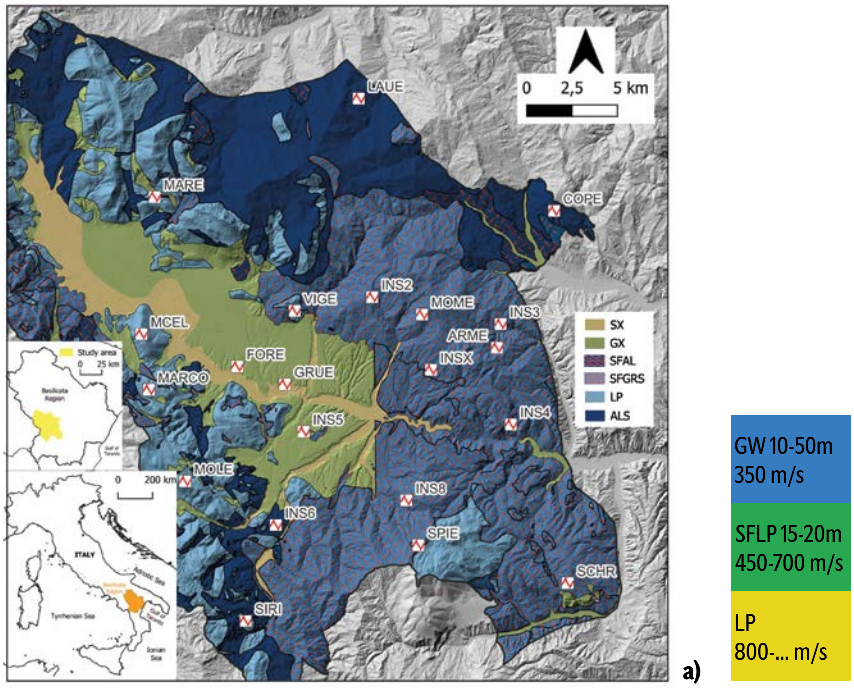

FIGURE 4.11
(a) map of the recording stations in Val d'Agri area selected for 1D numerical modelling. The basemap consists of the geological-technical map modified by Mendicelli et al. (2024) and discussed in Section 2.3.2;
(b) Engineering geological log for MARE station. Codes are the engineering geology classes adopted in Italian standards of the third order seismic Microzonation studies (GW: Well sorted gravels, mixed gravels and sands; SFLP: Fractured/weathered LP; LP: Lapideous rock).

FIGURE 4.12
Comparison between the amplification functions obtained from the GIT analysis (red curve) and those evaluated by using the 1D deterministic (black curve) and semi-stochastic (blue curves) models. The horizontal bars indicate the AF values estimated for each period range and for each analysis (full-stochastic in green, semi-stochastic in blue, deterministic in black, and empirical in red). From left to right: sites with shallow sedimentary cover (MARE), intermediate sedimentary cover (SPIE), and thick sedimentary cover (GRUE). Bottom panels display the 1D models used for the semi-stochastic (blue lines) and deterministic modelling.

First of all, we compared the empirical amplification functions with those obtained from 1D deterministic numerical modelling, in order to assess discrepancies between amplification functions derived from simplified 1D models and those inferred from empirical observations (FIGURE 4.12). When grouping the sites according to the depth of the seismic bedrock (shallow, intermediate, and deep), the comparison reveals a progressive divergence as the bedrock depth increases. While the agreement is generally acceptable for shallow and intermediate sites, significantly mismatches are observed in deeper basin settings. This discrepancy underscores that 1D stratigraphic models, even when well-constrained, cannot account for the multidimensional wave propagation that dominates the measured response.

This is particularly evident for sites where the seismic bedrock occurs at greater depths, highlighting the limitations of simplified 1D modelling. Unlike the experimental approach, which inherently captures the full complexity of the local seismic response, 1D simulations focus exclusively on vertical stratigraphic amplification.

The comparison of AFs values, derived from 1D stochastic and deterministic modelling approaches with the empirical amplification functions for the three considered period ranges (FIGURE 4.12), highlights an additional important insight: the AF value estimated over a limited frequency range may not fully capture the complexity of the entire amplification function, when it includes both peaks and troughs within that interval. In such cases – which are quite common, if a local seismic response is of interest (and not large areas estimates), the AF estimator risks underestimating or misrepresenting seismic site responses, particularly in geologically complex settings such as valleys and intermontane basins. Consequently, using a single integral AF value for deep basins local seismic response might lead to a significant underestimation of the seismic demand.

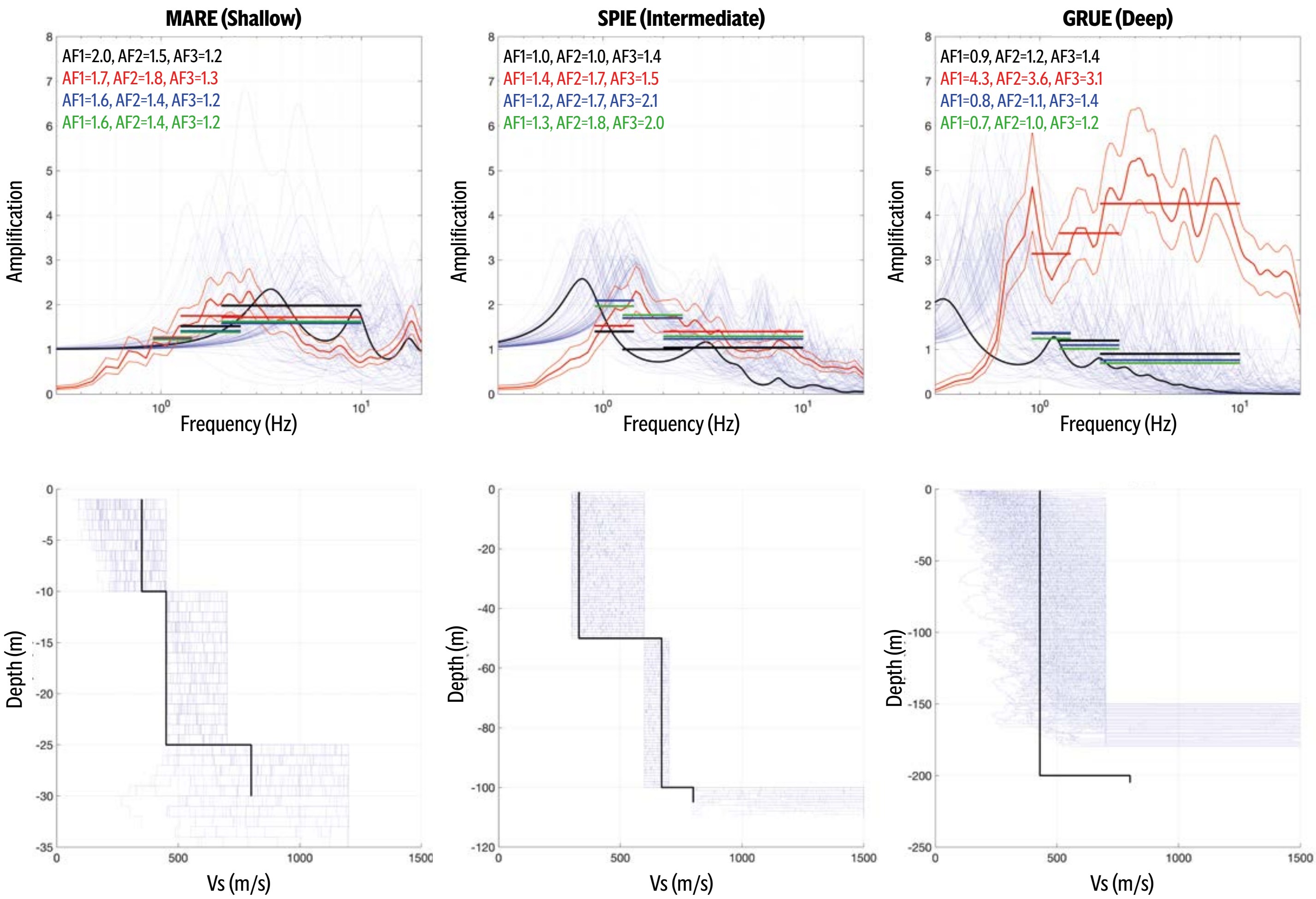

A further comparison was done with respect to the numerical Amplification Factors computed for the Basilicata region in Section 3.3.2 (FIGURE 4.13). The three AF distributions are plotted for all seismic-stratigraphic columns and for all 100 realizations per column.
Empirical AF values obtained from the GIT are superimposed on the boxplots considering the station locations and their intersection with the ID of the stratigraphic columns on map.
In this case, FIGURE 4.13 indicates that the stochastic models proposed are, on average, adequate to capture the variability of the experimental estimates, confirming that the parametrization plays a crucial role.

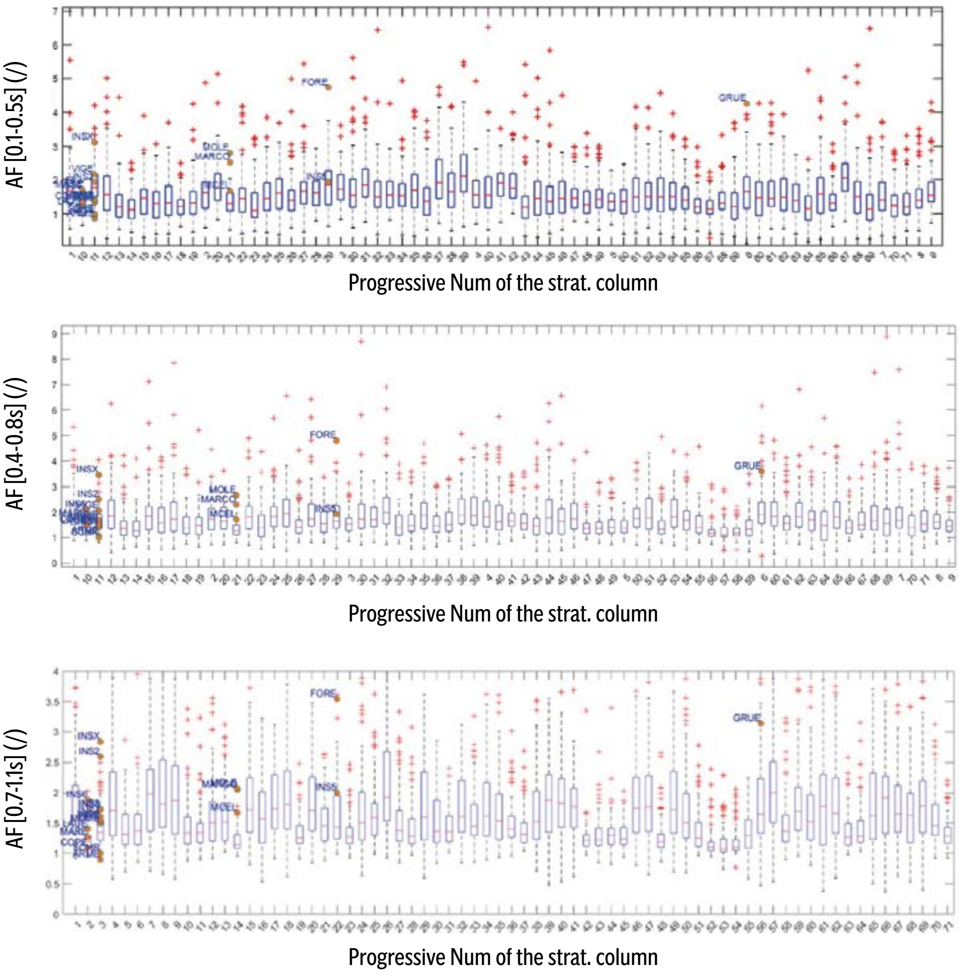

FIGURE 4.13
Comparison between the AF obtained from the GIT analysis (orange points) and those evaluated by using the 1D stochastic models (box-plots). The three boxplots show the 25th and 75th percentiles, the median, and the full AF range for each column described in Section 3.3.2 and in Table 3.7 (the x-axis corresponds to the seismic-stratigraphic column ID).

4.2 Comparison between geognostic-data–derived estimates and modelling-based estimates: the Brescia test site

The study of the area of Brescia (FIGURE 4.14) was carried out with the aim of providing estimates useful for assessing the expected seismic amplification effects in a plain environment where the morphological contribution is nearly negligible.

FIGURE 4.14
Overview of the study area.

Simulations were carried out on 278 borehole stratigraphies, each including expert-assigned codes of the geologic–technical units. The S-wave velocity values used were the median values obtained from statistics based on 214 direct and indirect geophysical measurements (MASW, DH, and inversion of the HVSR curves).

Higher amplifications are observed in the polygons where CL crops out and in the western sector (FIGURE 4.15).

The AF values resulting from large-scale stochastic modelling remain lower than those derived from the regional charts. See FIGURE 4.16 where the results of a second level of the SM study for Brescia is available.

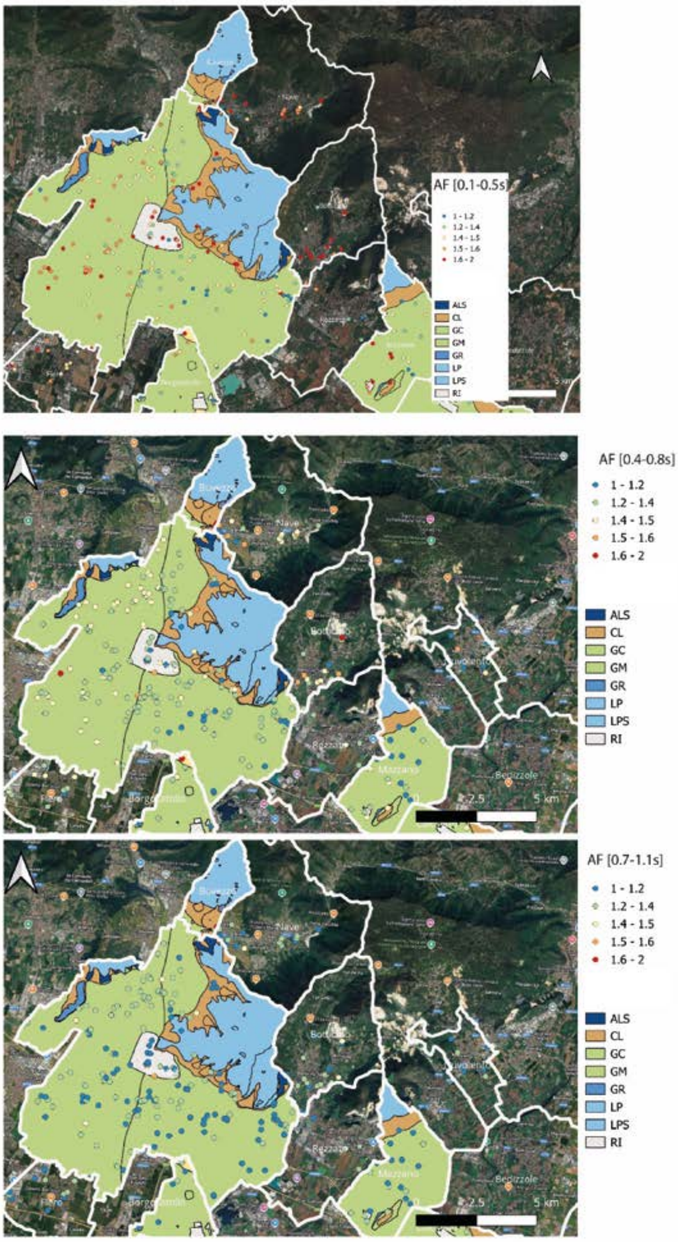

FIGURE 4.15
AF values at 278 borehole stratigraphies. The basemap consists of a geological–technical map compiled from all available studies in the area (from the original DB of SM studies).

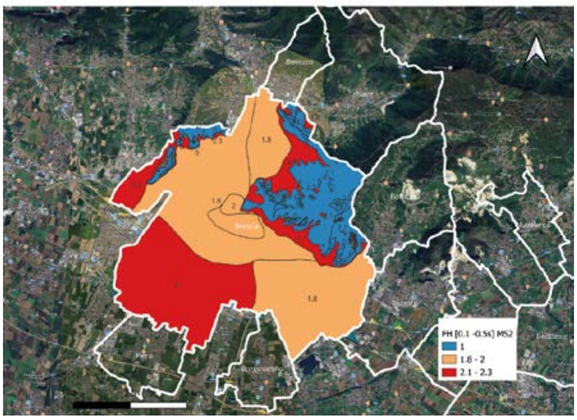

FIGURE 4.16
Sketch of the seismic microzonation study of level 2 for the municipality of Brescia (Gasparetti and Quassoli,2016).

Sensitivity analyses were also carried out to obtain amplification factors (AF), varying both the S-wave velocity variability laws and the inter-correlation laws between layers.

In each box, the central red mark indicates the median, and the bottom and top edges of the box

indicate the 25th and 75th percentiles, respectively. The whiskers extend to the most extreme data points not considered outliers, while the outliers are plotted individually using the '+' marker symbol. The box- plots in FIGURE 4.16 show the variations in AF obtained with using the soil mechanical behaviour described in Section 3.1 with respect the one obtained assuming no variation of Vs, and Vs values of each layer equal to the median values obtained from statistics based on direct and indirect geophysical measurements for the first period range (0.1–0.5 s, i.e., 'short period').
In this first period range, variability spans from 1 to 2, although outliers reach amplification factor values as high as about 4.

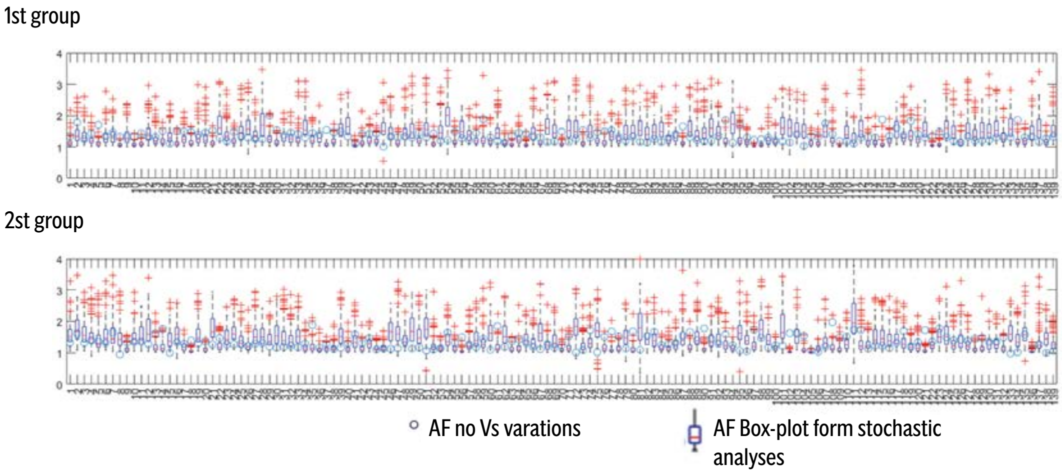

FIGURE 4.17
Comparisons among: 1) AFs obtained at 278 boreholes, assuming as S-wave velocity values the median values obtained from statistics based on direct and indirect geophysical measurements (blue circles) and the ones computed using the soil mechanical behaviour of Section 3.1 (box-plots). For clarity, the figure is divided into two subplots: the upper one displays the results for the first 139 seismostratigraphic columns, and the lower one those for the remaining 139. The total is therefore 278 (139×2), corresponding to the number of boreholes that reach the bedrock.

Moreover, the three plots of FIGURE 4.18 show the amplification factor values obtained from the "deterministic" modelling (vertical axis), as a function of the amplification factor values obtained from the stochastic modelling (horizontal axis).

From left to right, the plots correspond to the three period ranges: 0.1–0.5 s (short period), 0.4–0.8 s (intermediate period), and 0.7–1.1 s (long period). The bisector divides the Cartesian plane into two half-spaces: in the lower half-space, the stochastic simulations can be considered conservative with respect to the deterministic simulations (which use only the median Vs-variation values), whereas in the upper half-space the stochastic simulations cannot be considered conservative. As we move toward longer periods – that is, toward the right – the AF values obtained from the stochastic simulations become more conservative for the same stratigraphic column. At short periods, the stochastic simulations are unable to fully capture the variability of the shallow layers; however, this confirms that the proposed method is not intended to replace Level-3 SM. Instead, it is a tool designed to support hazard assessments that incorporate site effects over large areas.

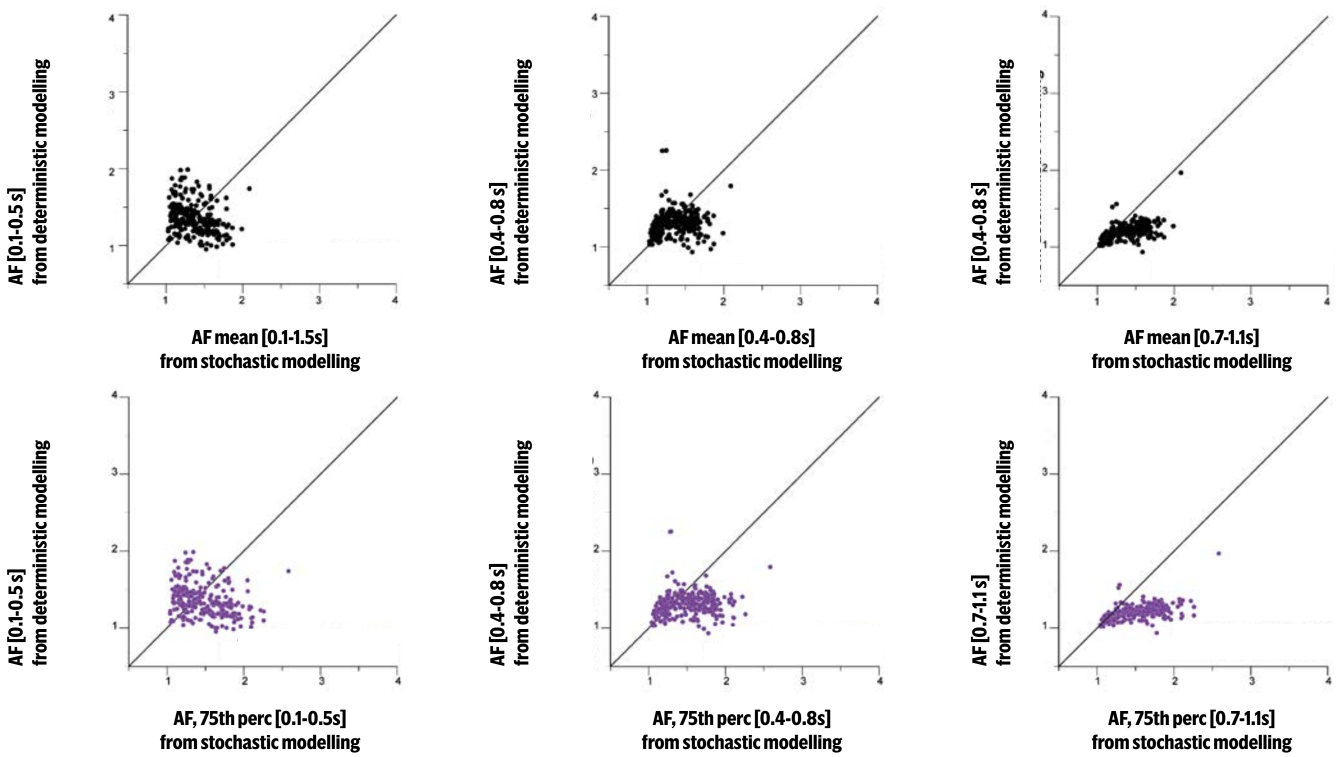

FIGURE 4.18
Comparison among the AF values obtained from the "deterministic" modelling (vertical axis) and AFs obtained from the stochastic modelling (horizontal axis), produced using the soil mechanical behaviour of Section 3.1

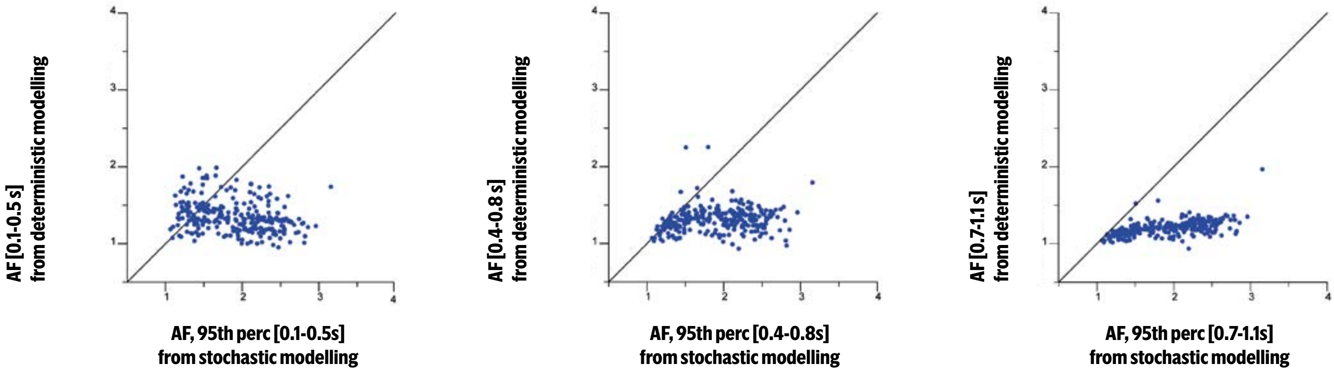
AF [0.1-0.5 s]
from deterministic modelling
AF, 95th perc [0.1-0.5s]
from stochastic modelling
AF [0.4-0.8 s]
from deterministic modelling
AF, 95th perc [0.4-0.8s]
from stochastic modelling
AF [0.7-1.1 s]
from deterministic modelling
AF, 95th perc [0.7-1.1s]
from stochastic modelling

5. Testing proxies relative to topographic and stratigraphic amplification factors in the Italian seismic code (NTC18)

5. Testing proxies relative to topographic and stratigraphic amplification factors in the Italian seismic code (NTC18)

5.1 Numerical testing of topographic proxies

5.1.1 Introduction

A vast body of scientific literature has long highlighted the determining influence of surface topography on local seismic response (Geli et al. 1988; Ashford and Sitar 1997). Specific geomorphological configurations, such as sharp ridges, steep slopes, cliffs, isolated reliefs, and headlands, can amplify or attenuate seismic waves through complex processes of focusing, diffraction, and topographic resonance. Despite its theoretical importance, direct measurements of these phenomena remain scarce, as experimental evaluation is often complicated by the overlapping of local stratigraphic conditions and the objective difficulty of identifying "neutral" reference sites. However, macroscopic evidence of damage from past earthquakes, especially in Italy, confirms the criticality of this issue: many historical settlements and villages are located on hilltops or ridges, making topographic seismic risk a central element in the national architectural and urban planning context.

5.1.2 The Standards

In ordinary engineering practice, however, it is not realistic to expect complex numerical modeling to be performed for common structures to evaluate these effects. It is therefore essential to have simplified and effective proxies that provide reliable preliminary estimates. These proxies are currently implemented in the main regulations, such as Eurocode8 (CEN, 2003) and the Italian Technical Standards for Construction (NTC18, 2018). These codes provide topographic amplification factors (AF) exclusively for two-dimensional morphologies, such as elongated ridges; if the real conformation is not assimilable to a 2D setting, the simplified approach fails, and advanced numerical modeling becomes necessary. Specifically, the standards classify landforms into four main categories (FIGURE 5.1). Reliefs with a height of less than 30 meters or slopes with an average inclination of less than 15° fall into Class T1, for which no amplification is considered (AF = 1). Class T2 identifies cliffs and isolated slopes with an inclination greater than 15° (AF = 1.2). Ridges whose crest width is significantly smaller than the base are divided into two groups: Class T3 for slopes between 15° and 30° (AF = 1.2) and Class T4 for even steeper inclinations (AF = 1.4). These coefficients represent the maximum expected effect at the edge of the cliff or ridge. The standard then assumes that these values decrease linearly along the profile of the relief, until returning to unity (AF = 1) at the base. Furthermore, adopting a conservative approach, any de-amplification effects typical of negative morphologies (such as narrow valleys) are not considered.

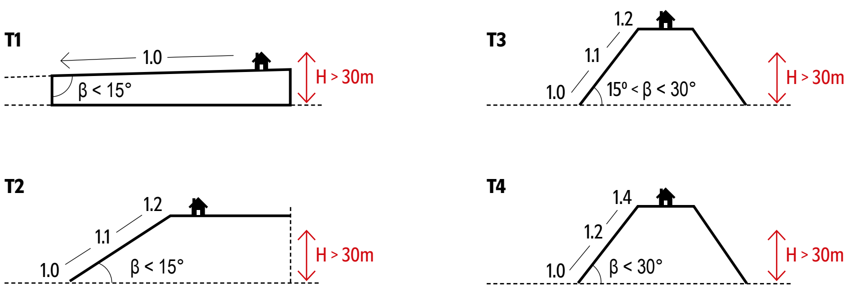

FIGURE 5.1 Morphological classes and expected amplification factors considered by the seismic norms (EC8 (CEN; 2003) and in its Italian version (NTC18, 2018).

As evidenced by the limited indications on landforms provided by the codes, their practical application is hindered by the difficulty of objectively parameterizing the territory to correctly assign these classes, leaving the identification of amplifying morphologies to the professional's subjective judgment. To bridge this regulatory gap, the PRIN SERENA project has systematically investigated the characteristics of geomorphological proxies, with the aim of providing a reliable methodological framework that allows for the widespread and objective application of numerical procedures based on spatial analysis.

5.1.3 The GIS-Based Workflow

The starting point was the development of a computerized workflow implemented in a GIS (Geographic Information Systems) environment using the Python programming language and the ArcPy™ libraries available in ArcGIS Pro (Fantozzi et al. 2023). This workflow allows for the analysis of vast portions of the territory using spatial databases and detailed mapping outputs (FIGURE 5.2). The precision of this system depends strictly on the resolution of the topographic data: for this reason, the project adopted the TINITALY digital elevation model (DEM) with a resolution of 10 meters (Tarquini et al. 2007), ideal for capturing the morphological variations necessary at the scale of engineering design and seismic microzonation.

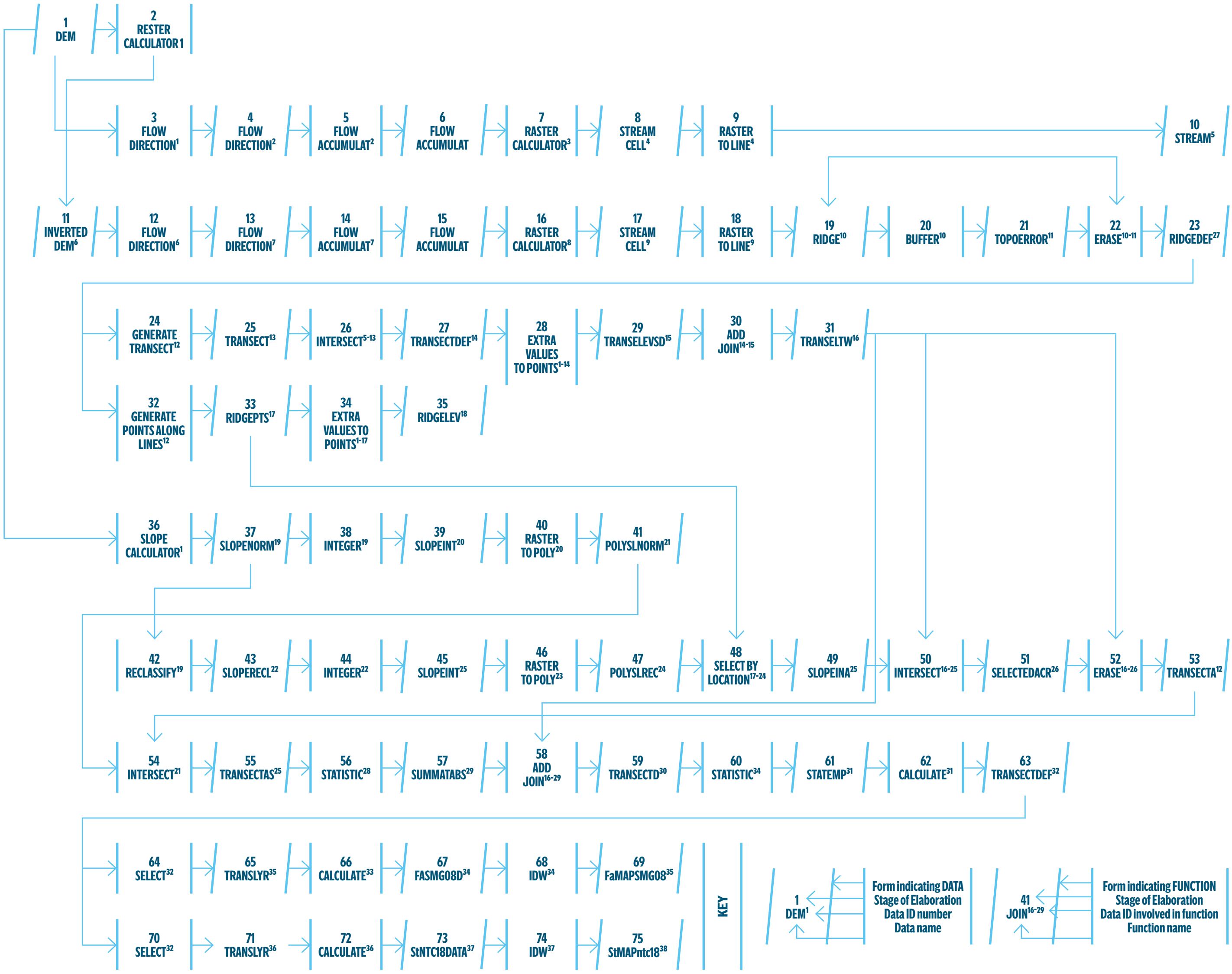

FIGURE 5.2
Workflow of the numerical procedure for the automatic identification of areas prone to topographic seismic amplification effects by the current seismic codes. From Fantozzi et al. (2023).

The core of this work consists of an automated logic for the identification of landforms and the systematic extraction of transects. The methodology first defines the ridgelines (representing the top of the reliefs) and the hydrographic network, which is unequivocally assumed as the "base" of the relief. Between these two morphological boundaries, the system automatically generates a dense grid of profiles that are strictly perpendicular to the ridges. This approach ensures that each transect is representative of the real slope geometry, maintaining a spatial resolution consistent with the source DEM. From this automated processing, a high-value output is generated for territorial planning: a comprehensive spatial database that stores the essential geometric parameters for every profile (height H, relative height h, base width L, crest width W, and inclination I) (FIGURE 5.3). Everything that "revolves around" this extraction translates into a high-value output for planning: the system generates complete spatial databases and high-resolution susceptibility maps.

These maps allow for the visualization of the exact spatial distribution of classes T1, T2, T3, and T4 on a regional scale, quantifying the areas subject to amplification (AF) according to the guidelines of the

Standards. By defining restrictive criteria and "reference morphologies," it was possible to formalize procedures for detecting landforms potentially subject to amplification, drastically reducing interpretative subjectivity.

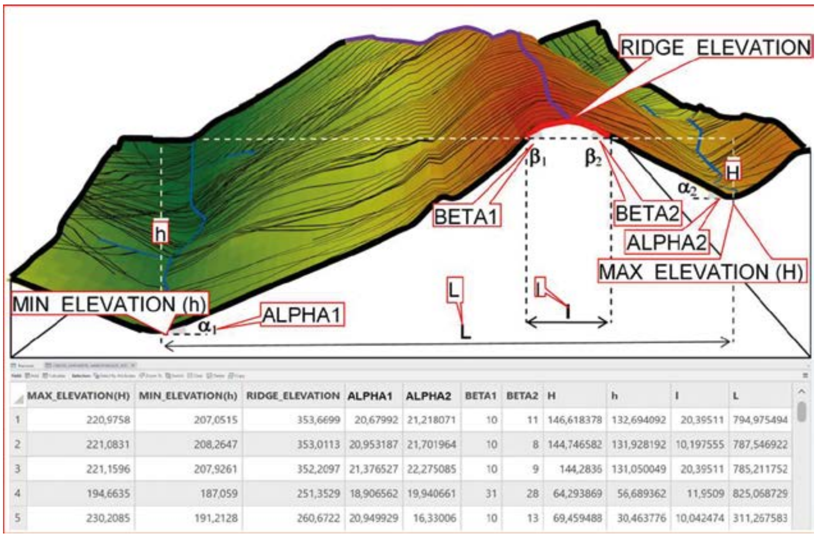

	MAX_ELEVATION(H)	MIN_ELEVATION(h)	RIDGE_ELEVATION	ALPHA1	ALPHA2	BETA1	BETA2	H	h	l	L
1	220,9758	207,0515	353,6699	20,67992	21,218071	10	11	146,618378	132,694092	20,39511	794,975494
2	221,0831	208,2647	353,0113	20,953187	21,701964	10	8	144,746582	131,928192	10,197555	787,546922
3	221,1596	207,9261	352,2097	21,376527	22,275085	10	9	144,2836	131,050049	20,39511	785,211752
4	194,6635	187,059	251,3529	18,906562	19,940661	31	28	64,293869	56,689362	11,9509	825,068729
5	230,2085	191,2128	260,6722	20,949929	16,33006	10	13	69,459488	30,463776	10,042474	311,267583

FIGURE 5.3 Morphometric values representative of standard morphological configurations for a single profile. The meanings of the table attribute values are described in the red callout boxes in the sketch. From Fantozzi et al. (2023).

5.1.4 Numerical testing: the case study of Siena

The validity of this automated system and the regulatory proxies themselves was tested through specific case studies, with one case study focused on the urban area of Siena. (Ariano et al. 2026/Manuscript under review). Chosen for its conformation of elongated ridges and, above all, for its seismic-stratigraphic peculiarity, Siena is built on deposits of Pliocene marine sediments that present relatively uniform geomechanical characteristics throughout the relief (FIGURE 5.4). This homogeneity is fundamental, as it allows for the isolation of "shape" (topographic) effects from "deposit" (stratigraphic) effects, preventing the two phenomena from overlapping indistinguishably.

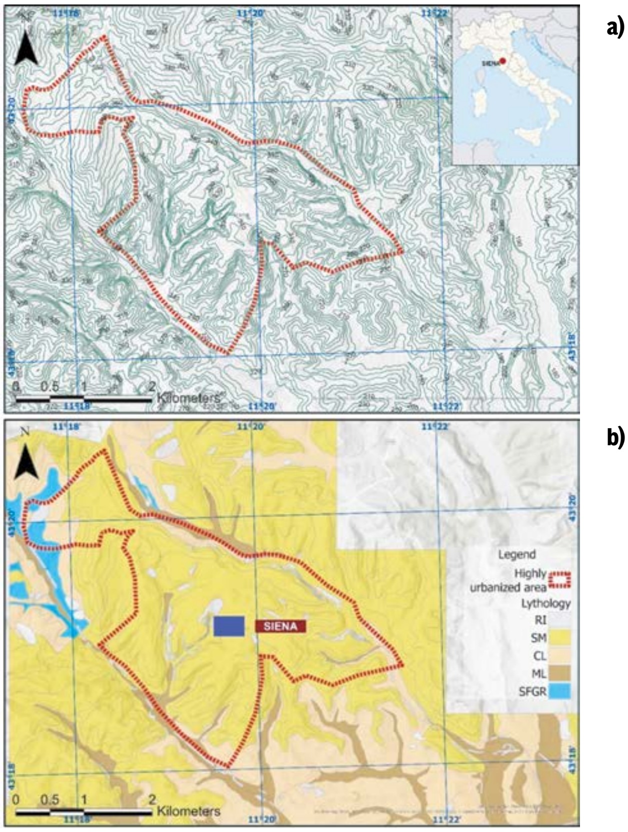

FIGURE 5.4 a) contour levels in the municipality of Siena. The settlement is clearly located on areas of higher elevation, with abrupt slope changes evident in regions where contour lines are more closely spaced. The red dashed line delineates the area with a higher residential density in the surroundings of Siena's historic centre. b) Geological–technical map of the historic center of Siena, based on the Seismic Microzonation study (SM-WB 2008). Areas outside the study extent are not displayed. Lithological units are labeled according to the legend.: RI – anthropogenic soils; SM – silty sands (marine terrace deposits); CL – inorganic clays of medium–low plasticity; ML – inorganic silts and fine silty/clayey sands (intermontane basin deposits); SFGR – cemented, fractured or weathered granular substrate. The red dashed line delineates the same area of the "top figure", while the blue rectangle refers to an area examined in Figure 5.7. The figures have been generated using Esri ArcGIS Pro Layout tools (ESRI 2023). Base data: SRTM DEM (NASA), accessed May 2025.

A large set of morphologies associated with slopes, scarps, and crests defined in the Code were identified based on the automatic procedure described in the previous section (FIGURE 5.5). To check amplification factors defined in the norm for the configurations in FIGURE 5.1, possible expected amplification effects have been numerically estimated along profiles obtained by the approach describe above.

FIGURE 5.5
Transects relative to the morphological classes in Figure 5.1 identified by the computer-aided procedure by Fantozzi et al. (2023). T1 class morphologies are not shown.

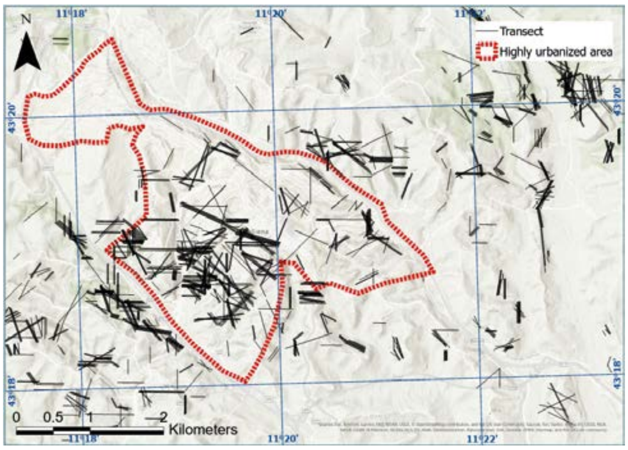

To this purpose and by following the assumption that each profile is the expression of a 2D morphology, a two-dimensional finite element (FEM) analysis has been performed by using software AlgoShake2D (Algoritmiqa, 2025), which is the new proprietary version of the code LSR2d, tested, e.g., by Faraone et al. (2023). This numerical tool relies on the same numerical procedure adopted in the older QUAD4M (Hudson et al. 1993). The input motion is applied as a set of acceleration time histories to all nodes at the base boundary of the mesh, which is modelled as a compliant base.

Twelve representative transects, covering the different morphological configurations, were randomly selected for numerical modelling. The selection of the transects was carried out in proportion to the occurrence of the various morphological types identified within the study area, to ensure a comprehensive representation of the overall topographic setting. Several relatively 'flat' profiles (with a maximum elevation above the reference level lower than 30 m) were included to test the hypothesis that such configurations produce negligible amplification effects. In the whole area, no profile has been found corresponding to the T3 morphological class. All transects extend between two topographic minima, with an average length of 500 meters and a maximum of 900 (TABLE 5.1).

The simulation adopted linear visco-elastic constitutive equations and was driven by a seismic input consisting of seven spectro-compatible accelerograms, selected via Rexel-Web (Russo et al. 2022) based on the reference seismic hazard map of Italy (Meletti and Montaldo, 2007). These records were selected to be compatible with the reference target spectrum defined by the Italian seismic code (NTC18) for a return period of 475 years, considering rock outcropping conditions (soil class A) and flat topography. To ensure consistency with the local seismic hazard, the database search was constrained within a magnitude range of 3.5–6.0 and an epicentral distance range of 0–40 km.

TABLE 5.1
Comparison between outcomes of the numerical modelling and amplification factors by the norm (EC8, 2003). For each transect, the total length (in meters), the maximum relative elevation (DH) and the average slope (b) are reported along with the respective, morphological class (Figure 5.1). The maximum amplification expected from the norm (AF_Standards) is also reported along with the AF estimates provided by numerical modelling in the three ranges of periods.

Transect	Lenght (m)	ΔH (m)	β (°)	Class	AF_Standards	Max AF_Simulation		
						I°(0.1 - 0.5 s)	II°(0.4 - 0.8 s)	III°(0.7 - 1.1 s)
1	465	17	10,0	T1	1,0	1,1	1,1	1,1
2	278	43	10,5	T1	1,0	1,3	1,2	1,1
3	346	45	10,0	T1	1,0	1,1	1,1	1,1
4	906	28	10,0	T1	1,0	1,1	1,1	1,1
5	388	51	10,0	T1	1,0	1,2	1,2	1,2
6	670	34	10,0	T1	1,0	1,1	1,1	1,1
7	442	38	17,6	T2	1,2	1,2	1,2	1,1
8	664	44	17,0	T2	1,2	1,1	1,1	1,2
9	352	42	16,0	T2	1,2	1,2	1,2	1,1
10	442	36	16,8	T2	1,2	1,1	1,2	1,1
11	408	51	15,5	T2	1,2	1,3	1,3	1,2
12	456	63	30,1	T4	1,4	1,3	1,3	1,2

While the AF values in the norm are assumed to be frequency-independent, in the numerical analyses three amplification values have been obtained relative to three period ranges (I°: 0.1-0.5s, II°: 0.4-0.8s, III°:0.7-1.1s). This allows checking at what extent AF values depend on the vibration periods. This comparison has been performed at each point of the relevant profiles. An example of this comparison is reported in (FIGURE 5.6).

It is worth noting that the code adopts a conservative approach, and no de-amplification effect is assumed to exist: this last aspect should be accounted for when numerical outcomes will be compared with the amplification estimates provided by the proxies.

As concerns outcomes in TABLE 5.1, one can see that maximum AF values from the norm underestimate the ones obtained from numerical modelling relative to all transects of morphological class T1. This is true for all the period ranges. A conservative value is instead provided in case of Transect 12 (Class T4). In the most frequent configurations (T2 classes), the norm provides conservative values in 4 out of 5 cases considered.

In order obtain a more general comparison, whole set of AF values along each transect has been considered. In TABLE 5.2, the statistics are reported relative to the differences between the AF values from the norm and those from simulations at each point of the respective transect. One can see that, in general, average differences are close to zero, which means that norm provides nearly unbiased AF values relative to the three rages of period. As concerns T1 morphologies, average values are negative which means that the norm slightly underestimates actual amplification effects. In the other cases, the small bias is towards positive values in that the norm tends to overestimate AF values from modelling. The standard deviation of discrepancies between norm and numerical evaluations indicate that these are below 0.1 values with a probability higher than 84% (1s) along all the profiles and for all the vibration periods and are below 0.2 with a probability higher 95% (2s).

TABLE 5.2
Table 5.2. Statistics relative to the comparison of the AF values provided along each transect for each transect in Table 5.1 by the norm (EC8, 2003) and those obtained from numerical modelling.
For each transect, the average difference and respective standard deviations are reported relative to the three ranges of periods.
Negative averages indicate that AF values from the norm tend to underestimate the ones provided by numerical modelling.

Transect	Class	AF [0.1-0.5s]		AF (0.4-0.8s)		AF(0.7-1.1s)	
		μ	σ	μ	σ	μ	σ
1	T1	-0,03	0,04	-0,04	0,04	-0,03	0,03
2	T1	-0,09	0,12	-0,12	0,08	-0,07	0,04
3	T1	-0,04	0,04	-0,06	0,05	-0,04	0,04
4	T1	-0,02	0,03	-0,03	0,03	-0,04	0,02
5	T1	-0,07	0,07	-0,13	0,09	-0,09	0,06
6	T1	-0,02	0,03	-0,04	0,04	-0,07	0,06
7	T2	0,11	0,05	0,06	0,05	0,07	0,04
8	T2	0,08	0,05	0,05	0,03	0,03	0,02
9	T2	0,04	0,04	0,01	0,02	0,05	0,03
10	T2	0,09	0,03	0,05	0,03	0,07	0,02
11	T2	0,05	0,07	-0,01	0,06	0,01	0,02
12	T4	0,14	0,09	0,10	0,08	0,14	0,09

FIGURE 5.6
Outcome of numerical simulations relative to a Transect. The lower part of the figure shows the morphological profile of the analysed transect, with elevation on the vertical axis and transect length on the horizontal axis. The upper part of the figure graphically compares the AF values: the regulatory value and those derived from 2D numerical modeling across the three reference period intervals.

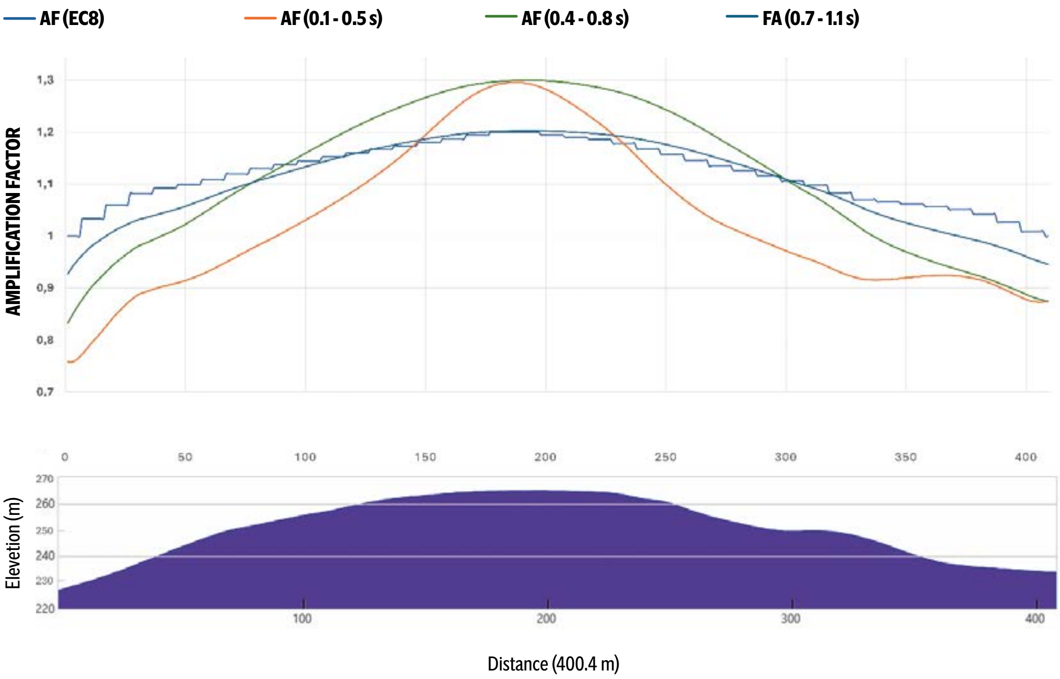

5.1.5 Applicability of NTC18 topographic proxies

The analysis of the results of this comparison brought to light crucial issues regarding the objectives and implicit limitations of the standard itself. The first problem concerns the expected accuracy: the very coarse classification of the coefficients (1.0, 1.2, 1.4) implicitly suggests that variations below 0.2 are not considered significant relative to the overall uncertainties (such as the direction of the impinging seismic waves).

However, this assumption contrasts with the regulatory prescription that imposes a rigorous linear decay of the amplification factor along the slope, making it difficult to statistically evaluate the "weight" of the discrepancies observed between the calculated models and the standard.

Furthermore, the question arises as to whether regulatory factors should be considered as conservative estimates or as expected averages. The numerical comparison suggests that, in situations conforming to classes T2, T3, and T4, the standard provides estimates of the maximum amplification effects at the summit that are tendentially conservative. Conversely, for "minor" morphologies (reliefs less than 30m or slight slopes, Class T1), the standard appears to underestimate the phenomenon, ignoring amplifications of the order of 1.1 calculated by the numerical model.

Along the slopes, the regulatory proxies provide on average unbiased values (with mean differences close to zero), but in many specific cases reach discrepancies of the order of 0.1. Depending on how the "undeclared" objectives of the standard are interpreted, these discrepancies may be considered negligible or, conversely, significant for design purposes.

Beyond these numerical tolerances, the main problem emerging from the comparison concerns the selection of morphologies. By applying rigorous criteria, consistent with both wave physics and current codes, the number of real situations assimilable to a purely 2D morphology is drastically reduced. This implies that the proxies provided by NTC/EC8 (and their automatic mapping) can be safely applied in only a very limited number of contexts, making them ineffective for a general mapping of topographic risk on a large scale (FIGURE 5.7).

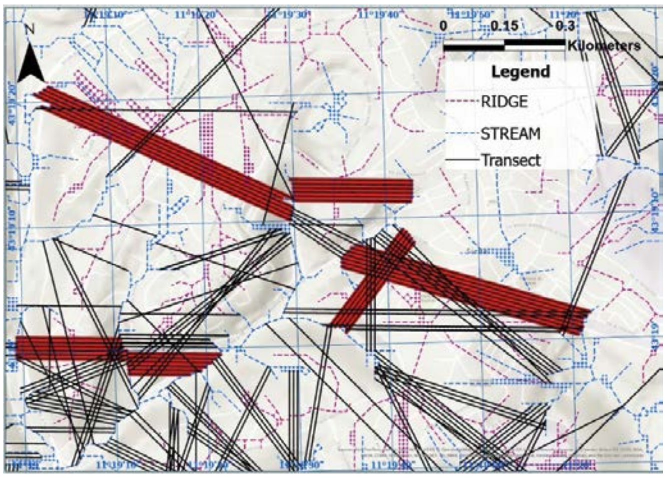

FIGURE 5.7
Extract from a Map Frame produced using ArcGIS Pro, showing the historic centre of Siena, refer to the blue rectangle in Figure 5.4b. The layout displays ridge lines as dashed purple lines and drainage lines as dashed blue lines. The black lines represent the transects identified using the EC8-based proxy. The red buffer, shown only on selected transects, highlights those correctly classified as two-dimensional morphologies for this case study.

The research conducted has addressed a fundamental gap in the management of topographic seismic Hazard. The primary objective was achieved through the formalization of an analytical, objective, and automated workflow capable of translating the sometimes-ambiguous geometric prescriptions of seismic codes (NTC18, EC8) into rigorous computational parameters.

However, the application of this protocol has brought to light intrinsic criticalities within the regulations themselves that cannot be ignored. The systematic comparison between regulatory proxies and advanced numerical modelling (conducted in the Siena case study) highlighted that the "ideal" two-dimensional geometry envisioned by legislators is, in practice, an abstraction rarely found in the complex geomorphological reality of Italy. The analyses clearly show that the number of real-world situations assimilable to a purely 2D morphology is extremely limited; this raises questions about the actual effectiveness of proxies designed for symmetric and infinitely elongated profiles when applied to asymmetric ridges, irregular reliefs, or complex urban contexts (Ariano et al. 2026).

From an engineering safety perspective, the results indicate that the amplification factors (AF) proposed by the codes tend to be conservative for steeper classes (T2, T3, T4), ensuring an acceptable margin of safety for design. Conversely, a concerning tendency toward underestimation was identified for "minor" reliefs (Class T1), where calculated amplifications in the order of 1.1 are ignored by the code, introducing a potential unaccounted risk in areas erroneously considered "neutral." Furthermore, the regulatory requirement for a linear decay of the amplification factor along slopes proved to lack solid statistical support in numerical models, suggesting the need to revise the spatial distribution of amplification effects along the relief profile.

Looking ahead, the findings unequivocally indicate that the natural progression of this research line must involve moving beyond the two-dimensional constraint. While 2D proxies represent a necessary starting point, they are unable to capture crucial physical phenomena such as three-dimensional focusing, lateral diffraction, and relief asymmetry, which can significantly alter the local seismic response. The next methodological step, already under development, involves the integration of 3D morphometric analyses capable of characterizing the territory in a holistic and spatially continuous manner. These new indicators must be calibrated through advanced 3D seismic modeling, thereby providing the engineering community and planning authorities with predictive tools that are increasingly consistent with the physical and geological reality of the territory.

5.2 Experimental testing of NTC18 proxies for stratigraphic and topographic classes

A statistical correlation analysis was completed at the national scale between different site proxies archived in the site characterization CRISP database (http://crisp.ingv.it/; Mercuri et al. 2023), to evaluate the most appropriate indicators deduced from experimental measurements that can describe the site transfer function (Cultrera and Mercuri, 2025).

CRISP is an advanced, freely accessible database implemented for the site characterization of stations within the Italian Seismic Network (RSN), operated by the INGV. It is structured to integrate different types of information that define the site response conditions, such as station metadata, geological and stratigraphic characterization, seismological analysis of recorded data, on-site geophysical information, site and topographic classification according to current Italian building code (NTC18) and European (EC8) regulations.

The core of the analysis focuses on the Horizontal-to-Vertical spectral ratio (HVSR), derived from both earthquake (HVeq) and ambient noise (HVnoise) measurements at 320 common stations, as a primary indicator of site effects. This seismological proxy is then correlated with other site indicators, including Lithological classification, Site and Topography Class (NTC18, 2018), Local Magnitude (ML) correction term (indicating magnitude over/underestimation at a site).

This extensive dataset allowed us to group the HVSR curves into four distinct clusters (FIGURE 5.8a) based on their shapes (e.g., flat, low-frequency amplification, high-frequency amplification, large intermediate-frequency amplification), revealing that: i) approximately half of the permanent stations exhibit significant amplification, with amplitudes exceeding 2; ii) although HVSR from noise generally mirrored that from earthquakes, it often showed lower or equal amplitudes but higher resonance frequency amplitudes, likely due to different wavefield compositions. The correlation between HVSR and other proxies displayed a weak but statistically significant dependence on lithology, site classes and magnitude residuals. Specifically, as soil characteristics degrade, the resonance frequency decreases, and its amplitude slightly increases (FIGURE 5.8b). Furthermore, local magnitude tends to be overestimated at sites exhibiting HVSR amplification at frequencies below 2-3Hz and a decrease toward negative values in ML residuals was observed corresponding to the degradation of soil properties (e.g., hard sites in class A yielded positive residuals, while soft sites in class C showed negative residuals). No correlation was found with topographic classes.

The analysis demonstrates a weak but statistically significant dependence of HVSR on lithology, site classes, and ML residuals. The primary suggestion of the research is that integrating seismological data, including HVSR curves, fundamental frequency, and amplitude, can substantially optimize soil class definitions within the updated Eurocode 8 framework, overcoming some of the limitations and uncertainties associated with current building code classifications.

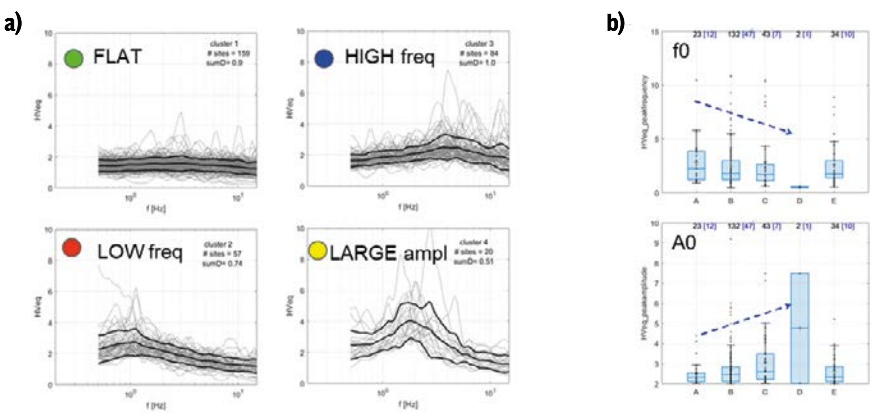

FIGURE 5.8
a) HVSR curves on earthquake from 320 sites grouped in 4 clusters: grey lines refer to each station result, black lines represent the mean +- 1 standard deviation; each plot displays the number of curves (# sites) and the within-cluster sums of observation-to-centroid distances, normalized to the maximum value among the 4 clusters (sumD).
b) Frequency peak (f_0), its amplitude (A0) versus site class from NTC18; numbers in black next to the boxplots indicate the samples used for each class (i.e. the number of sites with a frequency peak), while numbers in square brackets indicate sites belonging to that site class but without a frequency peak, i.e. having flat HVSR curve. Modified after Cultrera and Mercuri, 2025.

6. Estimate of susceptibility areas for seismically induced landslides

6. Estimate of susceptibility areas for seismically induced landslides

Slope stability is governed by the interaction between predisposing factors (geological and geomorphological) and triggering forcings: rainfall is the most frequent trigger (Crozier, 2010), although snowmelt, thermal variations, anthropogenic pressures and seismic shaking may also contribute significantly (Gariano and Guzzetti, 2016; Jaafari, 2024). Landslide susceptibility has been investigated using statistical and machine learning approaches (Loche et al. 2022; Lombardo and Mai, 2018; Reichenbach et al. 2018), heuristic methods (Ruff and Czurda, 2008), hybrid approaches (Pham et al. 2019; Wang et al. 2020) and physically based models (Alvioli et al. 2023; Mergili et al. 2014a,b), the latter being capable of explicitly representing mechanical processes through the integration of geotechnical parameters, hydrological conditions and, where available, seismic input.

A critical issue common to all approaches concerns the availability, quality, and representativeness of input data. Uncertainty associated with geotechnical parameters and the spatial heterogeneity of materials may compromise the reliability of model estimates (Shao and Xu, 2022), thus requiring observational calibration procedures (Marin et al. 2021) and probabilistic treatments of uncertainty (Pakyuz-Charrier et al. 2018; Wang et al. 2010; Zhang et al. 2010), implemented within reproducible frameworks and evaluated using objective performance metrics (e.g. AUC–ROC; Mevoli et al. 2026).

These challenges are further amplified in the case of coseismic landslides, where geotechnical uncertainties are compounded by those related to the characterisation of seismic input, local site response variability and the selection of representative dynamic parameters (Jibson et al. 2000; Keefer, 1984; Marano et al. 2010). In this context, purely statistical approaches show limited capability to coherently integrate geotechnical variables and mechanical parameters (Del Gaudio and Wasowski, 2004; Lombardo and Tanyas, 2022; Tanyas et al. 2019), reinforcing the need for models in which physical processes are explicitly represented.

Within this framework, the application of physically based models requires a robust and coherent definition of input parameters, as well as calibration and validation procedures capable of ensuring that simulations are representative of real conditions and their associated uncertainties.

On the basis of these premises, the following sections systematically describe the operational workflow developed within the project, highlighting the logical progression from the construction of geological–technical datasets to distributed slope stability modelling under both static and seismic conditions.

Section 6.1 presents the activities devoted to the geotechnical characterisation of the national lithological cartography. First, section illustrates the construction of the national geotechnical parameter dataset (Monte et al. 2024a, b), derived from a systematic review of the international literature and subsequent association with national lithological classes. The outcome is a structured and statistically characterized database from which spatially distributed maps of cohesion, friction angle, porosity and associated uncertainty are derived, providing the quantitative input for stability analyses.

Section 6.2 describes the activities focused on susceptibility to rotational–translational landslides. The probabilistic observational calibration (back-analysis) procedure implemented using the physically based model *r.slope.stability* (https://www.landslidemodels.org/r.slope.stability/) is presented, based on Monte Carlo sampling and systematic comparison with high-quality landslide inventories. The supra-regional applications under both static and pseudostatic conditions are then illustrated, integrating spatially distributed PGA maps. The results show the model response under different hydrological scenarios, with and without seismic input, highlighting the combined effects of forcings on the probability of instability *(pfail)*, the factor of safety *(FS)* and the depth of critical slip surfaces. They demonstrate the robustness and transferability of the workflow towards national-scale applications.

Finally, Section 6.3 outlines the activities concerning susceptibility to rockfalls. The three-dimensional physically based model *r.stone* (Guzzetti and Alvioli, 2025; Alvioli et al. 2024a), implemented in GRASS

GIS, is described for the simulation of trajectories and runout, both in a "static" configuration (with sources controlled by morphometric factors) and in a seismically induced configuration, through a phenomenological coupling between detachment probability and ground shaking based on PGA.

6.1 National geotechnical parameter dataset

Physically based modelling of landslide susceptibility requires the availability of representative and spatially distributed geotechnical parameters capable of describing the mechanical behaviour of materials under both static and pseudo-static conditions. However, geological and lithological maps commonly used for territorial-scale applications do not provide quantitative information on the key geotechnical parameters, thus limiting their direct use in stability models. Within the Project PRIN SERENA, efforts were made to bridge this gap through the construction of a structured geotechnical database and its integration with the existing national-scale lithological cartography (Bucci et al. 2022), as the Geological–Technical Map (Bucci et al. 2026 – in preparation), described in the previous section, was still under development at the time.

The activity focused on the systematic collection of key geotechnical parameters for slope stability modelling, in particular effective cohesion, effective friction angle and porosity, selected because they are directly involved in the definition of shear strength. Data were retrieved through a critical review of the international peer-reviewed scientific literature, conducted according to rigorous and reproducible criteria. Overall, more than 100 scientific publications were analysed, from which over 2,300 geotechnical parameter records were extracted, referring to approximately 1,800 samples and more than 200 different lithotypes distributed worldwide.

For each record, detailed information was collected regarding material type, geographical location, data acquisition methods (laboratory testing, in situ testing or indirect estimates), and the values of the geotechnical parameters. Particular attention was paid to verifying data quality and reliability, harmonizing units of measurement and excluding values not representative of natural material conditions. This process resulted in a coherent dataset suitable for use as a basis for regional- and national-scale analyses.

Given the high variability of lithotypes reported in the literature, it was necessary to associate the collected geotechnical parameters with the lithological classes of the Lithological Map of Italy proposed by Bucci et al. (2022). This operation, conducted on an expert-judgement basis, enabled more than 200 lithotypes to be grouped into a limited number of homogeneous lithological classes represented in the Bucci et al. (2022) cartography, consistent with the distributed modelling approach adopted in the project. For each lithological class, descriptive statistics (median, percentiles and quartile coefficients of variation, CQV in FIGURE 6.1) were computed to represent both the characteristic values of the geotechnical parameters and the associated degree of uncertainty. These statistics were then used to derive spatially distributed geotechnical maps at national scale, supporting the integration of parameters into landslide susceptibility models (FIGURE 6.1).

The activity also led to the publication of a peer-reviewed article in an international journal, in which the data collection and harmonization methodology, the database structure and the main potential applications in the fields of geomechanically modelling and slope stability are described in detail: Monte et al. (2024b).

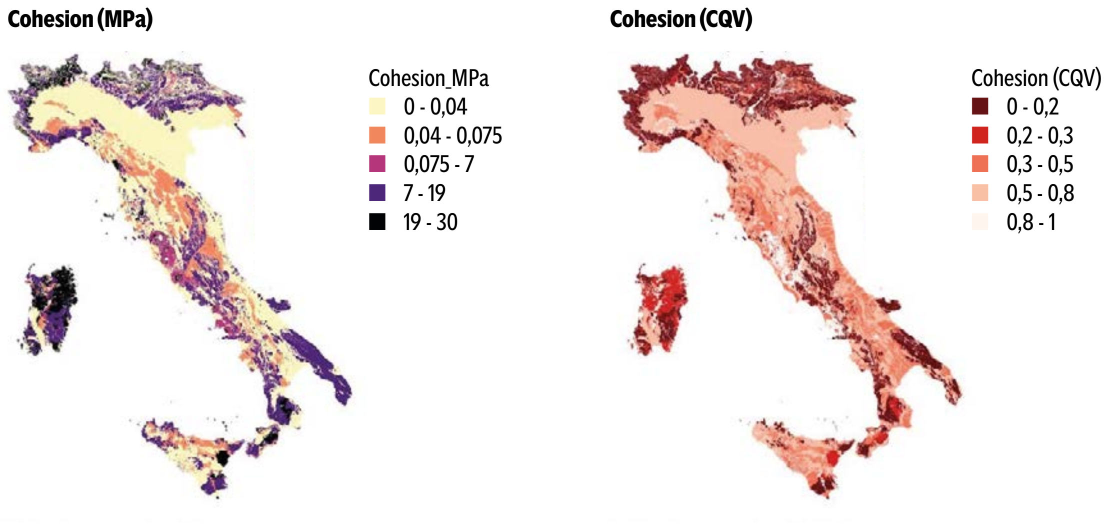

FIGURE 6.1 National maps of the main geotechnical parameters (cohesion, friction angle and porosity) and their associated uncertainty (CQV), derived from the linkage between the geotechnical dataset and the lithological classes of Bucci et al. (2022). From Monte et al. (2024a, b).

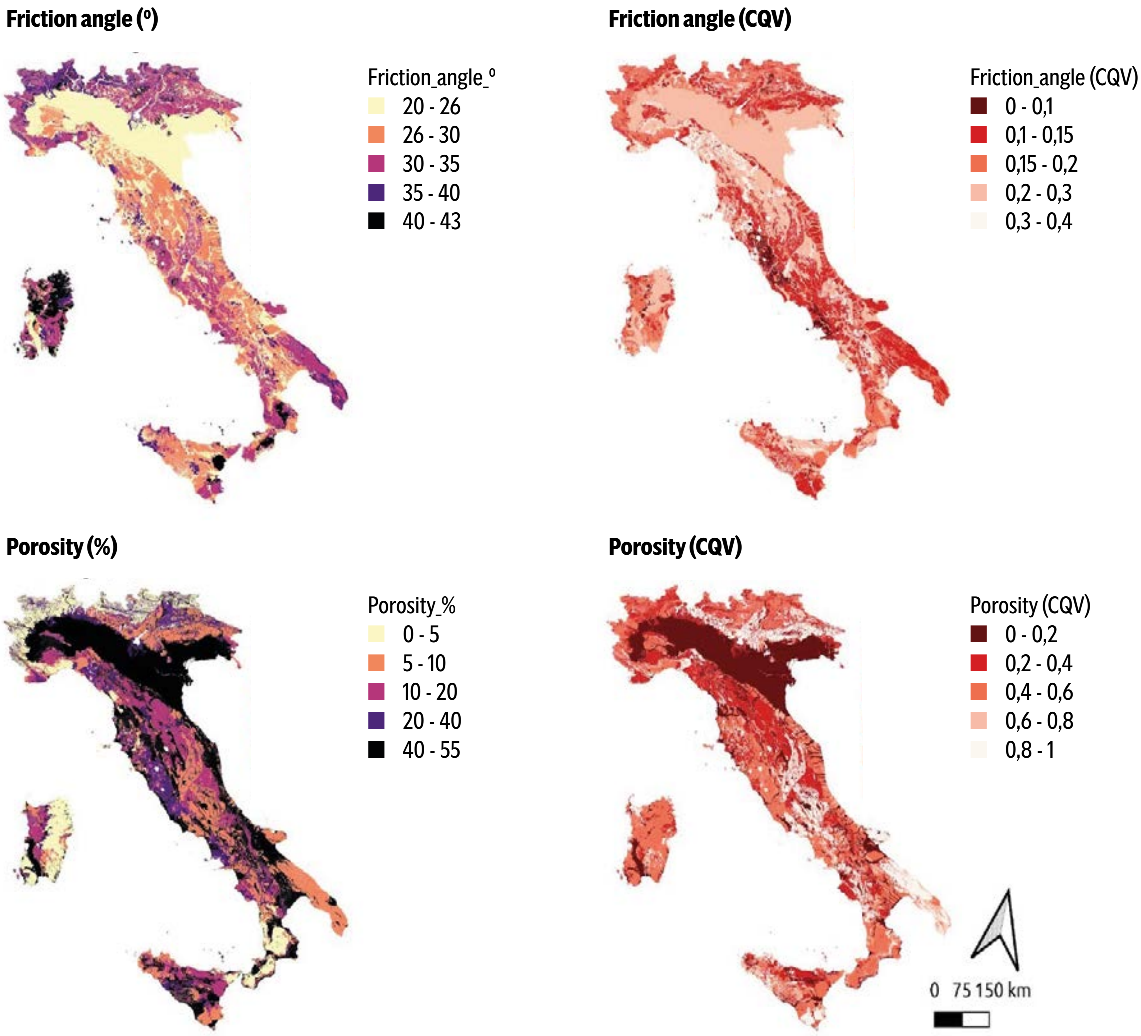

6.2 Susceptibility to Rotational–Translational Landslides

6.2.1 Observational Calibration (Back-Analysis) and Probabilistic Treatment of Uncertainty

Starting from the national dataset of geotechnical parameters (Monte et al. 2024a, b), associated with the Lithological Map of Bucci et al. (2022), a parametric reorganization was developed based on the new geological–technical classes illustrated in Section 6.1. The aim was to provide a more effective description of the mechanical behaviour of geological units in relation to slope stability and seismic response.

However, prior to employing these parameters in landslide susceptibility modelling, a calibration procedure was undertaken to reduce the uncertainties associated with parameter values. This aspect is particularly relevant at regional scale, where parameters derived from the international literature, although statistically robust, may not fully reflect the local combination of lithology, weathering/fracturing state, thickness of superficial deposits and land-use conditions. To address this issue, we defined an observational calibration (back-analysis) procedure designed for regional contexts and replicable across extensive domains.

The calibration strategy was implemented using the open-source software *r.slope.stability* (Mergili et al. 2014a, b), a physically based model developed within the GRASS GIS environment for distributed regional-scale slope stability analysis. The model adopts a three-dimensional limit equilibrium formulation based on the Mohr–Coulomb failure criterion and allows exploration of a wide set of potential three-dimensional slip surfaces, represented by ellipsoids varying in depth, inclination and orientation. This configuration enables the simulation of both shallow translational mechanisms and deeper rotational instabilities, making it particularly suitable for applications over extensive and geologically heterogeneous territorial domains.

A relevant feature of the model is the possibility of representing a stratified system composed of a superficial soil layer and one (or more) underlying bedrock units, to which different geotechnical properties can be assigned. Furthermore, *r.slope.stability* allows analyses to be performed under static conditions, considering only gravitational and hydrological components, and subsequently to incorporate seismic input (through a Peak Ground Acceleration, PGA, value), ensuring consistency with the objectives of project concerning slope stability under seismic shaking conditions.

The approach adopted to refine the range of geotechnical parameters for slope stability modelling is based on the comparison between (i) stability maps derived from modelling and (ii) the spatial distribution of observed landslides (inventories referring to non-seismically induced landslides), in order to identify the combinations of cohesion (*c*) and friction angle (*φ*) with the greatest capability to discriminate between unstable and stable areas.

The procedure is structured as follows.

i) Definition of initial parameter ranges.
For the bedrock, the initial ranges of effective cohesion (*c*), effective friction angle (*φ*) and maximum porosity (used as a proxy for potential water content) were derived from the dataset of Bucci et al. (2026 – in preparation), which integrates the parameter ranges defined for lithotypes (Monte et al. 2024a, b) within the new geological–technical classification. For the soil layer, the following intervals were adopted: 0–19 kPa for c and 15°–45° for φ, with water content ranging between 0–50% and a unit weight of 13,000 N/m^3 (Monte et al. b); soil thickness was assigned using the *Rooting Depth of Italy* dataset (Rivieccio et al. 2020).

ii) Definition of calibration units and representation of uncertainty.
Calibration of c and φ was performed separately for each combination of lithological unit and land-use class (reclassified into urban, agricultural, woodland, grassland and other, based on Corine Land Cover data), in order to account for possible systematic differences in the mechanical properties of superficial materials. To represent the intrinsic uncertainty of geotechnical properties, parameter variability was explicitly modelled through Monte Carlo sampling. For each ellipsoidal slip surface hypothesised by the *r.slope.stability* model and for each lithological unit–land-use combination, random series of c and φ values were generated, with cohesion sampled from lognormal distributions and friction angle from normal distributions, within the assigned ranges.

iii) Probabilistic simulations and comparison with inventories.
The multiple parameter combinations generated for different ellipsoidal slip surfaces were used by *r.slope.stability* to compute the factor of safety *(FS)*. At cell scale, the probability of failure (pfail) was estimated as the frequency of unstable conditions (*FS* < 1) across the different Monte Carlo realisations for each individual ellipsoid representing a potential slip surface. The lowest *pfail* value among those generated by the various ellipsoids was then assigned to each cell.
The resulting maps were subsequently compared with the IFFI landslide inventory, specifically considering the portion of each landslide polygon identified as the initiation zone.

iv) Optimisation and parameter selection.
Calibration quality was assessed using objective classification metrics, in particular *AUC–ROC* and Balanced Accuracy (BA). The procedure led to calibrated parameter ranges that were often narrower than the initial ones, indicating a refinement of estimates and improved consistency with local conditions represented in the inventories. A complete application of the workflow was described for the Molise case study (Monte et al. in press), through 150 iterative runs aimed at identifying parameter combinations with maximum discriminant capability.

To ensure that all Italian lithological units were involved in the calibration phase, specific territorial domains characterised by high levels of completeness and accuracy in landslide inventories were identified. These areas, selected for their detailed mapping and representativeness of different morphological and lithological contexts, were used as benchmarks for the application of back-analysis and for model performance evaluation. For the Molise study area, the IFFI landslide inventory (Trigila et al. 2010) was used, which in this region is characterised by high quality and detail (Loche et al. 2022). Other areas considered include Valcamonica–Valseriana, Lecco, Sanremo, Staffora, Umbria–Marche, Lunigiana, the Setta River basin, Basento and Messina. Together, these constitute a set of calibration sites ensuring adequate sampling of Italy's geological–technical and geomorphological variability. The landslide inventories available in these areas were produced by CNR IRPI and have been employed in various applications (e.g. Marchesini et al. 2014).

The use of these reference domains made it possible to derive calibrated parameter ranges consistent with observed instability conditions, reducing reliance on average values derived solely from literature and improving the territorial representativeness of the geotechnical parameters assigned to lithological and geological–technical units. The multi-area calibration also strengthened the transferability of the resulting parameter set, making it suitable for modelling applications over extensive domains. The calibrated geotechnical parameters were subsequently adopted as input for the supra-regional susceptibility analyses described in the following sections.

6.2.2 Supra-Regional Applications: Static and Pseudostatic Analyses with PGA

Hydrological scenarios

Slope stability simulations were performed considering two idealised hydrological configurations, introduced to represent limiting conditions of water content within the materials. The first configuration corresponds to completely dry conditions, in which both the soil cover and the underlying bedrock are assumed to be unsaturated. The second configuration represents fully saturated conditions, with saturation affecting both the soil layer and the bedrock. These hydrological settings were consistently adopted in both the static and pseudostatic analyses described below.

Static analyses

Static analyses were conducted to assess slope stability under the sole action of gravitational and hydrological forcings, providing a baseline framework for comparison with the pseudostatic simulations. Potential failure geometries were explored using three-dimensional ellipsoidal slip surfaces, imposing a maximum depth at the centre of the ellipsoid of 10 m, in order to represent both shallow mechanisms and relatively deeper instabilities. Soil thickness was assigned in a spatially variable manner, as described in Section 6.1, while the maximum depth of the bedrock was set to 50 m.

The planimetric dimensions of the ellipsoids were varied, with lengths ranging from 20 to 200 m and widths from 20 to 150 m. To avoid unrealistic geometries, the length-to-width ratio was constrained within the interval $1 \leq L/W \leq 2.39$. Slip surfaces were sampled with high spatial density to ensure adequate exploration of the space of potential instability conditions.
Static simulations were performed in probabilistic mode, using the geotechnical parameters and sampling distributions defined in Section 6.1. From the simulation results, spatially distributed maps of mean factor of safety *(FS)*, probability of failure *(pfail)* and the main geometric properties associated with the critical slip surface were derived.

Pseudo-static analyses

Pseudostatic simulations were carried out to evaluate slope stability under seismic loading. These analyses build upon the previously described static configurations, with the addition of a seismic forcing component, thus enabling explicit assessment of the contribution of ground shaking to the reduction of stability conditions.
A pseudostatic approach was adopted, in which earthquake effects are represented by introducing an equivalent horizontal force applied to the potentially unstable mass. Pseudostatic analyses were conducted in probabilistic mode, using the same geotechnical parameters and sampling distributions as in the static analyses, thereby ensuring methodological consistency across the different simulated scenarios.
Operationally, a raster map of Peak *Ground Acceleration (PGA),* expressed in m/s^2 and describing the spatial distribution of expected maximum ground acceleration at the surface, was added to the input data used for the static analyses. The *PGA* map employed refers to four Italian regions (Emilia-Romagna, Umbria, Marche and Tuscany) and was produced as part of the activities the SERENA project (Section 3.4).
Within the *r.slope.stability* modelling framework, seismic loading is incorporated into the three-dimensional limit equilibrium formulation as a horizontal force F′ acting on each potentially unstable column, defined as:

eq.6.1) $$F' = G'K,$$

where G′ represents the effective weight of the column and K is the seismic coefficient, defined as:

eq.6.2) $$K = \frac{PGA\, C_s}{g},$$

where g denotes gravitational acceleration and C_s is the dimensionless pseudostatic coefficient, which controls the fraction of peak ground acceleration transferred to the potentially unstable mass in the form of an equivalent horizontal force.

In the present study, the coefficient C_s was set equal to 1. This choice is justified by the fact that the *PGA* maps used already explicitly and spatially incorporate the effects of the seismic source, wave propagation and site conditions. Within this supra-regional-scale application framework, the assumption $C_s = 1$ allows the full information contained in the *PGA* to be directly transferred to the pseudostatic calculation, avoiding additional simplifications or arbitrary assumptions regarding seismic load reduction.

The force F′ is then decomposed into components parallel and normal to the potential slip surface and included in the calculation of the factor of safety *(FS)*, contributing to a reduction of the stabilising component of the normal stress and an increase in the shear stress acting along the failure surface.

Application of the methodology at regional and supra-regional scales

A first complete application of the methodology developed within the PRIN SERENA Project is presented in a manuscript currently under submission, in which the entire operational workflow is implemented, from the geological–technical characterisation of the territory to the observational calibration of geotechnical parameters, and finally to landslide susceptibility modelling under both static and pseudostatic conditions, within a multi-forcing framework that considers the interaction between rainfall and seismic shaking.

The study was applied to the 16 August 2018 seismic event in Molise and represents the first application of landslide susceptibility modelling with seismic input using the *r.slope.stability* software. The results provide concrete evidence of the technical feasibility and robustness of the approach at regional scale, highlighting the model's capability to coherently integrate geological–technical, hydrological and seismic information.
Building on the experience gained in the Molise case study, the methodology was subsequently extended to supra-regional scale, encompassing the territories of Tuscany, Emilia-Romagna, Umbria and Marche. The selection of these areas was motivated by the availability of spatially distributed seismic input cartography, in particular raster maps of *Peak Ground Acceleration (PGA)* obtained in the Section 3.4.
Within these territorial domains, it was therefore possible to systematically apply both static stability analyses and pseudostatic analyses, considering the two previously defined hydrological configurations (fully saturated and completely dry conditions).

Results

The maps of probability of failure (*pfail,* FIGURE 6.2) reveal a systematic model response across the different simulated scenarios, with clear differences both between static and pseudostatic conditions and between dry and saturated hydrological settings. In general, the introduction of seismic loading leads to a widespread increase in the probability of instability, which is further amplified under saturated conditions. The pseudostatic–saturated configuration represents the most critical scenario, with extensive portions of the territory characterised by high *pfail* values.
The spatial distribution of areas with higher probability of failure is consistent with the lithological and geological–technical framework (FIGURE 2.3): clayey covers (C), sandy deposits (S), gravels (G), superficial lithified cover units (LC), and fractured or weathered bedrock units (SFAL, SFALS, SFCOS) exhibit particularly high susceptibility, whereas more competent lithologies (LP, LPS) generally display lower susceptibility values, except in sectors characterised by steeper slopes.

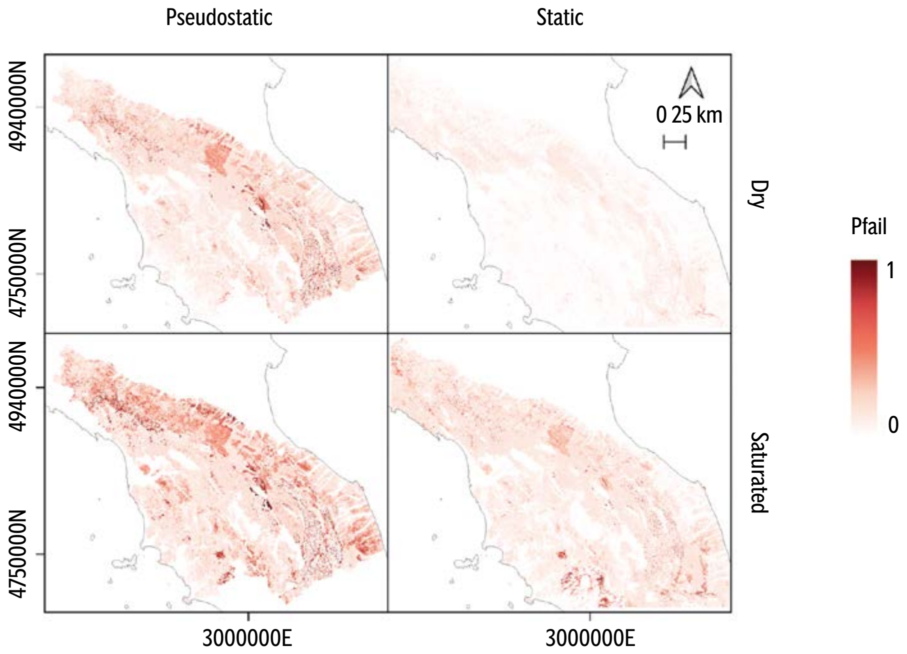

FIGURE 6.2
Maps of probability of failure (pfail) for pseudostatic (left) and static (right) analyses, under dry (top) and saturated (bottom) conditions. Darker tones indicate higher pfail values (0–1).

The factor of safety *(FS)* maps (FIGURE 6.3) provides a complementary and consistent picture with respect to pfail. Under pseudostatic conditions, both in dry and saturated scenarios, large portions of the study area exhibit *FS* values close to unity, indicative of widespread limit equilibrium conditions. This configuration is particularly evident in the pseudostatic–saturated scenario, where the combined effect of reduced effective stresses and the equivalent horizontal force associated with *PGA* results in a generalised decrease in the factor of safety.

Conversely, in the static simulations an overall increase in *FS* values is observed, with extensive areas characterised by greater stability, especially under dry conditions. In this case as well, the spatial distribution of *FS* values reflects the geological–technical framework: clayey units (C, S, G and LC) and fractured alternations (SFAL, SFALS, SFCOS) more frequently display values close to or below 1, whereas compact lithified rocks (LP) tend to maintain higher *FS* values.

FIGURE 6.3
Maps of the factor of safety (FS) for pseudostatic (left) and static (right) analyses, under dry (top) and saturated (bottom) conditions. Values close to 1 indicate limit equilibrium conditions; higher values indicate greater stability.

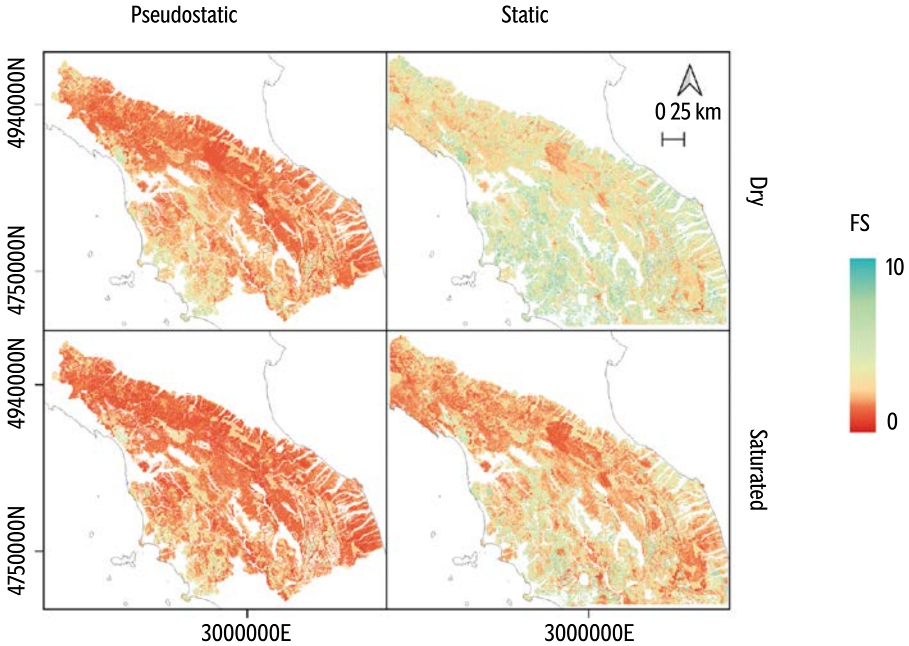

The maps of the depth of the critical slip surfaces (FIGURE 6.4) provide essential additional information regarding the potential geometry of failure phenomena. Across all scenarios, marked spatial variability in depth is observed, with higher values concentrated along the main morphostructural alignments and in mountainous sectors characterised by greater relief energy.

In the pseudostatic–saturated scenario, in addition to the increase in probability of instability, there is a tendency for the activation of deeper critical slip surfaces compared with static conditions, suggesting the potential involvement of larger volumes. Saturation, by reducing effective strength, promotes in several contexts the deepening of failure surfaces, particularly within stratified and fractured successions (SFAL, SFALS, SFCOS). In compact rock units, deeper critical surfaces tend to be concentrated in morphologically steeper sectors, whereas in weaker or more fractured lithologies they appear more extensive and distributed over broader areas.

FIGURE 6.4
Depth (m) of the critical slip surfaces identified by the model for pseudostatic (left) and static (right) analyses, under dry (top) and saturated (bottom) conditions. Higher values indicate deeper failure surfaces associated with conditions close to limit equilibrium.

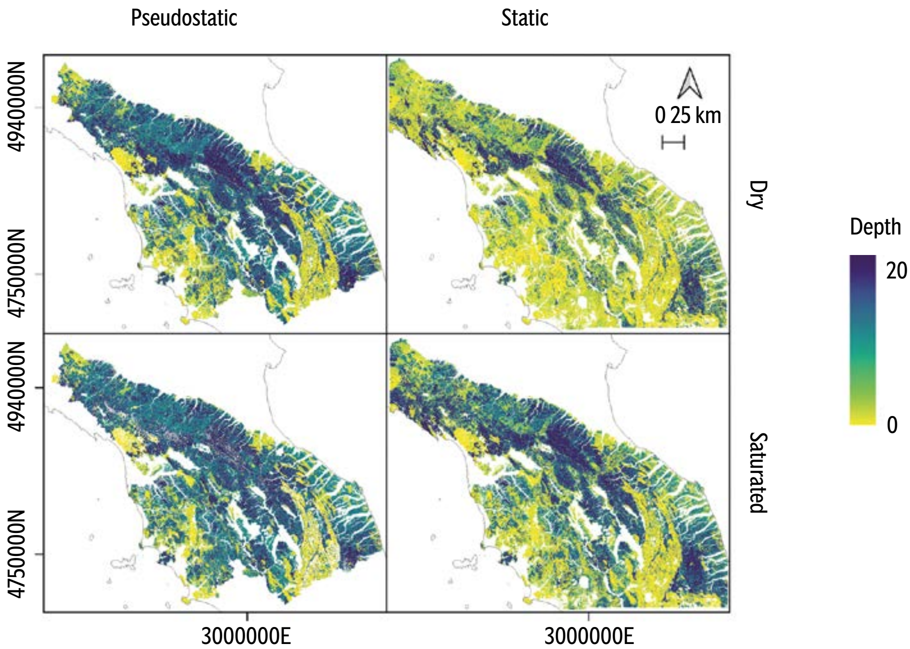

Overall, the integrated analysis of the pfail, FS and critical slip surface depth maps highlights a coherent model response to the different forcing scenarios and a clear correspondence with the geological–technical map. The interaction between the mechanical properties of materials, hydrological conditions and seismic input not only influences the probability of initiation, but also modulates both the degree of stability and the geometric scale of the potentially mobilisable volumes.

The pseudostatic–saturated scenario emerges as the most critical, both in terms of the areal extent of instability conditions and the depth of the failure surfaces, outlining a framework of high susceptibility in lithotechnical contexts that are mechanically weaker or structurally predisposed to instability.

6.3 Susceptibility to Rockfall Landslides

6.3.1 Physically Based Model for the Simulation of Rockfall Runout

Slope stability modelling across Italy was carried out using the software r.stone, a GRASS GIS module. A complete description of the software inputs, outputs and options is available on the official GRASS GIS add-on webpage for *r.stone:* https://grass.osgeo.org/grass-stable/manuals/addons/r.stone.html.

The three-dimensional physically based rockfall model adopted here was originally developed by Guzzetti et al. (2002) as proprietary software. It was subsequently translated and released as a GRASS GIS module named *r.stone* within the framework of the HySTC/RETURN project (Alvioli et al. 2024a). The r.stone module performs three-dimensional modelling of rockfall trajectories. A landslide block is idealised as a point mass, and the model simulates its trajectory as a sequence of falling, bouncing and rolling phases. The trajectory follows a digital terrain model (DTM), starting from one or more user-defined source points with a non-zero initial velocity, and stops downslope when all its kinetic energy has been dissipated (i.e. when a minimum velocity is reached) through bouncing and/or rolling on the ground.

Normal and tangential restitution coefficients describe the fraction of kinetic energy lost at each rebound, while a friction coefficient accounts for energy loss during rolling. The implementation of STONE within *r.stone* requires, in addition to the DTM, a minimum set of raster input maps, including a source map and three raster maps of numerical coefficients (see **TABLE 6.1** and Alvioli et al. 2021). The output consists of a raster map whose values correspond to the number of trajectories crossing each grid cell after completion of the simulation.

TABLE 6.1
Numerical values of the parameters used in STONE, with lithological classes from Bucci et al. (2021). STONE was configured to perform random sampling of parameter values within a ±5% range around the nominal values listed here. Values originally from Alvioli et al. (2021).

Class ID	Lithological Class	Dynamic Friction	Normal Restitution	Tangential Restitution
L1	Anthropic deposits	0.65	35	55
L2	Alluvial, lacustrine, marine, eluvial and colluvial deposits	0.80	15	40
L3	Coastal deposits, not related to fluvial processes	0.65	35	55
L4	Landslides	0.65	35	55
L5	Glacial deposits	0.65	35	55
L6	Loosely packed elastic deposits	0.35	45	55
L7	Consolidated elastic deposits	0.40	55	65
L8	Marl	0.40	55	65
L9	Carbonates-siliciclastic and marl sequence	0.40	60	70
L10	Chaotic rocks, melange	0.35	45	55
L11	Flysch	0.40	55	65
L12	Carbonate Rocks	0.40	55	65
L13	Evaporites	0.35	45	55
L14	Pyroclastic rocks and ignimbrites	0.40	55	65
L15	Lava and basalts	0.30	65	75
L16	Intrusive igneous rocks	0.30	65	75
L17	Schists	0.35	60	70
L18	Non-schists	0.30	65	75
L19	Lakes, glaciers	0.95	10	10

Within the software, the input DTM is treated as a regular triangular network constructed dynamically at runtime. Rockfall trajectories are computed using second-order parametric equations following a roto-translation of the coordinate system within the execution triangle. The calculation of each trajectory includes the random selection of an initial direction angle and cell-by-cell values of restitution and friction coefficients sampled from Gaussian distributions centred on the values specified in the corresponding input raster and bounded within ±10% of the central value. Owing to the random selection of the initial direction and parameters, and to the possibility of simulating multiple trajectories from each source cell, the output has a probabilistic interpretation.

In the following, we describe separately the modelling of rockfalls at national scale, independent of any specific triggering mechanism or event, and subsequently the modelling of earthquake-induced rockfalls in the study areas corresponding to the Italian regions of Tuscany, Umbria, Marche and Emilia-Romagna.

6.3.2 National-Scale Modelling

For the source map at national scale, we adopted a generalised version of the map introduced by Alvioli et al. (2021), who developed a method to parameterise a probability function *P(S)* based on expert mapping and statistical generalisation.

The function *P(S)* represents the probability that a grid cell, characterised by slope angle S on the TINITALY DEM, acts as a rockfall source, and has the following form:

Eq. 6.3) $P(S)_{s \leq a} = 0,$

Eq. 6.4) $P(S)_{s > a} = c\left(\frac{s}{90}\right),$

where the parameter c in Equations (6.4) was obtained through quantile regression of data derived from expert-based mapping (Alvioli et al. 2021), and the value of a was selected such that P(S) > 0.2. Since the number of trajectories simulated by STONE from each source cell is proportional to P(S), this assumption ensures that a minimum number of trajectories is generated, so that the results constitute a representative sample.

Separate regressions for parameter c were performed for each physiographic unit, shown in FIGURE 6.5 together with the corresponding parameter values. The original map introduced by Alvioli et al. (2021) was limited to areas adjacent to the national railway network; here, we adopt the same parameterisation shown in FIGURE 6.5 for the whole of Italy. The results of this generalisation were first obtained by Sarkar and Alvioli (2025a,b) within the framework of a separate research project (Alvioli and Melelli, 2025).

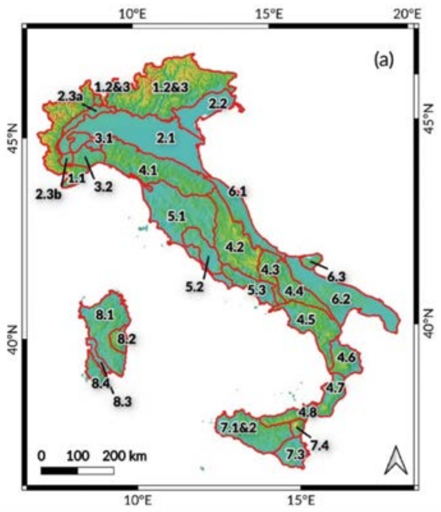

Area	c	Area	c
1.1	5.54	4.7	5.98
1.2	4.32	4.8	6.39
1.2	4.32	5.1	8.32
2.1	6.86	5.2	2.92
2.2	13.00	5.3	7.43
2.3a	8.59	6.1	5.41
2.3b	4.30	6.2	36.67
3.1	2.92	6.3	3.00
3.1	5.71	7.1-2	14.72
4.1	6.78	7.3	11.81
4.2	6.41	7.4	19.10
4.3	9.70	8.1	19.57
4.4	9.64	8.2	6.50
4.5	7.06	8.3	23.22
4.6	8.31	8.4	23.20

FIGURE 6.5 Physiographic regions of Italy, originally defined by Guzzetti and Reichenbach (1994) and modified by Alvioli et al. (2021). The coefficients obtained from the non-linear quantile regression using Equation (4) in the latter publication are reported in the table. Figure adapted from Alvioli et al. (2020).

The resulting raster map, containing non-zero integer values ranging from 0 to 100, is used by STONE to simulate a number of trajectories corresponding to the integer value assigned to each cell.

Each model realisation produces a raster map whose values represent the number of simulated trajectories crossing each grid cell. In order to derive a rockfall susceptibility zonation, it is necessary to define the coupling between the static model described in this section and the seismic forcing. This is addressed in the following section.

6.3.3 Modelling of Earthquake-Induced Rockfalls

In this subsection, we describe the phenomenological procedure used to couple seismic shaking with the three-dimensional model *r.stone* (Alvioli et al. 2022a, b).

Following a seismic event, the main ground effects include landslides. In Italy, the most common type of earthquake-induced landslides consists of rockfalls. Assessing the spatial extent and magnitude of an earthquake-triggered landslide event can be important both for preparedness planning and for emergency response operations. Here we describe an approach first developed by Alvioli et al. (2022b), subsequently refined and applied at broader scale to the 1976 Friuli earthquake by Alvioli et al. (2024b) and Alvioli et al. (2025), and at national scale by Alvioli et al. (2023).

The method is based on the simple observation that, for a given seismic event for which both *Peak Ground Acceleration (PGA)* and the triggered landslides are known, the spatial frequency of landslides is an increasing function of *PGA*. Assuming that the probability of a grid cell acting as a potential landslide source can be decomposed into a static morphometric factor and a ground-shaking factor, as follows:

Eq. 6.5) $$P^{dynamic}_{seismic},(S, ..., PGA) = P_{static}(S, ...)\, P_{seismic}(PGA),$$

where S is the slope angle, and "dynamic" denotes a time-dependent probability component. A simple model for the static probability, dependent solely on slope angle S, was introduced in Eq. (6.4), Section 3.1, and first proposed by Alvioli et al. (2021) for physics-based rockfall susceptibility assessment along the Italian national railway network. The ellipsis in *P*static (*S*, ...) in Eq. (6.5) indicates that more complex models for static source areas could be considered, such as models incorporating relative relief, as in Alvioli et al. (2022a), or relief and roughness, as in Pokharel et al. (2023), or multivariate models, as in Alvioli et al. (2026).

A simple model for the seismicity-dependent factor in Eq. (6.5) can be obtained by linearly transforming the *PGA* values recorded within the study area for a specific seismic event into the interval [0,1], as follows:

Eq. 6.6) $$P^{linear}_{seismic}(PGA) = \frac{PGA - PGA_{min}}{PGA_{max} - PGA_{min}},$$

where *PGAmin* and *PGAmax* are the minimum and maximum values of the *PGA* raster map. A more realistic model can be obtained through a non-linear mapping. A parametric function that has proven effective is the Normalised Tunable Sigmoid Function (NTSF), defined over the interval [0,1] as follows:

Eq. 6.7) $$P^{NTSF}_{seismic}(PGA) = \frac{1}{2} + \frac{1}{2}\,\frac{PGA' - kPGA'}{2k - 2k\,|PGA'| + 1'},$$

where k is a parameter controlling the slope of the function, and PGA' is defined as:

Eq. 6.8) $$PGA' = 2\,\frac{PGA - PGA_{cut}}{PGA_{max} - PGA_{cut}},$$

with the additional parameter *PGAcut*. The parameters in Equations (6.7) and (6.8) can be calibrated for a specific area, provided that an inventory of observed landslides is available for a given seismic event, together with the corresponding *PGA* raster map. FIGURE 6.6 shows different *PGA*-based functions (Eq. 6.7) for various parameter values. Previous (unpublished) studies have shown that optimal agreement with observed landslides is typically achieved for *PGAcut* = 0.017 and −0.5 < k < − 0.7.

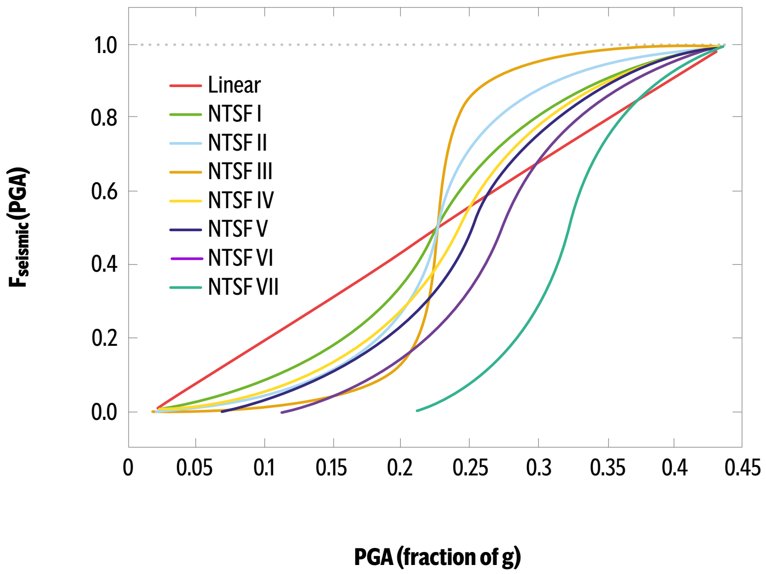

FIGURE 6.6 Different methods for mapping PGA values within the interval [0,1] for the activation of static sources based on seismic triggering (cf. Eq. (6.5)). The various curves corresponding to Equations (6.6)-(6.8), plotted with different colour were tested for the Friuli, Umbria–Marche and L'Aquila inventories. For greater details, see also Table 6.2.

TABLE 6.2
List of the parameters required to obtain the different curves in Figure 6.6. For curves NTSF IV, V, VI and VII, the value of PGA cut in Equation (6.8) was set equal to the 25th, 50th, 75th and 90th percentiles of all values in the PGA map, respectively.

NTSF	PGA_{cut}	k
I	0.017	-0.5
II	0.017	-0.7
III	0.017	-0.9
IV	0.048	-0.5
V	0.067	-0.5
VI	0.111	-0.5
VII	0.209	-0.5

FIGURE 6.7 presents an example of the results for the 1976 Friuli earthquake. The method can be applied to any ground-shaking scenario represented by the PGA map of a specific seismic event.
We suggest that this framework may be suitable for rapid assessment of rockfall impact as soon as ground-shaking estimates (derived from empirical or numerical models) become available following a seismic event.

a)

b)

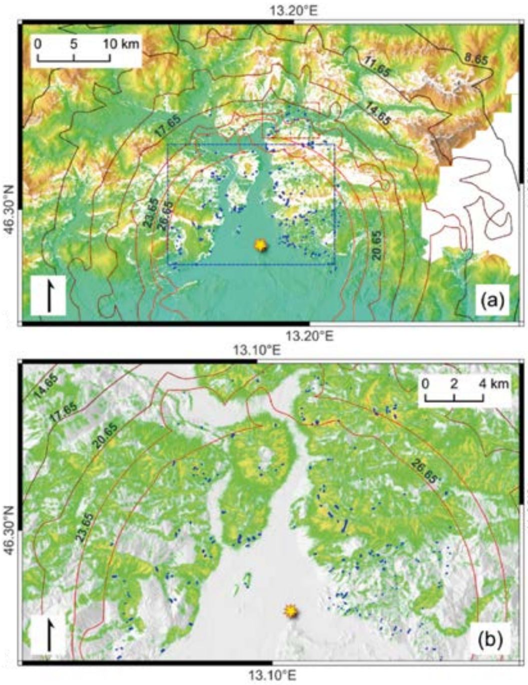

FIGURE 6.6
(a) Map of the optimal rockfall source area, obtained from Equations (3), (5), and (6) using the approximation referred to as NTSF I. Source areas are shown in white, without distinction among probability classes, for clarity. Blue points represent rockfalls observed after the seismic event, and red lines indicate contour lines of the PGA map. (b) Output of the STONE model realization using the source map shown in the upper panel as input. The runout map simulated by STONE is displayed using a green, yellow, and red colour ramp, corresponding to increasing values of the number of trajectories per cell. Figure adapted from Alvioli et al. (2024b).

6.3.4 Application to the SERENA Project Study Area

The SERENA project considered the regions of Emilia-Romagna, Tuscany, Umbria and Marche as the study area for the simulation of earthquake-induced rockfalls (see FIGURE 6.8). As part of the project activities, a map of *Peak Ground Acceleration (PGA)* was produced for the aforementioned regions, incorporating site amplification effects.

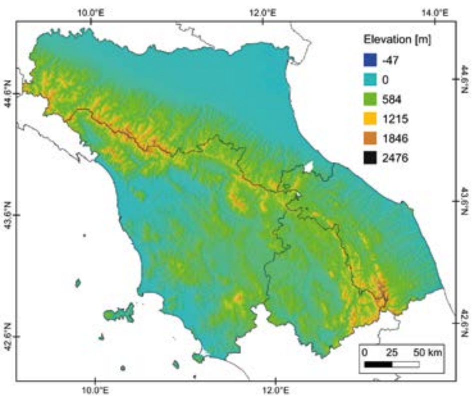

FIGURE 6.8
Study area selected within the PRIN SERENA project for the assessment of the runout of potential earthquake-induced rockfalls using the physically based model r.stone (Alvioli and Melelli, 2025). The figure shows a hillshade map overlaid in transparency on the TINITALY digital terrain model (Tarquini et al. 2007), with 10 m resolution, used for the r.stone simulations.

The minimum value in the *PGA map* is *PGAmin* = 0.027 (in units of gravitational acceleration, *g),* and the maximum value is *PGAmax* = 0.6. The map is shown in **FIGURE 6.9**.

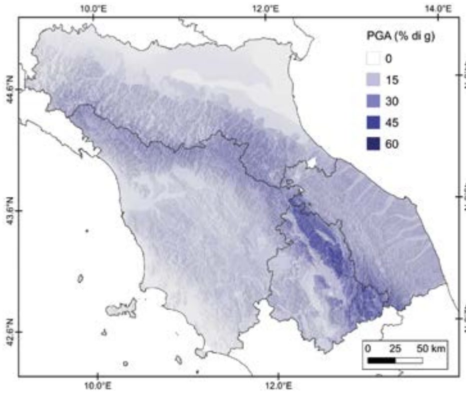

FIGURE 6.9
Raster map of Peak Ground Acceleration (PGA) produced in scope the PRIN SERENA project, overlaid transparently on a hillshade map of the TINITALY DTM shown in Figure 6.8.
The PGA map was used in Equations (6.5)–(6.8) to couple seismic shaking with rockfall triggering, for the physically based simulation of runout.

In the following, we present the results of simulations performed with r.stone. We show the outputs obtained from model realisations initialised with "static" source maps, i.e. not dependent on a specific triggering mechanism, and with "dynamic" sources, corresponding to a seismic trigger according to the model described by Eqs. (6.5)-(6.8). We recall that static sources represent all grid cells that may generate block detachment with the probability defined by Eqs. (6.3)-(6.4), whereas dynamic sources represent the combination of this probability with the probability of triggering due to seismic shaking, according to Eqs. (6.5)-(6.8).
The simulation results are shown in **FIGURE 6.10** for the entire study area, and in **FIGURES 6.11–6.14** for progressively smaller sub-areas; the rectangles in **FIGURE 6.10** define the areas displayed in the subsequent figures. From **FIGURE 6.11** it is immediately evident that imposing the seismic trigger reduces the spatial extent of non-zero results. Indeed, the model is constructed such that the presence of morphologically potential source cells (based on slope S) is irrelevant in regions where seismic shaking is null.

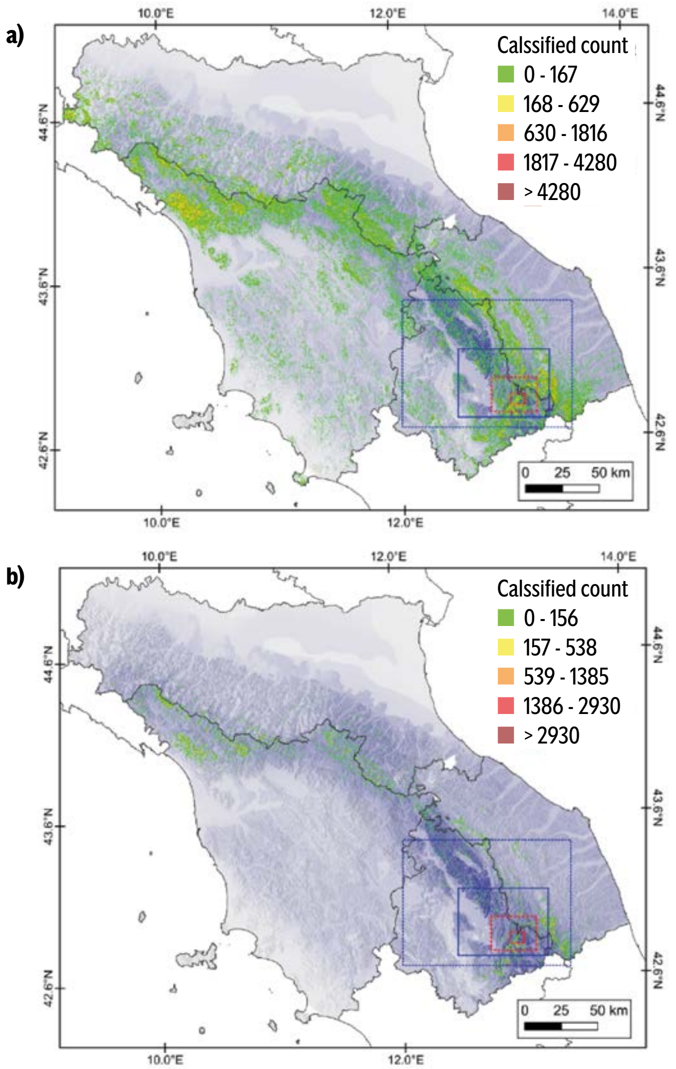

FIGURE 6.10
The two panels show the raster map of rockfall runout obtained from the r.stone model.
a): result obtained with the model initialised using all potential source cells derived from morphometric considerations according to Equations (6.3)–(6.4).
b) result obtained with sources restricted to potential earthquake-induced rockfalls, using the PGA map (shown in transparency as in Figure 6.9) and applying Equations (6.5)–(6.8).

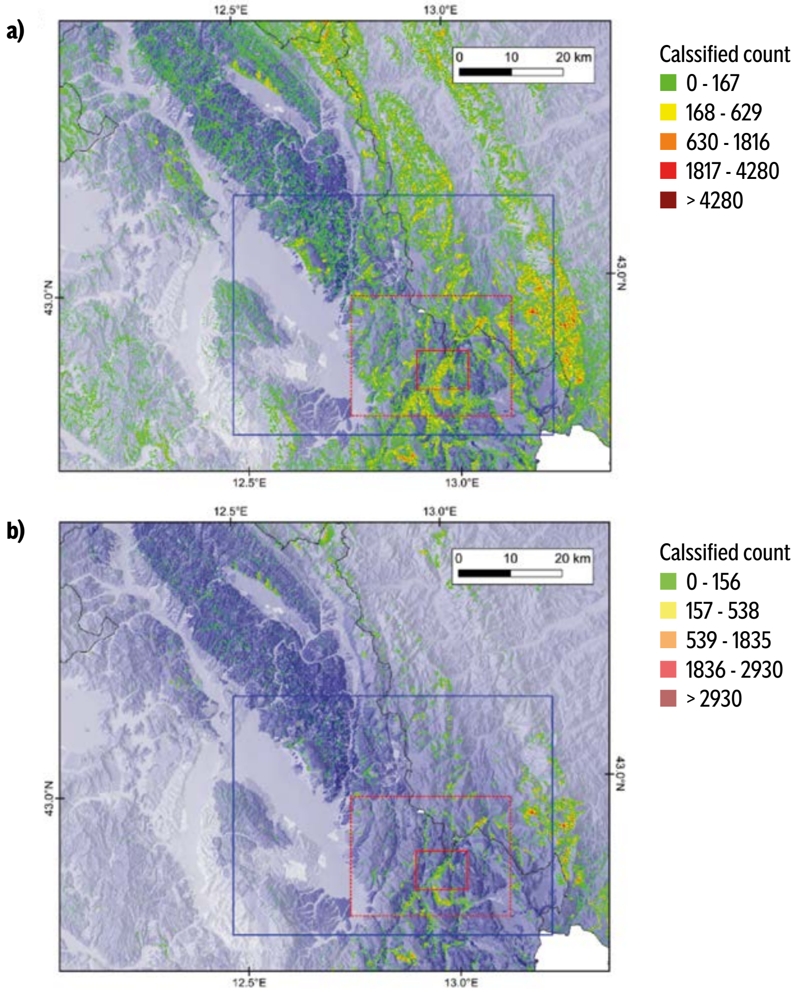

FIGURE 6.11
Detail of the area outlined by the blue dashed rectangle in Figure 6.10. a): result obtained with the model initialised using all potential source cells derived from morphometric considerations.
b) result obtained with sources restricted to potential earthquake-induced rockfalls, using the PGA map (shown in transparency as in Figure 6.9).

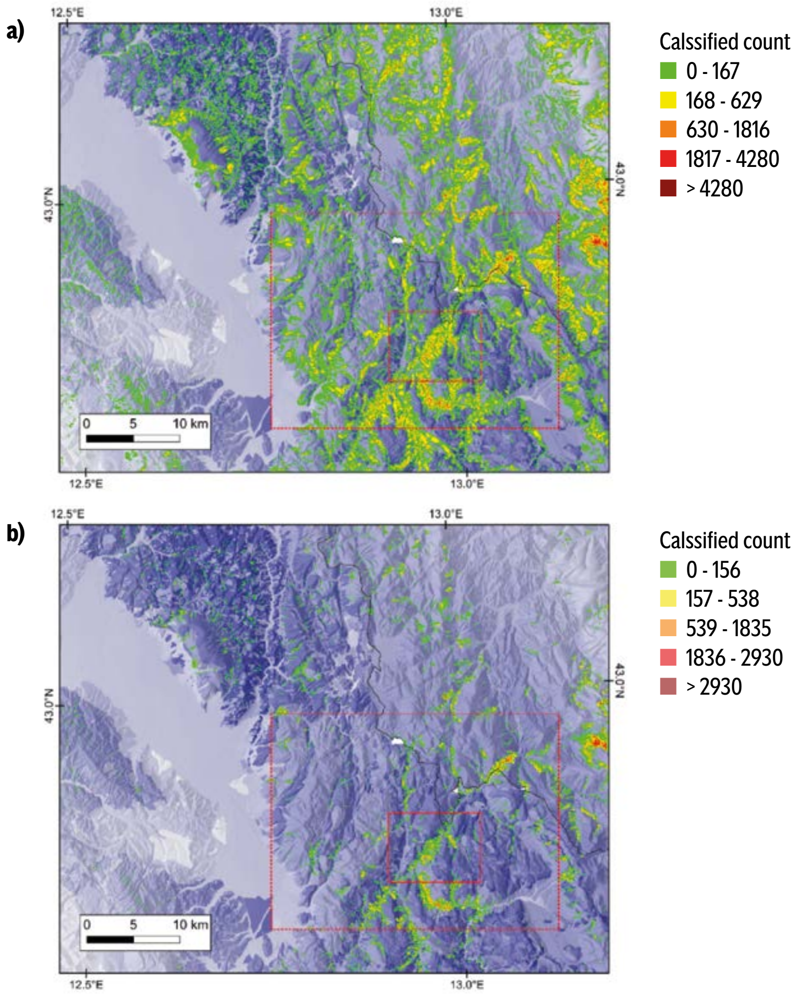

FIGURE 6.12
Detail of the area outlined by the blue solid-line rectangle in Figures 6.10 and 6.11. a): result obtained with the model initialised using all potential source cells derived from morphometric considerations.
b) result obtained with sources restricted to potential earthquake-induced rockfalls, using the PGA map (shown in transparency as in Figure 6.9).

FIGURE 6.13
Detail of the area enclosed by the red dashed rectangle in Figures 6.10, 6.11 and 6.12. a): result obtained with the model initialised using all potential source cells derived from morphometric considerations. b) result obtained with sources restricted to potential earthquake-induced rockfalls, using the PGA map (shown in transparency as in Figure 6.9).

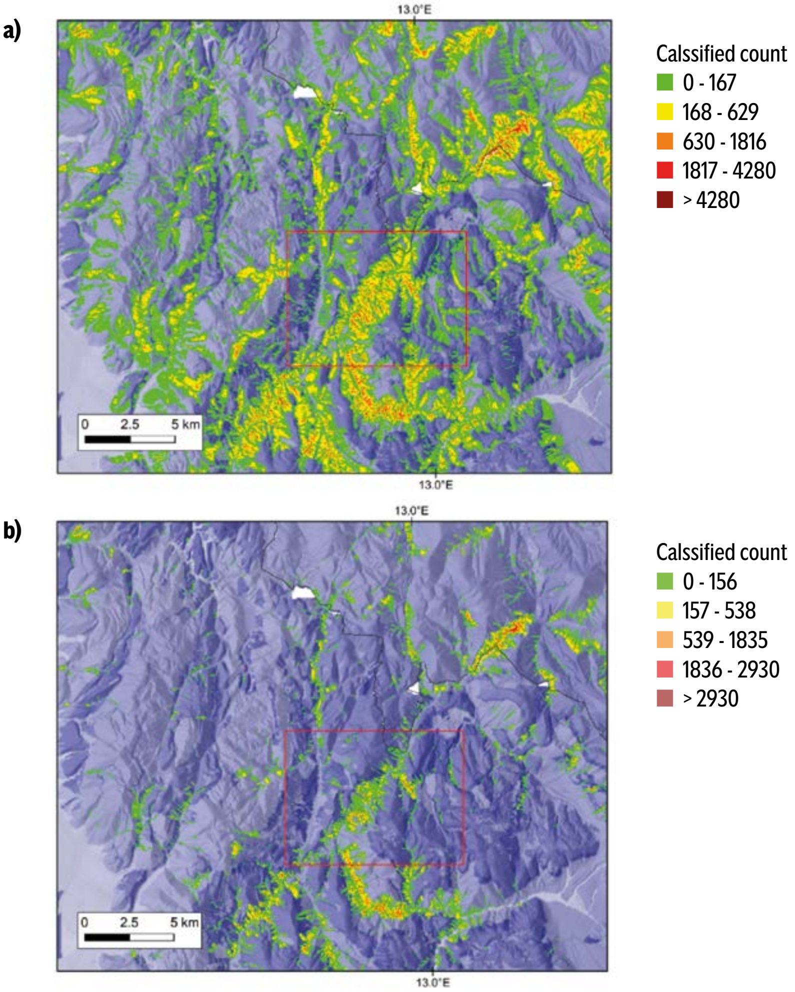

FIGURE 6.14
Detail of the area within the red dashed rectangle in Figs. 6.10, 6.11, 6.12 and 6.13. a): result obtained with the model initialised using all potential source cells derived from morphometric considerations. b) result obtained with sources restricted to potential earthquake-induced rockfalls, using the PGA map. In this figure, the PGA raster map shown in the previous figures has been omitted.

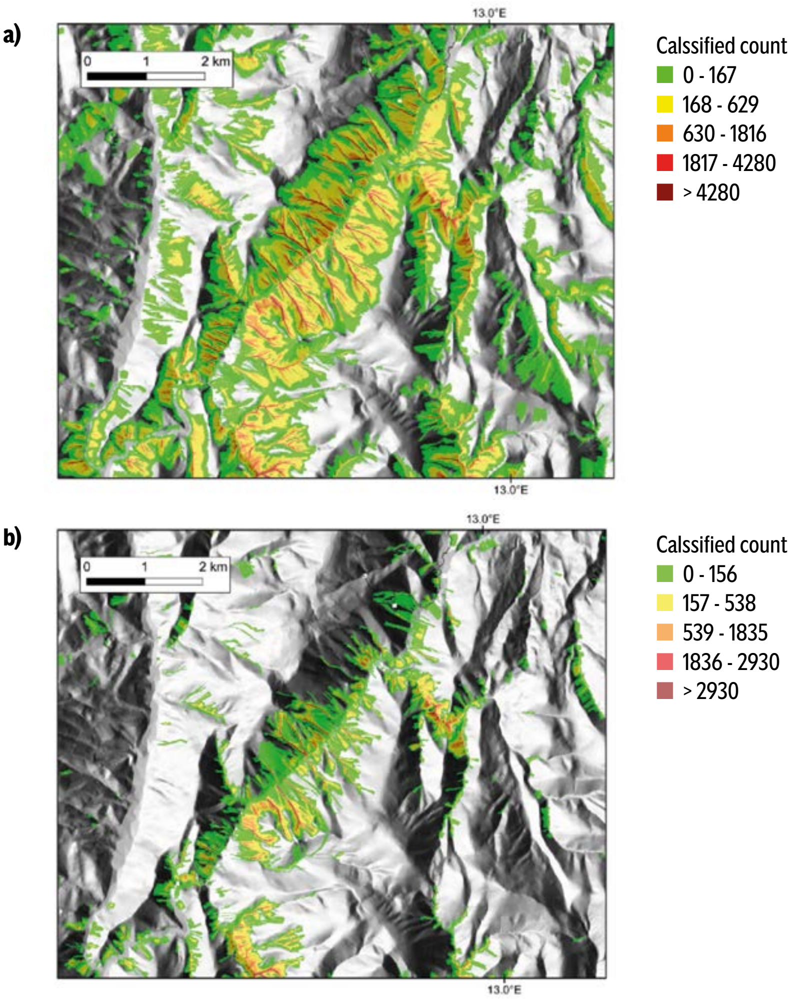

Specifically, the static rockfall source map contains approximately 49.5 million non-zero cells, whereas the map of potential earthquake-induced sources contains approximately two million. The source maps themselves are not shown in the figures for brevity. Correspondingly, the runout map derived from static sources contains about 330,000 non-zero cells, while that obtained from dynamic (seismically triggered) sources contains approximately 100,000 non-zero cells.

As previously noted, the outputs of *r.stone* are raster maps whose values represent the number of simulated trajectories crossing a given cell; these are therefore positive integers, with an upper limit depending on the number of simulated trajectories. The value distribution is highly skewed, with a very large number of cells close to unity and a long tail extending towards very large values.

For visualisation purposes, and to provide a meaningful representation of the results, classification schemes suitable for highly skewed distributions are typically adopted. An equal-interval classification would result in the lowest class containing the vast majority of cells, while a quantile classification would produce a highest class spanning an excessively wide value range; in both cases, the classification would poorly represent the actual distribution.

In this report, as in several published studies, we adopt a head–tail classification algorithm. This procedure consists of computing the mean value of the raster, assigning all values below the mean (which are far more numerous than those above) to the lowest class, then computing the mean of the remaining values, assigning values between the first and second means to the second class, and iterating the process until four classes are obtained; the fifth class is represented by the remaining highest values. FIGURES 6.10 – 6.14 are classified according to this method; the legends display the threshold differences between the five classes, coloured from green to dark red.

7. Open-Source Geospatial Content Management System

7. Open-Source Geospatial Content Management System

The Geospatial content Management System constitutes a central component of the PRIN SERENA Project, as it provides the infrastructural and methodological backbone for the management, organization, and dissemination of data and results. Given the large volume and heterogeneity of datasets involved — ranging from geological and geomorphological information to geotechnical and seismo-stratigraphic data — the implementation of a coherent and efficient data management strategy was essential.
The activities developed within the PRIN SERENA Project are designed to ensure that data were properly archived, harmonized, analysed, and ultimately made accessible through dedicated web services. In this context, the activities carried out in this framework supports not only the internal workflow of the project, but also its broader objective of producing reproducible and shareable scientific outputs. The activities were articulated into three strategic activities designed to guide project operations:

- → Data archiving, management, and harmonization protocols;
- → Framework for data analysis and map production oriented toward a coherent probabilistic approach to uncertainty management;
- → Provision of web-services to develop a WebGIS interface for sharing project outcomes.

This chapter details the operational architecture, technical choices, and governance policies adopted for the Project. These frameworks are designed to ensure compliance with FAIR (Findable, Accessible, Interoperable, Reusable, Mons et al. 2017; Wilkinson et al. 2016) principles while addressing complex issues regarding intellectual property and data ownership within a multi-institutional research consortium.

7.1 Strategic Data Management Architecture

To effectively manage the heterogeneous nature of data generated by multiple participating institutions – ranging from raw seismic profiles to processed geological maps – a dual-layered management architecture was defined. This strategy ensures seamless collaboration during the processing phase while optimizing accessibility for public dissemination in the final phase, regardless of the specific datasets eventually loaded into the system.
The workflow, illustrated in FIGURE 7.1, distinguishes between two primary categories of data: Raw Data (internal processing) and Maps/Documents (public sharing). This separation allows for distinct management protocols tailored to each stage of the data lifecycle.
The overall workflow can be conceptualized as a continuous process in which raw and intermediate data are first collected, shared, and processed within a collaborative environment, and are subsequently transferred to a publication-oriented platform once they have been validated.
This separation ensures both flexibility during the research phase and reliability in the dissemination phase.

1. **Data Collection & Ingestion:** The project initiates with the acquisition of various datasets from local surveys, existing databases, and field campaigns.

2. **Raw Data Processing (NextCloud Environment):** Unprocessed data, internal documents, and large-scale archives are stored and collaboratively processed within a secure cloud environment based on NextCloud. This phase supports iterative editing, quality control, versioning, and the generation of intermediate results before final publication.

3. **Dissemination & Service Provision (GeoPortal Environment):** Once data undergo harmonization and validation according to PRIN SERENA Project standards, they are migrated

to the Geoportal (based on GeoNode). Here, metadata is enriched, access levels are defined, and WebGIS services (WMS/WFS) are generated for public or restricted distribution.

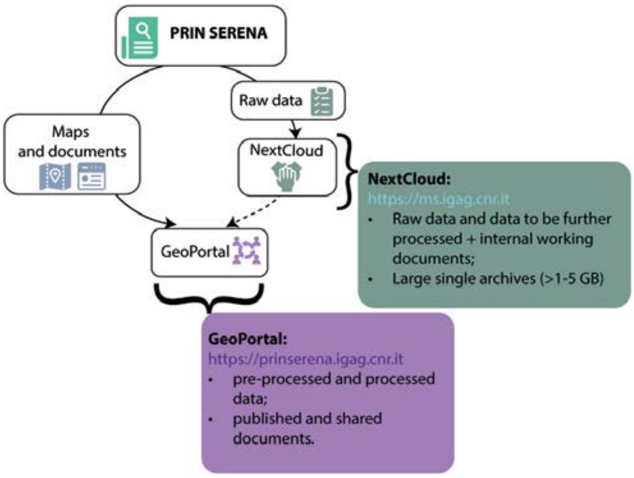

FIGURE 7.1 PRIN SERENA Conceptual Data Management Workflow.

7.1.1 A Collaborative Raw Data Management (NextCloud)

The collaborative component is based on NextCloud, an open-source solution for cloud storage and file sharing that is widely used in different environments. This environment facilitates real-time collaboration without compromising data integrity prior to publication, serving as the “sandbox” for WP activities.

→ **Functional Scope:** Provides a unified interface for file sharing, version control, and document management. It is specifically suited for handling large binary files (e.g., >1 GB) often encountered in geophysical datasets and seismic profiles.
→ **Collaboration Model:** Each participant is granted access to a dedicated workspace through a personal account associated with the project, enabling collaborative workflows that include file sharing, version control, and synchronized updates.

This setup facilitates continuous interaction among research units, allowing data to be progressively refined and validated. The use of Nextcloud is particularly advantageous for handling large datasets and non-final data products, which may undergo multiple stages of processing before reaching a stable and publishable form. By maintaining these data within a controlled internal environment, the project ensures that only validated and well-documented datasets are subsequently made available through public platforms.

7.1.2 Dissemination & Geospatial Services (GeoNode)

For the final dissemination of results, the project utilizes a **WebGIS platform** (https://prinserena.igag.cnr.it) based on **GeoNode** (https://geonode.org/), an open-source platform specifically designed to support the storage, visualization, and sharing of geospatial information within a WebGIS framework. This system transforms static datasets into dynamic geospatial information services, aligning with OGC (Open Geospatial Consortium) standards for maximum interoperability (FIGURE 7.2).

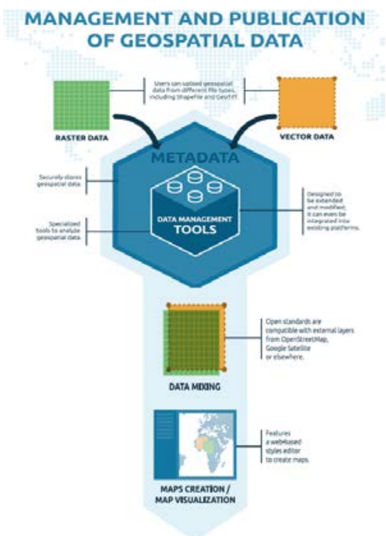

FIGURE 7.2 Data Managment in GeoNode, source: https://docs.geonode.org/en/5.0.x/start/index.html.

The PRIN SERENA Geoportal serves as the primary interface through which both project participants and external users can access data and results. It provides a comprehensive set of tools that allow users to upload datasets, create and edit metadata, visualize spatial information through interactive maps, and share resources according to defined access policies. In this way, the geoportal acts not only as a repository but also as an active environment for data exploration and dissemination.

A key feature of the geoportal is its ability to manage different types of resources in an integrated manner. Geospatial layers, documents, and composite maps are all treated as first-class entities, each associated with detailed metadata that describe their content, origin, and usage conditions. This metadata-driven approach is essential for ensuring that datasets remain understandable and reusable over time.
The Geoportal architecture provides the ability to handle multiscale maps dynamically. The system is designed to:

- → Store all data in their original projections and resolutions within a central database.
- → Automatically reproject vector and raster layers to the widely used Web Mercator projection for efficient on-the-fly rendering in the WebGIS interface.
- → Allow users to create compositions that display different datasets based on zoom levels, ensuring clarity when visualizing high-resolution geological maps alongside national-scale topographic or geological layers.

User access to the geoportal is regulated through a system of authentication and permissions. While public users can freely explore and interact with datasets that have been explicitly made available, registered users – the project participants – are granted additional capabilities, including the ability to upload new data, modify existing resources, and define access permissions. This dual-level access model allows the platform to function both as an internal working tool and as a public dissemination interface.

- → **Functional Scope:** Enables users to search a catalog of layers and documents, visualize them in interactive maps, download data via standard web services (WMS, WFS), and access specific metadata. It supports the creation of custom maps composed of one or more layers.
- → **Service Provision:** The platform is designed to act as a server providing standard OGC services:
  - → **WMS (Web Map Service):** For rendering map images on-the-fly for web integration.
  - → **WFS (Web Feature Service):** For querying and downloading vector features directly to external GIS software (e.g., QGIS, ArcGIS).
  - → **WCS (Web Coverage Service):** For accessing raster data efficiently.
- → **Access Control:** Supports granular permissions. While the public can view “publicly shared” resources without authentication, registered users possess rights to upload new layers, edit metadata, or access restricted datasets based on their institutional group affiliation.

7.2 Open Science Framework and Data Governance

The data management strategy adopted in the PRIN SERENA project is grounded in the principles of Open Science, with particular reference to the FAIR framework. The FAIR principles – Findable, Accessible, Interoperable, and Reusable – provide a conceptual guideline for ensuring that datasets are organized in a way that maximizes their scientific value. In practice, this means that data are accompanied by structured metadata, stored in accessible repositories, and formatted according to interoperable standards that facilitate their integration with other datasets.

It is important to note that FAIR data do not necessarily coincide with open data. While open data are freely accessible and reusable without restriction, FAIR data may be subject to limitations related to intellectual property, confidentiality, or institutional agreements. In this sense, the project adopts a balanced approach that promotes accessibility while respecting legal and ethical constraints.

Issues of intellectual property and data ownership are addressed through a shared framework agreed upon by all participating institutions. Scientific results, methodological developments, and software implementations remain the intellectual property of the researchers and institutions that produced them. At the same time, datasets acquired within the project are jointly owned by the contributing partners, whereas pre-existing data retain their original ownership. This distinction is particularly relevant in multidisciplinary projects, where data originate from multiple sources and institutional contexts.
To ensure long-term traceability and citability of datasets, the project makes use of persistent identifiers in the form of Digital Object Identifiers (DOIs). The adoption of DOI standards, supported by infrastructures such as DataCite, allows each dataset to be uniquely identified and linked to its metadata, thereby enhancing its visibility, reproducibility, and scientific impact.

7.2.1 DOI Registration and Data Citation Infrastructure

To ensure persistent identification and valorization of research outputs, the project employed the Digital Object Identifier (DOI) system managed by CNR's editorial unit *(Unità Editoria)*.

This infrastructure is planned to support long-term data citation and discovery.

CNR utilizes two specific agencies depending on the type of output being registered:

1. **mEDRA:** Primarily used for articles, serials, and monographs (commercial or open access). All CNR structures have autonomy to register DOIs here via the mEDRA portal.

2. **DataCite:** Used specifically for datasets, collections, workflows, software, images, models, and grey literature (theses, technical standards).

The PRIN SERENA project has initiated the registration of a dedicated **Data Repository** with DataCite. This repository allows the assignment of DOIs to all datasets produced during the project lifecycle, ensuring that every layer or processed result can be uniquely cited. To align with the *Repository Discovery* initiative of DataCite, this repository is registered in the REgistry of REsearch Data Repository (RE3Data), enhancing its visibility within the global scientific network.

Project participants have the option to request the registration of DOIs for datasets in the dedicated data repository. This enables researchers and policymakers to cite specific data layers or processed results with precision, contributing to the recognition of open science practices.

7.3 Metadata, Interoperability, and Web Services

Metadata play a crucial role in the overall data management strategy, as they provide the descriptive and contextual information necessary to interpret and reuse datasets. In the PRIN SERENA GeoPortal, metadata are created according to internationally recognized standards, such as ISO 19115 and ISO 19139, ensuring compatibility with other geospatial data infrastructures.

Key mandatory metadata fields include:

→ **Identification:** Title, Abstract, Keywords, DOI.
→ **Spatial Extent:** Geographic bounding boxes and coordinate reference systems (CRS).
→ **Quality Assessment:** Reports on validation status, uncertainty levels, and processing history.
→ **Rights Management:** License type (e.g., Creative Commons), attribution requirements, and access restrictions.

The adoption of standardized metadata is closely linked to the concept of interoperability. By adhering to open standards defined by the Open Geospatial Consortium (OGC), the geoportal enables data to be accessed and used across different platforms and software environments. In particular, datasets can be served through web services such as WMS, WFS, and WCS, allowing users to visualize and download data directly within external GIS applications.

This interoperability significantly enhances the usability of the data, as it allows researchers and practitioners to integrate PRIN SERENA datasets into their own workflows without the need for manual data conversion or duplication.

8. Conclusions and future perspectives

8. Conclusions and future perspectives

The SERENA project faced a very challenging task of providing a regional scale map of site effects including ground motion amplification induced by 1D seismo-stratigraphic and topographic configurations, and seismo-induced landslides. This goal does not conflict with the needs of seismic microzonation study for a reliable estimate of expected co-seismic effects, and the regional estimates should not be considered as a possible alternative. However, financial limitations make SM studies affordable only for relatively small urbanized areas, leaving large areas – where vital and strategic structures and infrastructures (such as roads, lifelines, etc.) are located – unexplored. While municipal land planning may gain relatively small benefit from the approximate outcomes of regional scale studies, risk assessment supporting prevention strategies requires this large scale information to plan risk reduction strategies and allocate funds. Moreover, the availability of preliminary estimates of site effects can be highly beneficial when planning microzonation studies.

To provide an advancement in the large scale mapping of site effects, the SERENA project aimed at developing and testing different methodological approaches able to fully exploit data available at regional scale.

All the procedures described in the previous sections combine two types of numerical estimates:

1. a first kind of estimate, useful for covering the entire national territory, derived from the characterization of typical geological configurations at the national scale;

2. a second kind of estimate, obtained from seismic stratigraphies derived from the current revision of geological maps or available geological and geophysical data.

Both estimates are affected by significant uncertainties which must be considered in the development of the final product. These uncertainties are also mainly dependent by the epistemic and observational information available for each region and used in the different approaches to construct the seismo-stratigraphic columns.

These two numerical estimates should not be viewed as alternatives but rather as complementary, given the substantial independence of the information sources and methodological approaches used to derive them.

From the methodological point of view, managing the heterogeneities in the granularity of the available information was challenging. The Digital Elevation Model (DEM) of Italy provides topographic information with a 10m resolution, while the reference seismic hazard data are provided over a grid map with nodes spaced 0.25° in latitude and longitude. Furthermore, the situation is more complex for geological data, which is provided at different scales (1:250,000, 1:100,000, 1:25,000, 1:10,000) across different areas of the country. These maps were developed with different criteria and limitations. Specifically, 1:250,000 and 1:100,000 scale maps mostly identify outcropping geological bedrocks, and more recent deposits that play a significant role in seismic site response are generally lacking when they are relatively small and thin. Moreover, as concerns more detailed maps (1:10,000) were developed by Regional Administrations using slightly different criteria. This implies that discontinuities (or artifacts) may occur along the administrative boundaries due to the lack of continuity among the maps. Providing a homogeneous map would have required a substantial effort, which was beyond the scope of the present project. Consequently, different approaches, mostly based on expert judgements, were adopted to manage the different situations.

Another difficulty arose in defining representative geological logs, i.e. providing a third dimension to the maps. To address this, a novel approach has been developed which is considered a major methodological advancement of the project. This approach comprises in three steps.

First, specific domains were identified in the considered areas based on morphological and geological considerations (the GeoMorpho-Stratigraphic Unit or GMSU). Within each domain, primary geological bodies were identified and classified in terms of formation age and prevalent lithology, by using archetypal engineering geological units (EGUs). Based on these classifications, a typical general lithostratigraphic log was constructed by ordering EGUs with ages (the younger above the older) and incorporating the range of possible thicknesses for each EGU. GIS-based automatic procedures were thus developed to assess the site specific lithostratigraphic configuration for each outcrop by considering surrounding outcrops.

As a second step, primary seismic and geotechnical parameters were assigned to each EGU based on the statistical analysis of available data. Since no local information was considered, these characterizations were affected by uncertainties, which were parameterized based on available data. This information was used for numerical simulations relative to each log incorporating the relevant uncertainty. Numerical 1D simulations were carried out using the same equivalent linear numerical procedure and the input motion provided by the reference hazard map of Italy within the RVT framework. This allowed the definition of a probability distribution for amplification values representative of each considered outcrop.

The evaluation of possible testing procedures was another key element of the project. Two approaches were explored relative to stratigraphic and topographic effects based on empirical and numerical procedures.

First research activities focused on comparing different empirical techniques for estimating amplification factors with 1D numerical site amplification estimates for rigorous validation. The findings are summarized as follows:

→ Data Collection and Standardization. A comprehensive and multi-methodological dataset of empirical Amplification Factors (AF) was established. This includes estimates derived from Site-to-Site Residuals (dS2S), Generalized Inversion Technique (GIT), and Standard Spectral Ratio (SSR). This extensive data collection covers more than 1000 sites, encompassing both the national scale and selected regional areas (including Central Italy, North-East Italy, the Basilicata region, and the Ferrara area). To ensure robustness, the data were standardized within a centralized Spatial Data Infrastructure, facilitating semi-automatic comparative analysis and integration with the project's GIS platform.

→ Mutual Consistency of Empirical Estimates. Cross-validation of the different empirical methods demonstrated a high degree of correlation, with Spearman's coefficient consistently exceeding 0.9. This highlights the statistical robustness of the empirical approach, confirming that these methods capture the actual physical response of the site independently of the specific algorithm. However, systematic biases were identified, predominantly linked to the variability of the chosen reference rock conditions.

→ Benchmarking Numerical vs. Empirical Estimations. Comparisons between empirical observations and simplified estimates nationwide (about 900 sites) revealed that the latter act as unbiased predictors for only approximately 25-35% of investigated sites. Systematic discrepancies were observed: 1D models typically overestimate amplification on rock and stiff sites (roughly 65% of sites, primarily along the Apennine belt and the Tyrrhenian side) while underestimating it in deep alluvial basins (e.g., Po Plain, Fucino) where 2D/3D effects are dominant, as the generation of basin-edge surface waves and the focusing/defocusing of seismic energy which significantly enhance amplification levels. A detailed regional-level comparison, exploiting 1D numerical stochastic models obtained within the SERENA project for Tuscany, Marche, Umbria, Piedmont, and Lombardy, was also conducted (about 860 sites). These regional analyses confirmed and further detailed the trends in the normalized residual distribution that were initially observed at the national scale.

→ Advanced Spatialization Strategies. To move from point-based station data to continuous areal maps, advanced geostatistical frameworks were implemented. These include Universal Kriging in Central Italy using site proxies (Vs_{30} and lithostratigraphic trends) as predictors, and high-resolution cluster analysis in the Alto Garda and Ferrara areas, leveraging horizontal-to-vertical spectral ratios (HVSR) from noise as proxies for spectral amplification zonation. A statistical correlation analysis was also completed at the national scale between different site proxies archived in the CRISP database, relative to the permanent INGV seismic network stations, to evaluate the most appropriate modalities for the spatialization of the punctual results deduced from experimental measurements.

While traditional hazard assessments rely on stratigraphic proxies to theoretically predict site effects, our research establishes that empirical methods have reached a degree of maturity that allows for the direct observation of amplification ground motion. This data-driven approach is grounded in extensive observational databases at national (permanent networks) and local (seismic sequences campaigns and local experiments) levels. The large data collection ensures that amplification estimates can be considered as statistically robust physical evaluation of site response, as one of the major outcomes of this work package is the consistency among established empirical techniques: independent methods – SSR, GIT, and dS2S – identify the same relative amplification patterns across diverse geological contexts. The methods exhibit a remarkable agreement, capturing the “true” physical response of the site despite differences in their mathematical formulation and confirming that independent data sources converge on consistent site response patterns.

A critical challenge identified during the analysis is the operational definition of the reference site. In seismic regulations, an ideal bedrock is typically defined by Vs_{30} = 800 m/s. In reality, however, rock sites often exhibit complex behaviours, including weathering or high-frequency attenuation (k0). In Central Italy, a systematic deviation was initially observed between different methods due to these reference site characteristics. By applying a period-dependent generic-to-reference scaling factor, we were able to remove these biases and align the distributions. This proves that empirical methods are equivalent and robust once the reference ground motion baseline is rigorously calibrated.

The numerical approach was also crucial for evaluating topographic amplification effects. In this case, the estimates were inferred from the application of proxies provided by current seismic codes (EC08, NTC18). In this case, it was of main importance the possibility of a univocal identification of the morphological configurations where the proxies were applicable. A GIS based code was developed on purpose and 2D numerical simulations were carried on evaluating feasibility of proxies. The analysis revealed that: a. the proxies are appliable in a very restricted number of cases, by leaving undetermined the possible presence of such effects else were; b. when applied, proxies provide amplification factors generally conservative relative to larger structures (elevation above 30m) but are largely under conservative when relatively small reliefs are of concern. This suggests that new proxies should be developed to obtain an extensive estimate of possible topographic amplification effects.

The combination of geomorphological characterization and numerical simulations was also considered to assess the hazard of seismically induced landslides and rockfalls by a quantitative and reproducible procedure for estimating susceptibility to rotational-translational landslides over extensive domains, using a physically based approach. The implemented methodological chain coherently integrates: (i) geotechnical parameterisation derived from the national dataset and reorganised according to the new geological-technical classification; (ii) observational calibration of parameters through back-analysis of high-quality landslide inventories; and (iii) explicit representation of uncertainty through Monte Carlo sampling. This framework addresses the typical challenges of distributed modelling at regional scale, related to material variability and parameter representativeness, reducing reliance on average literature values and anchoring simulations to observational constraints. Supra-regional applications under static and pseudostatic conditions demonstrate a systematic model response to hydrological scenarios and to the introduction of seismic input *(PGA)*. The *pfail* and *FS* maps show that the combination of saturation and pseudostatic loading represents the most severe scenario, with increased probability of instability and widespread conditions close to limit equilibrium. Depth maps further indicate that, in specific lithotechnical and morphological contexts, the combined effect of forcings may promote the activation of deeper critical surfaces, suggesting a potential increase in the volumes that may be mobilised. The spatial consistency of the results with the geological–technical map confirms the decisive role of predisposing factors (mechanical properties and structural condition of materials), while the increase in instability from static to pseudostatic scenarios quantifies the effect of seismic forcing within the limit equilibrium framework. Overall, the workflow developed within the SERENA Project provides a calibrated, probabilistic and transferable procedure for distributed slope stability modelling, ready to be extended to broader territorial domains and, prospectively, to the entire national territory using spatially distributed seismic inputs, in line with the overarching objectives of the SERENA project.

With regards to rockfall susceptibility, it is important to note that using a PGA map does not correspond to a specific seismic event, and extracted from that work. Instead, the map employed here represents the maximum expected ground shaking in the study area. Therefore, the resulting map represents a susceptibility map for earthquake-induced rockfalls and cannot be considered as a hazard map strictu sensu, as it provides only spatial information and does not include information on expected block size or on the temporal dimension of occurrence.

From a data management point of view, the combined use of NextCloud for secure internal collaboration and GeoNode for standardized public dissemination, resulted in a coherent system that supports the entire lifecycle of project data.

Data were initially collected and shared within the collaborative environment, where they were processed and refined through iterative interactions among project partners.
Once a dataset reached the sufficient level of quality and completeness, it was transferred to the GeoPortal https://prinserena.igag.cnr.it, where it was enriched with metadata and made available for visualization and dissemination.

Collaboration among scientific partners was streamlined via specialized cloud platforms capable of handling large geospatial datasets. Datasets were planned to be traceable (via DOIs), high-quality (ISO metadata), and fully interoperable with external systems (OGC standards).

The adoption of open-source technologies, adherence to FAIR principles, and implementation of standardized metadata and interoperability protocols collectively contributed to the creation of high-quality, traceable datasets. These features not only facilitate collaboration among project partners but also enhance the visibility and impact of the project's results within the broader scientific community. PRIN SERENA Project datasets will be maintained also in the future to support land-use planning, risk reduction strategies, and emergency management across the Italian peninsula.

Further research is needed to define an improved method for combining numerical estimates obtained by adopting different approaches, so as to fully exploit future updates and incorporate new and more accurate data. Dedicated procedure will allow handling uncertainty through a Bayesian approach, where incoming information will be weighed by considering respective levels of uncertainty.

Based on the different amount of information available for each study area, slightly different approaches were considered as discussed in the text. Because of time limitations and with the aim of providing estimates relative to the whole Italian area, no direct comparison was performed among the outcomes provided form the same area by considering the different levels of approximation. Beyond the possible limitations of the numerical approach here considered, this comparison would be of great importance to evaluate the impact of lacking information on the final outcomes and, above all, assessing respective uncertainty level. This comparison could also be the basis of a possible strategy devoted to the probabilistic combination of estimates provided by considering different levels of details in input data, including those provided by SM studies.

The future of SM lies in a hybrid approach: anchored in direct empirical observation and extended spatially through advanced geostatistics and machine learning. By prioritizing empirical data as the foundation of the hazard assessment chain, we can significantly reduce uncertainty, mitigate risks in complex areas, and provide more accurate tools for urban planning and resilience.

We propose a critical shift in professional microzonation workflows, as empirical AFs should be used as benchmark for linear numerical simulations. Professionals could validate the linear behaviour of their numerical models versus available empirical evidence before introducing non-linear parameters. This approach ensures that simulations are physically anchored and minimizes the risk of underestimating hazards in geologically complex areas. This would require a centralized Spatial Data Infrastructure, essential to ensure interoperability between observational databases and professional analysis software, guaranteeing that professionals access the most up-to-date and standardized values.

From the methodological point of view, an effort should also be made to: (i) isolate local site response from regional propagation signatures by prioritizing recordings of local earthquakes; (ii) investigate the effect of the reference site definition; (iii) increase the collection of experimental data in specific site condition, such as topography or complex basins.

The inherent limitation of empirical estimates is their point-based nature, as they are strictly valid only at the recording station's location. This constraint is further complicated by significant local variability, where sites separated by merely hundreds of meters can exhibit distinct amplification behaviours. Consequently, the primary goal is the transition from a single-point assessment to continuous areal coverage using reliable and robust proxies. The future challenge is therefore to bridge these spatial gaps, necessitating the delineation of homogeneous zones to be used for SM purposes. This is achieved by uncovering the complex relationships and statistical correlations between geological, geophysical, topographical, and seismological variables through advanced statistical analysis (e.g., canonical correlation) to identify the minimum, most effective, and sensitive set of geophysical and geological proxies that can predict the site amplification functions and be used as robust indicators of site effect. Moreover, spatialization strategies include the implementation of Universal Kriging and Machine Learning models to extrapolate point data across broader areas, integrating deterministic trends such as geology, slope-based Vs,30 and other proxies.

In this context, numerical modelling can also provide important constraints on the spatial variability of site response, helping to guide and support the spatialization of empirical observations. A closer integration between empirical approaches and physics-based numerical simulations therefore represents a key direction for future research, enabling a more robust and physically consistent characterization of site amplification at the regional scale.

The activities carried out within the SERENA Project establish a robust framework that has supported the scientific objectives of the project and will continue to support its contribution to the broader scientific community.

9. Reference list

Appendix: Scientific Outputs of the Project

Peer Reviewed Publications

National Conference Proceedings

International Conference Proceedings

9. Reference list

Acunzo, G., Falcone, G., di Lernia, A., Mori, F., Mendicelli, A., Naso, G., …, Moscatelli, M. (2024).
NC92Soil: A computer code for deterministic and stochastic 1D equivalent linear seismic site response analyses. Computers and Geotechnics **165**, 105857. https://www.sciencedirect.com/science/article/pii/S0266352X23006146

Aimar, M., Ciancimino, A., Foti, S. (2020).
An assessment of the NTC18 stratigraphic seismic amplification factors. Italian Geotechnical Journal **1**, 5–21.

Albarello, D. (2017).
Extensive application of seismic microzoning: methodological and socio-political issues in the Italian experience. Bollettino di Geofisica Teorica ed Applicata **58**, 4, 253–264. https://doi.org/10.4430/bgta0205

Albarello, D., Paolucci, E. (2024).
Possible measure of soil factors in the Italian seismic code. Bulletin of Earthquake Engineering. https://doi.org/10.1007/s10518-024-02021-9

Albarello, D., Carfagna, N., Fantozzi, P.L. (2025).
The impact of 1D seismostratigraphical amplification effects on probabilistic seismic hazard maps at regional scale: the case of Tuscany (Central Italy). Bull. Earthq. Eng. **23**, 3043–3055. https://doi.org/10.1007/s10518-025-02167-0

Algoritmiqa (2025).
AlgoShake 2D [software]. https://www.algoritmiqa.com/algoshake-2d/. Accessed 30 Oct 2025

Alvioli, M. (2020).
Administrative boundaries and urban areas in Italy: a perspective from scaling laws. Landscape and Urban Planning **204**, 103906. https://doi.org/10.1016/j.landurbplan.2020.103906

Alvioli, M., Guzzetti, F., Marchesini, I. (2020).
Parameter-free delineation of slope units and terrain subdivision of Italy. Geomorphology **358**, 107124. https://doi.org/10.1016/j.geomorph.2020.107124

Alvioli, M., Santangelo, M., Fiorucci, F., Cardinali, M., Marchesini, I., Reichenbach, P., Rossi, M., Guzzetti, F., Peruccacci, S. (2021).
Rockfall susceptibility and network-ranked susceptibility along the Italian railway. Engineering Geology **293**, 106301. https://doi.org/10.1016/j.enggeo.2021.106301

Alvioli, M., De Matteo, A., Castaldo, R., Tizzani, P., Reichenbach, P. (2022a).
Three-dimensional simulations of rockfalls in Ischia, Southern Italy, and preliminary susceptibility zonation. Geomatics, Natural Hazards and Risk **13**, 2712. https://doi.org/10.1080/19475705.2022.2131472

Alvioli, M., Fiorucci, F., Marchesini, I., Santangelo, M., Ardizzone, F., Bucci, F., Rossi, M., Guzzetti, F., Reichenbach, P., Moscatelli, M., Mendicelli, A., Mori, F., Falcone, G., Massaro, S. (2022b).
Metodologie integrate multi-scala per la zonazione della pericolosità da frana sismo-indotta in Italia: DP-2 Analisi alla mesoscala regionale. Rapporto di progetto WP3.

Alvioli, M., Falcone, G., Mendicelli, A., Mori, F., Fiorucci, F., Ardizzone, F., Moscatelli, M. (2023).
Seismically induced rockfall hazard from a physically based model and ground motion scenarios in Italy. Geomorphology **429**, 108652. https://doi.org/10.1016/j.geomorph.2023.108652

Alvioli, M., Guzzetti, F., Antonello, A. (2024a).
r.stone – The STONE rockfall module. https://grass.osgeo.org/grass-stable/manuals/addons/r.stone.html

Alvioli, M., Poggi, V., Peresan, A., Scaini, C., Tamaro, A., Guzzetti, F. (2024b).
A scenario-based approach for immediate post-earthquake rockfall impact assessment. Landslides **21**, 1.

https://doi.org/10.1007/s10346-023-02127-2

Alvioli, M., Melelli, L. (2025).
Project URGERE: "2022M7EP3M_PE10_PRIN2022 – URban GEodiversity for a Resilient Environment", 2022–2025. CUP B53D23007260006. Finanziato dall'Unione europea – Next Generation EU. https://urgere-project.irpi.cnr.it/

Alvioli, M., Antonello, A., Guzzetti, F. (2026).
Selection of rockfall sources for three-dimensional modeling with r.stone in GRASS GIS. (in preparation)

Amanti, M., Chiessi, V., Muraro, C., Puzzilli, L., Roma, M., Catalano, S., Romagnoli, G., Tortorici, G., Cavuoto, G., Albarello, D., Fantozzi, P.L., Paolucci, E., Pieruccini, P., Caprari, P., Mirabella, F., Della Seta, M., Esposito, C., Di Curzio, D., Francescone, M., Pizzi, A., Macerola, L., Nocentini, M., Tallini, M. (2020).
Geological and geotechnical models definition for 3rd level SM studies in Central Italy. Bull. Earthq. Eng. **18**, 5441–5473. https://doi.org/10.1007/s10518-020-00843-x

Andrews, D.J. (1986).
Objective determination of source parameters and similarity of earthquakes of different size.
In: Das, S., Boatwright, J., Scholz, C.H. (Eds.), Earthquake Source Mechanics. American Geophysical Union, Monograph **37**, 259–267. https://doi.org/10.1029/GM037p0259

Ariano, M., Fantozzi, P.L., Albarello, D. (2026).
Numerical testing proxies of seismic codes relative to topographic amplification effects: the case study of the Siena urban area (Central Italy). Under review in Bulletin of Earthquake Engineering.

Ashford, S.A., Sitar, N. (1997).
Analysis of topographic amplification of inclined shear waves in a steep coastal bluff. Bull. Seismol. Soc. Am. **87**, 692–700. https://doi.org/10.1785/BSSA0870030692

Barnaba, C., Laurenzano, G., Moratto, L., Sugan, M., Vuan, A., Priolo, E., Romanelli, M., Di Bartolomeo, P. (2014).
Strong-motion observations from the OGS temporary seismic network during the 2012 Emilia sequence in northern Italy. Bulletin of Earthquake Engineering **12**, 2165–2178. https://doi.org/10.1007/s10518-014-9610-4

Bindi, D., Zaccarelli, R., Razafindrakoto, H., Yen, M.H., Cotton, F. (2023).
Empirical shaking scenarios for Europe: a feasibility study. Geophys. J. Int. **232**, 990–1005. https://doi.org/10.1093/gji/ggac382

Bindi, D., Pacor, F., Luzi, L., Puglia, R., Massa, M., Ameri, G., Paolucci, R. (2011).
Ground motion prediction equations derived from the Italian strong motion database. Bulletin of Earthquake Engineering **9**, 1899–1920.

Borcherdt, R.D. (1970).
Effects of local geology on ground motion near San Francisco Bay. Bulletin of the Seismological Society of America **60**, 29–61. https://doi.org/10.1785/BSSA0600010029

Bucci, F., Santangelo, M., Fongo, L., Alvioli, M., Cardinali, M., Melelli, L., Marchesini, I. (2021).
A new digital lithological map of Italy at 1:100,000 scale. https://doi.org/10.1594/PANGAEA.935673

Bucci, F., Santangelo, M., Fongo, L., Alvioli, M., Cardinali, M., Melelli, L., Marchesini, I. (2022).
A new digital lithological map of Italy at the 1:100,000 scale for geomechanical modelling. Earth System Science Data **14**, 4129–4151. https://doi.org/10.5194/essd-14-4129-2022

Cara, F., Cultrera, G., Riccio, G., et al. (2019).
Temporary dense seismic network during the 2016 Central Italy seismic emergency for microzonation studies. Scientific Data **6**, 182. https://doi.org/10.1038/s41597-019-0188-1

Carbone, S., Catalano, S., Lazzari, S., Lentini, F., Monaco, C. (1991).
Presentazione della carta geologica del Bacino del Fiume Agri (Basilicata). Mem. Soc. Geol. It. **47**, 129–143.

Castelbarco, T., Lanzano, G., Brunelli, G., Sgobba, S., Pacor, F., Luzi, L., Pergalani, F., WP6 PRIN SERENA. (2025).
1D response analysis of seismic stations in ITACA for Seismic Microzonation purposes. 43° Convegno Nazionale GNGTS, 11–14 febbraio 2025, Bologna.

Castro, R.R., Anderson, J.G., Singh, S.K. (1990).
Site response, attenuation and source spectra of S waves along the Guerrero, Mexico, subduction zone. Bulletin of the Seismological Society of America **80**, 1481–1503.

Catalano, S., Grassi, S., Imposa, S., Tortorici, G., Cavuoto, G., Di Fiore, V., Alleanza, G.A., Chiaradonna, A.,

De Silva, F., D'Onofrio, A., Silvestri, F., Romagnoli, G. (2019).
The subsoil model for seismic microzonation study: the interplay between geology, geophysics and geotechnical engineering. In: Earthquake Geotechnical Engineering for Protection and Development of Environment and Constructions – Silvestri & Moraci (Eds). Proceedings of the VII ICEGE, Rome, 17–20 June, 948–959. ISBN 978-0-367-14328-2.

CEN (2003).
EN 1998-1 Eurocode 8: Design of structures for earthquake resistance – Part 1: General rules, seismic actions and rules for buildings. Draft No. 6, Doc CEN/TC247/SC8/N335, Brussels. http://www.cen.eu/cenorm/homepage.htm

Cesarano, M., Porchia, A., Romagnoli, G., Catalano, S., Mendicelli, A., Nocentini, M., Peronace, E., Naso, G., Moscatelli, M. (2022).
Multiscale geothematic maps for territorial planning from data collected for the Italian Seismic Microzonation Project. Italian Journal of Geosciences **141**, 35–52. https://doi.org/10.3301/IJG.2022.03

Crozier, M.J. (2010).
Deciphering the effect of climate change on landslide activity: A review. Geomorphology **124**, 260–267. https://doi.org/10.1016/j.geomorph.2010.04.009

Cultrera, G., Mercuri, A. (2025).
Statistical analysis of site effect indicators at the Italian seismic network: inside the site characterization database CRISP. Bull. Earthquake Eng. **23**, 4365–4390. https://doi.org/10.1007/s10518-025-02212-y

D'Agostino, A., Porchia, A., Tortorici, G., Pavano, F., Cavuoto, G., Moscatelli, M., Ortolano, G., Catalano, S. (2025).
'Stratigraphically Homogeneous Zones': automated construction and restitution procedure for engineering geology use. Journal of Maps **21**, 1, 2504064. https://doi.org/10.1080/17445647.2025.2504064

Darendeli, M.B. (2001).
Development of a new family of normalized modulus reduction and material damping curves. Ph.D. thesis.

Decreto Legislativo (2021).
Decreto Legislativo 2021/200 del 8 novembre 2021, Attuazione della direttiva (UE) 2019/1024. GU n.285 del 30-11-2021 – Suppl. Ordinario n. 42.

Del Gaudio, V., Wasowski, J. (2004).
Time probabilistic evaluation of seismically induced landslide hazard in Irpinia (Southern Italy). Soil Dyn. Earthq. Eng. **24**, 915–928. https://doi.org/10.1016/j.soildyn.2004.06.019

Di Giulio, G., Gaudiosi, I., Cara, F., Milana, G., Tallini, M. (2014).
Shear-wave velocity profile and seismic input derived from ambient vibration array measurements: the case study of downtown L'Aquila. Geophysical Journal International **198**, 2, 848–866.

EPRI (1993).
Guidelines for Determining Design Basis Ground Motions. Electric Power Research Institute.

Esri (2023).
ArcGIS Pro: Release 3.3.

Falcone, G., Acunzo, G., Mendicelli, A., Mori, F., Naso, G., Peronace, E., Porchia, A., Romagnoli, G., Tarquini, E., Moscatelli, M. (2021).
Seismic amplification maps of Italy based on site-specific microzonation dataset and one-dimensional numerical approach. Engineering Geology **289**, 106170. https://doi.org/10.1016/j.enggeo.2021.106170

Fantozzi, P.L., Paolucci, E., Pieruccini, P., Albarello, D. (2023).
Automatic identification of sites prone to topographic seismic amplification effects by the current seismic codes. Soil Dyn. Earthq. Eng. **174**, 108212. https://doi.org/10.1016/j.soildyn.2023.108212

Faraone, C., Colantonio, F., Vessia, G. (2023).
Seismic amplification effects induced by ancient shallow cavities underneath the urban area of the historical city center of Chieti, Italy. Eng. Geol. **324**, 107259.

Felicetta, C., Russo, E., D'Amico, M., Sgobba, S., Lanzano, G., Mascandola, C., Pacor, F., Luzi, L. (2023).
Italian Accelerometric Archive v4.0. INGV – Dipartimento della Protezione Civile. https://doi.org/10.13127/itaca.4.0

Felicetta, C., Mascandola, C., Spallarossa, D., Pacor, F., Hailemikael, S., Di Giulio, G. (2021).
Quantification of site effects in the Amatrice area (Central Italy): Insights from ground-motion recordings of the 2016–2017 seismic sequence. Soil Dyn. Earthq. Eng. **142**, 106565. https://doi.org/10.1016/j.soildyn.2020.106565

Gallipoli, M.R., Albarello, D., Mucciarelli, M., Bianca, M. (2011).
Ambient noise measurements to support emergency seismic microzonation: the Abruzzo 2009 earthquake experience. Bollettino di Geofisica Teorica e Applicata **53**, 539–559. https://doi.org/10.4430/bgta0031

Gallipoli, M.R., Laurenzano, G., Calamita, G., Tortorici, G., Taverna, P., Porchia, A., Catalano, S., Klinb, P., Barnaba, C. (2026).
How reliable are 1D models in reproducing the site seismic amplification functions? A case study in the Val d'Agri Basin, Italy. Submitted to Engineering Geology.

Gariano, S.L., Guzzetti, F. (2016).
Landslides in a changing climate. Earth-Sci. Rev. **162**, 227–252. https://doi.org/10.1016/j.earscirev.2016.08.011

Gasparetti, D., Quassoli, G. (2016).
Seismic Microzonation study of level 2 of the municipality of Brescia.

Gaudiosi, I., Romagnoli, G., Albarello, D., Fortunato, C., Imprescia, P., Stigliano, F., Moscatelli, M. (2023).
$G/G_0(\gamma)$ and $D(\gamma)$ curves joined with engineering geological units in Italy. Scientific Data.
https://www.nature.com/articles/s41597-023-02412-8

Gaudiosi, I. (2024).
Input parameters for batch analyses in the PRIN SERENA Project (Ver. 1.0). Zenodo.
https://doi.org/10.5281/zenodo.13950083

Gaudiosi, I., Mendicelli, A., Porchia, A., Catalano, S., D'Agostino, A., Pennica, F., Tortorici, G., Moscatelli, M. (2026).
NC92Soil typical outputs for a seismic input associated with ID 27202 (Version 1.0). Zenodo.
https://doi.org/10.5281/zenodo.18533806

Geli, L., Bard, P.-Y., Jullien, B. (1988).
The effect of topography on earthquake ground motion: A review and new results. Bull. Seismol. Soc. Am. **78**, 42–63.

Guzzetti, F., Reichenbach, P. (1994).
Towards a definition of topographic divisions for Italy. Geomorphology **11**, 57–74.
https://doi.org/10.1016/0169-555X(94)90042-6

Guzzetti, F., Crosta, G., Detti, R., Agliardi, F. (2002).
STONE: a computer program for the three-dimensional simulation of rock-falls. Comput. Geosci. **28**, 9, 1079–1093.
https://doi.org/10.1016/S0098-3004(02)00025-0

Guzzetti, F. (2016).
Forecasting natural hazards, performance of scientists, ethics, and the need for transparency. Toxicological & Environmental Chemistry **98**, 9, 1043–1059. https://doi.org/10.1080/02772248.2015.1030664

Guzzetti, F., Alvioli, M. (2025).
r.stone – GRASS GIS manual. https://github.com/OSGeo/grass-addons/commits/grass8/src/raster/r.stone

Hailemikael, S., Amoroso, S., Gaudiosi, I. (2020).
Guest editorial: seismic microzonation of Central Italy following the 2016–2017 seismic sequence. Bull. Earthq. Eng. **18**, 5415–5422. https://doi.org/10.1007/s10518-020-00929-6

Hailemikael, S., Cultrera, G., Lanzano, G., Barnaba, C., Laurenzano, G., Gallipoli, M.R., Martini, G., Peloso, A., Sgobba, S., Pacor, F. (2026).
On the consistency of site amplification estimates from empirical and numerical methods in Italy. Submitted to Bulletin of Earthquake Engineering.

Hudson, M.B., Idriss, I.M., Beikae, M. (1993).
QUAD4M: A computer program for evaluating the seismic response of soil structure by variable damping finite element procedures. Department of Civil & Environmental Engineering, University of California, Davis.

Jaafari, A. (2024).
An Overview of Triggering and Causing Factors of Landslides. In: Chatterjee, U., Lalmalsawmzauva, K.C., Biswas, B., Pal, S.C. (Eds.), Landslides in the Himalayan Region: Risk Assessment and Mitigation Strategy for Sustainable Management. Springer Nature, Singapore, 25–45. https://doi.org/10.1007/978-981-97-4680-4_2

Jibson, R.W., Harp, E.L., Michael, J.A. (2000).
A method for producing digital probabilistic seismic landslide hazard maps. Eng. Geol. **58**, 271–289.
https://doi.org/10.1016/S0013-7952(00)00039-9

Keefer, D.K. (1984).
Landslides caused by earthquakes. GSA Bulletin **95**, 4, 406–421.
https://pubs.geoscienceworld.org/gsa/gsabulletin/article/95/4/406/10164 (pubs.geoscienceworld.org in Bing)

Klin, P., Laurenzano, G., Priolo, E. (2018).
GITANES: A MATLAB package for estimation of site spectral amplification with the generalized inversion technique. Seismological Research Letters **89**, 1, 182–190. https://doi.org/10.1785/0220170080

Klin, P., Laurenzano, G., Barnaba, C., Priolo, E., Parolai, S. (2021).
Site amplification at permanent stations in Northeastern Italy. Bulletin of the Seismological Society of America **111**, 4, 1885–1904. https://doi.org/10.1785/0120200361

Kottke, A.R., Rathje, E.M. (2009).
Technical manual for Strata. Pacific Earthquake Engineering Research Center, Berkeley, CA.

Kottke, A.R., Wang, X., Rathje, E.M. (2013).
Technical Manual for Strata.

Lanzano, G., Luzi, L., Pacor, F., Felicetta, C., Puglia, R., Sgobba, S., D'Amico, M. (2019).
A revised ground motion prediction model for shallow crustal earthquakes in Italy. Bulletin of the Seismological Society of America **109**, 2, 525–540. https://doi.org/10.1785/0120180210

Lanzano, G., Felicetta, C., Pacor, F., Spallarossa, D., Traversa, P. (2022).
Generic-to-reference rock scaling factors for seismic ground motion in Italy. Bulletin of the Seismological Society of America 112, 1583–1606. https://doi.org/10.1785/0120210063

Lanzano, G., Brunelli, G., Sgobba, S., Felicetta, C., Pacor, F., Mascandola, C., Russo, E., Luzi, L. (2024).
ITACAs2s flatfile 2.0: table of empirical amplification functions of the Italian recording stations. INGV.
https://doi.org/10.13127/itaca.4.0/itacas2s_flatfile.2.0

Lanzano, G., Brunelli, G., Sgobba, S., Pacor, F. (2025).
Estimation of the seismic microzonation amplification factors from the GMMs site-to-site residuals: an application to the Italian strong-motion stations in ITACA 4.0. Bulletin of Earthquake Engineering **23**, 5229–5257.
https://doi.org/10.1007/s10518-025-02249-z

Laurenzano, G., Barnaba, C., Romano, M.A., et al. (2019).
The Central Italy 2016–2017 seismic sequence: site response analysis based on seismological data in the Arquata del Tronto–Montegallo municipalities. Bulletin of Earthquake Engineering **17**, 5449–5469.
https://doi.org/10.1007/s10518-018-0355-3

Laurenzano, G., Garbin, M., Parolai, S., Barnaba, C., Romanelli, M., Froner, L. (2023).
High-resolution local seismic zonation by cluster and correlation analysis. Soil Dynamics and Earthquake Engineering **173**, 108122. https://doi.org/10.1016/j.soildyn.2023.108122

Li, W., Assimaki, D. (2010).
Site- and motion-dependent parametric uncertainty of site-response analyses in earthquake simulations. Bull. Seismol. Soc. Am. **100**, 954–996.

Loche, M., Alvioli, M., Marchesini, I., Bakka, H., Lombardo, L. (2022).
Landslide susceptibility maps of Italy: Lessons learnt from dealing with multiple landslide types and the uneven spatial distribution of the national inventory. Earth-Sci. Rev. **232**. https://doi.org/10.1016/j.earscirev.2022.104125

Lombardo, L., Mai, P.M. (2018).
Presenting logistic regression-based landslide susceptibility results. Eng. Geol. **244**, 14–24.
https://doi.org/10.1016/j.enggeo.2018.07.019

Lombardo, L., Tanyas, H. (2022).
From scenario-based seismic hazard to scenario-based landslide hazard: fast-forwarding to the future via statistical simulations. Stoch. Environ. Res. Risk Assess. **36**, 2229–2242. https://doi.org/10.1007/s00477-021-02020-1

Luzi, L., Bindi, D., Puglia, R., Pacor, F., Oth, A. (2014).
Single-station sigma for Italian strong-motion stations. Bulletin of the Seismological Society of America **104**, 1, 467–483. https://doi.org/10.1785/0120130089

Luzi, L., D'Amico, M., Massa, M., Puglia, R. (2019).
Site effects observed in the Norcia intermountain basin (Central Italy) exploiting a 20-year monitoring. Bulletin of Earthquake Engineering **17**, 97–118. https://doi.org/10.1007/s10518-018-0444-3

Marano, K.D., Wald, D.J., Allen, T.I. (2010).

Global earthquake casualties due to secondary effects: a quantitative analysis for improving rapid loss analyses. Nat. Hazards **52**, 319–328. https://doi.org/10.1007/s11069-009-9372-5

Marchesini, I., Ardizzone, F., Alvioli, M., Rossi, M., Guzzetti, F. (2014).
Non-susceptible landslide areas in Italy and in the Mediterranean region. Nat. Hazards Earth Syst. Sci. **14**, 2215–2231. https://doi.org/10.5194/nhess-14-2215-2014

Marin, R.J., Velásquez, M.F., García, E.F., Alvioli, M., Aristizábal, E. (2021).
Assessing two methods of defining rainfall intensity and duration thresholds for shallow landslides in data-scarce catchments of the Colombian Andean Mountains. CATENA **206**, 105563. https://doi.org/10.1016/j.catena.2021.105563

Meletti, C., Montaldo, V. (2007).
Deliverable D2, DPC-INGV-S1 Project (in Italian). Available at: http://esse1.mi.ingv.it/d2.html

Mendicelli, A., Mori, F., Varone, C., Simionato, M., Moscatelli, M. (2024).
Mapping recent flood covers using machine learning techniques. 42° GNGTS General Assembly, 13–16 febbraio 2024, Ferrara.

Mercuri, A., Cultrera, G., Minarelli, L., Quintiliani, M., Bordoni, P., Famiani, D., Casale, P., Pischiutta, M., Ladina, C., Cara, F., Di Giulio, G., Pucillo, S., Tarabusi, G., INGV CRISP Working Group. (2023).
CRISP: an archive for the site characterization of permanent Italian seismic stations. Bull. Earthq. Eng. **21**, 2415–2439. https://doi.org/10.1007/s10518-023-01618-w

Mergili, M., Marchesini, I., Alvioli, M., Metz, M., Schneider-Muntau, B., Rossi, M., Guzzetti, F. (2014a).
A strategy for GIS-based 3-D slope stability modelling over large areas. Geosci. Model Dev. **7**, 2969–2982. https://doi.org/10.5194/gmd-7-2969-2014

Mergili, M., Marchesini, I., Rossi, M., Guzzetti, F., Fellin, W. (2014b).
Spatially distributed three-dimensional slope stability modelling in a raster GIS. Geomorphology **206**, 178–195. https://doi.org/10.1016/j.geomorph.2013.10.008

Mevoli, F.A., Borselli, L., Santangelo, M., Monte, N., de Lucia, D., Ugenti, A., Rossi, M. (2026).
Landslide susceptibility zoning through physically-based limit equilibrium method modelling. CATENA **263**, 109726. https://doi.org/10.1016/j.catena.2025.109726

Mons, B., Neylon, C., Velterop, J., Dumontier, M., da Silva Santos, L.O.B., Wilkinson, M.D. (2017).
Cloudy, increasingly FAIR; revisiting the FAIR Data guiding principles for the European Open Science Cloud. Information Services & Use **37**, 1, 49–56. doi: 10.3233/ISU-170824

Monte, N., Bucci, F., Mevoli, F.A., Santangelo, M., Reichenbach, P., Di Matteo, L., Marchesini, I. (2024a).
Geotechnical parametrization of the lithological map of Italy. https://doi.org/10.6084/m9.figshare.26326537.v1

Monte, N., Bucci, F., Mevoli, F.A., Santangelo, M., Reichenbach, P., Di Matteo, L., Marchesini, I. (2024b).
A dataset of geotechnical parameters based on international literature to characterise lithotypes in Italy. Scientific Data. https://www.nature.com/articles/s41597-024-04095-1

Monte, N., Bucci, F., Mevoli, F.A., Reichenbach, P., Alvioli, M., Santangelo, M., Marchesini, I. (in preparation).
Calibration of geotechnical parameters for slope stability assessment at the regional scale. Progress in Landslide Research and Technology, Vol. 4, Issue 2.

Mori, F., Mendicelli, A., Moscatelli, M., Romagnoli, G., Peronace, E., Naso, G. (2020).
A new Vs_{30} map for Italy based on the seismic microzonation dataset. Engineering Geology **275**, 105745. https://doi.org/10.1016/j.enggeo.2020.105745

Moscatelli, M., Albarello, D., Scarascia Mugnozza, G., Dolce, M. (2020).
The Italian approach to seismic microzonation. Bulletin of Earthquake Engineering **18**, 5425–5440. https://doi.org/10.1007/s10518-020-00856-6

NEHRP (2004).
NEHRP recommended provisions for seismic regulations for new buildings and other structures (FEMA 450). Building Seismic Safety Council, National Institute of Building Sciences, Washington, DC, USA.

NTC18 (2018).
Aggiornamento delle Norme Tecniche per le Costruzioni. Ministero delle Infrastrutture e dei Trasporti. https://www.gazzettaufficiale.it/eli/gu/2018/02/20/42/so/8/sg/pdf

Oth, A., Bindi, D., Parolai, S., Di Giacomo, D. (2011).
Spectral analysis of K-NET and KiK-net data in Japan, part II: On attenuation characteristics, source spectra, and site response of borehole and surface stations. Bulletin of the Seismological Society of America **101**, 667–687.

https://doi.org/10.1785/0120100135

Pakyuz-Charrier, E., Lindsay, M., Ogarko, V., Giraud, J., Jessell, M. (2018).
Monte Carlo simulation for uncertainty estimation on structural data in implicit 3-D geological modeling: a guide for disturbance distribution selection and parameterization. Solid Earth **9**, 385–402. https://doi.org/10.5194/se-9-385-2018

Panzera, F., Bergamo, P., Fäh, D. (2021).
Canonical correlation analysis based on site-response proxies to predict site-specific amplification functions in Switzerland. Bull. Seismol. Soc. Am. **111**, 1905–1920. https://doi.org/10.1785/0120200326

Paolucci, R., Aimar, M., Ciancimino, A., Dotti, M., Foti, S., Lanzano, G., Mattevi, P., Pacor, F., Vanini, M. (2021).
Checking the site categorization criteria and amplification factors of the 2021 draft of Eurocode 8 Part 1–1. Bull. Earthq. Eng. **19**, 4199–4234. https://doi.org/10.1007/s10518-021-01118-9

Parolai, S., Lai, C.G., Dreossi, I., Ktenidou, O.-J., Yong, A. (2022).
A review of near-surface QS estimation methods using active and passive sources. J. Seismol. **26**, 4, 823–862. https://doi.org/10.1007/s10950-021-10066-5

Pham, B.T., Prakash, I., Singh, S.K., Shirzadi, A., Shahabi, H., Tran, T.-T.-T., Bui, D.T. (2019).
Landslide susceptibility modeling using Reduced Error Pruning Trees and different ensemble techniques: Hybrid machine learning approaches. CATENA **175**, 203–218. https://doi.org/10.1016/j.catena.2018.12.018

Piana, F., Fioraso, G., Irace, A., Mosca, P., d'Atri, A., Barale, L., Falletti, P., Monegato, G., Morelli, M., Tallone, S., Vigna, G.B. (2017).
Geology of Piemonte Region (NW Italy, Alps–Apennines interference zone). Journal of Maps **13**, 2, 395–405. https://doi.org/10.1080/17445647.2017.1316218 (doi.org in Bing)

Pieruccini, P., Fantozzi, P.L., Carfagna, N., Gaudiosi, I., Albarello, D. (2024).
Mapping 1D seismic amplification effects in the range of periods of engineering interest based on geological data. Engineering Geology **341**, 107701. https://doi.org/10.1016/j.enggeo.2024.107701

Pilz, M., Cotton, F. (2019).
Does the one-dimensional assumption hold for site response analysis? A study of seismic site responses and implications for ground motion assessment using KiK-net strong-motion data. Earthquake Spectra **35**, 2, 883–905. https://doi.org/10.1193/050718eqs113m

Pokharel, B., Lim, S., Bhattarai, T.N., Alvioli, M. (2023).
Rockfall susceptibility along Pasang Lhamu and Galchhi–Rasuwagadhi highways, Rasuwa, Central Nepal. Bull. Eng. Geol. Environ. **82**, 183. https://doi.org/10.1007/s10064-023-03174-8

Priolo, E., et al. (2012).
The Ferrara thrust earthquakes of May–June 2012: preliminary site response analysis at the sites of the OGS temporary network. Annals of Geophysics **55**, 4. https://doi.org/10.4401/ag-6172

Priolo, E., Pacor, F., Spallarossa, D., Milana, G., Laurenzano, G., Romano, M.A., Felicetta, C., Hailemikael, S., Cara, F., Di Giulio, G., Ferretti, G., Barnaba, C., Lanzano, G., Luzi, L., D'Amico, M., Puglia, R., Scafidi, D., Barani, S., De Ferrari, R., Cultrera, G. (2020).
Seismological analyses of the seismic microzonation of 138 municipalities damaged by the 2016–2017 seismic sequence in Central Italy. Bulletin of Earthquake Engineering **18**, 5553–5593. https://doi.org/10.1007/s10518-019-00652-x

Reichenbach, P., Rossi, M., Malamud, B.D., Mihir, M., Guzzetti, F. (2018).
A review of statistically-based landslide susceptibility models. Earth-Sci. Rev. **180**, 60–91. https://doi.org/10.1016/j.earscirev.2018.03.001

Rivieccio, R., Di Bene, C., Paolanti, M., Marchetti, M., Napoli, R. (2020).
Soil rooting depth of Italy. J. Maps **16**, 36–42. https://doi.org/10.1080/17445647.2019.1690595

Rodriguez-Marek, A., Montalva, G., Cotton, F., Bonilla, F. (2011).
Analysis of single-station standard deviation using the KiK-net data. Bulletin of the Seismological Society of America **101**, 31242–31258. https://doi.org/10.1785/0120100252

Rollins, K.M., Evans, M.D., Diehl, N.B., Daily, W.D. (1998).
Shear modulus and damping relationships for gravels. J. Geotech. Geoenviron. Eng. **124**, 5.

Rollins, K.M., Singh, M., Roy, J. (2020).
Simplified equations for shear-modulus degradation and damping of gravels. J. Geotech. Geoenviron. Eng. **146**, 9.

Romagnoli, G., Tarquini, E., Porchia, A., Catalano, S., Albarello, D., Moscatelli, M. (2022).
Constraints for the Vs profiles from engineering-geological qualitative characterization of shallow subsoil

in seismic microzonation studies. Soil Dynamics and Earthquake Engineering **161**.

Ruff, M., Czurda, K. (2008).
Landslide susceptibility analysis with a heuristic approach in the Eastern Alps (Vorarlberg, Austria). Geomorphology **94**, 314–324. https://doi.org/10.1016/j.geomorph.2006.10.032

Russo, E., Felicetta, C., D'Amico, M., Sgobba, S., Lanzano, G., Mascandola, C., et al. (2022).
Italian Accelerometric Archive v3.2 [dataset]. INGV – National Civil Protection Department. https://doi.org/10.13127/itaca.3.2

Sarkar, N., Alvioli, M. (2025a).
Physically based and statistically based rockfall susceptibility along communication routes and in urban areas in Italy. EGU25-8583. https://doi.org/10.5194/egusphere-egu25-8583

Sarkar, N., Alvioli, M. (2025b).
Rockfall susceptibility along communication routes and in urban areas in Italy based on physical and statistical models. In: Proceedings of Geomorphometry 2025, 9–13 June, Perugia, Italy. M. Alvioli, L. Melelli, I. Marchesini (Eds.). CNR Edizioni, Rome. ISBN 978-88-8080-765-0. https://doi.org/10.5281/zenodo.15274240

Sgobba, S., Felicetta, C., Bortolotti, T., Menafoglio, A., Lanzano, G., Pacor, F. (2024).
A geostatistical modelling of empirical amplification functions and related site proxies for shaking scenarios in central Italy. Soil Dynamics and Earthquake Engineering **179**, 108496. https://doi.org/10.1016/j.soildyn.2024.108496

Shao, X., Xu, C. (2022).
Earthquake-induced landslides susceptibility assessment: A review of the state-of-the-art. Nat. Hazards Res. **2**, 172–182. https://doi.org/10.1016/j.nhres.2022.03.002

Shible, H., Hollender, F., Bindi, D., Traversa, P., Oth, A., Edwards, B., Klin, P., Kawase, H., Grendas, I., Castro, R.R., Theodoulidis, N., Gueguen, P. (2022).
GITEC: A generalized inversion technique benchmark. Bulletin of the Seismological Society of America **112**, 850–877. https://doi.org/10.1785/0120210242

SM Working Group (2015).
Guidelines for seismic microzonation. Conference of Regions and Autonomous Provinces of Italy – Civil Protection Department, Rome.

SM-WG (2008).
Guidelines for Seismic Microzonation. Conference of Regions and Autonomous Provinces of Italy – Civil Protection Department, Rome. https://www.centromicrozonazionesismica.it/it/download/category/9guidelinesforseismicmicrozonation

Strollo, A., Parolai, S., Bindi, D., Chiauzzi, L., Pagliuca, R., Mucciarelli, M., et al. (2012).
Microzonation of Potenza (Southern Italy) in terms of spectral intensity ratio using joint analysis of earthquakes and ambient noise. Bull. Earthq. Eng. **10**, 2, 493–516. https://doi.org/10.1007/s10518-011-9256-4

Stucchi, M., Meletti, C., Montaldo, V., Crowley, H., Calvi, G.M., Boschi, E. (2011).
Seismic Hazard Assessment (2003–2009) for the Italian Building Code. Bull. Seismol. Soc. Am. **101**, 1885–1911. https://doi.org/10.1785/0120100130

Tanyas, H., Rossi, M., Alvioli, M., van Westen, C.J., Marchesini, I. (2019).
A global slope unit-based method for the near real-time prediction of earthquake-induced landslides. Geomorphology **327**, 126–146. https://doi.org/10.1016/j.geomorph.2018.10.022

Tarquini, S., Isola, I., Favalli, M., Mazzarini, F., Bisson, M., Pareschi, M.T., et al. (2007).
TINITALY/01: a new triangular irregular network of Italy. Ann. Geophys. **50**, 407–424. https://doi.org/10.4401/ag-4424

TCSM – Technical Commission for Seismic Microzonation (2018).
Graphic and data archiving standards. National Department of Civil Protection, Rome (Version 4.1). https://centromicrozonazionesismica.it/documents/37/StandardMS_4_1.pdf

Trigila, A., Iadanza, C., Spizzichino, D. (2010).
Quality assessment of the Italian Landslide Inventory using GIS processing. Landslides **7**, 455–470. https://doi.org/10.1007/s10346-010-0213-0

Wald, D.J., Allen, T.I. (2007).
Topographic slope as a proxy for seismic site conditions and amplification. Bulletin of the Seismological Society of America **97**, 5, 1379–1395. https://doi.org/10.1785/0120060267

Wang, Y., Cao, Z., Au, S.-K. (2010).
Efficient Monte Carlo simulation of parameter sensitivity in probabilistic slope stability analysis. Comput. Geotech. **37**, 1015–1022. https://doi.org/10.1016/j.compgeo.2010.08.010

Wang, Y., Feng, L., Li, S., Ren, F., Du, Q. (2020).
A hybrid model considering spatial heterogeneity for landslide susceptibility mapping in Zhejiang Province, China. CATENA **188**, 104425. https://doi.org/10.1016/j.catena.2019.104425

Wilkinson, M., Dumontier, M., Aalbersberg, I., et al. (2016).
The FAIR Guiding Principles for scientific data management and stewardship. Sci. Data **3**, 160018. https://doi.org/10.1038/sdata.2016.18

Zhang, J., Wilson, H.T., Zhang, L.M. (2010).
Efficient probabilistic back-analysis of slope stability model parameters. Journal of Geotechnical and Geoenvironmental Engineering **136**, 1. https://ascelibrary.org/doi/abs/10.1061/(ASCE)GT.1943-5606.0000205

Appendix: Scientific Outputs of the Project

Peer Reviewed Publications

Albarello, D., Carfagna, N., Fantozzi, P.L. (2025).
The impact of 1D seismostratigraphical amplification effects on probabilistic seismic hazard maps at regional scale: the case of Tuscany (Central Italy). Bull. Earthq. Eng. https://doi.org/10.1007/s10518-025-02167-0

Cultrera, G., Mercuri, A. (2025).
Statistical analysis of site effect indicators at the Italian Seismic Network: inside the site characterization database CRISP. In stampa su Bull. Earthq. Eng., June 2025.

D'Agostino, A., Porchia, A., Tortorici, G., Pavano, F., Cavuoto, G., Moscatelli, M., Ortolano, G., Catalano, S. (2025).
"Stratigraphically Homogeneous Zones": automated construction and restitution procedure for engineering geology use. Journal of Maps **21**, 1, 2504064. https://doi.org/10.1080/17445647.2025.2504064

Foti, A., Pavano, F., Romagnoli, G., Tortorici, G., Catalano, S. (2023).
Structural geology of the eastern termination of the Mt. Kumeta–Alcantara line (NE Sicily, Italy). Journal of Maps **19**, 1, 2179436. https://doi.org/10.1080/17445647.2023.2179436

Fantozzi, P.L., Albarello, D., Pieruccini, P., Paolucci, E. (2023).
Morphometric analysis of predisposing factors for topographic seismic amplification effects. Soil Dyn. Earthq. Eng. **174**, 108212. https://doi.org/10.1016/j.soildyn.2023.108212

Gaudiosi, I., Romagnoli, G., Albarello, D., Fortunato, C., Imprescia, P., Stigliano, F., Moscatelli, M. (2023).
Shear modulus reduction and damping ratios curves joined with engineering geological units in Italy. Sci. Data **10**, 625. https://doi.org/10.1038/s41597-023-02412-8

Lanzano, G., Brunelli, G., Sgobba, S., Pacor, F. (2025).
Estimation of the seismic microzonation amplification factors from the GMMs site-to-site residuals: an application to the Italian strong-motion stations in ITACA 4.0. Bulletin of Earthquake Engineering (submitted).

Laurenzano, G., Garbin, M., Parolai, S., Barnaba, C., Romanelli, M., Froner, L. (2023).
High-resolution local seismic zonation by cluster and correlation analysis. Soil Dyn. Earthq. Eng. **173**, 108122. https://doi.org/10.1016/j.soildyn.2023.108122

Monte, N., Bucci, F., Mevoli, F.A., Santangelo, M., Reichenbach, P., Di Matteo, L., Marchesini, I. (2024).
A dataset of geotechnical parameters based on international literature to characterise lithotypes in Italy. Scientific Data. https://www.nature.com/articles/s41597-024-04095-1

Monte, N., Bucci, F., Mevoli, F.A., Reichenbach, P., Alvioli, M., Santangelo, M., Marchesini, I. (in press).
Calibration of geotechnical parameters for slope stability assessment at the regional scale.
In: P*rogress in Landslide Research and Technology,* ICL.

Pieruccini, P., Fantozzi, P.L., Carfagna, N., Gaudiosi, I., Albarello, D. (2024).
Mapping 1D seismic amplification effects in the range of periods of engineering interest based on geological data. Engineering Geology **341**. https://doi.org/10.1016/j.enggeo.2024.107701

Sgobba, S., Felicetta, C., Bortolotti, T., Menafoglio, A., Lanzano, G., Pacor, F. (2024).
A geostatistical modelling of empirical amplification functions and related site proxies for shaking scenarios in central Italy. Soil Dyn. Earthq. Eng. **179**, 108496. https://doi.org/10.1016/j.soildyn.2024.108496

National Conference Proceedings

Albarello, D., Catalano, S., De Franco, R., Barnaba, C., Cultrera, G. (2023).
Mapping seismic Site Effects at REgional and NAtional scale (SERENA): an ambitious PRIN Project. GNGTS General Assembly, 7–9 February 2023, Bologna.

Albarello, D., Catalano, S., Cavuoto, G., Fantozzi, P.L., Moscatelli, M., Pieruccini, P., Porchia, A., Tortorici, G., SERENA PRIN Project WP2 Working Group. (2023).
Geology-based classification of the national territory for the restitution of a multiscale map of stratigraphic amplification effects. GNGTS General Assembly, 7–9 February 2023, Bologna.

Albarello, D., Carfagna, N., Fantozzi, P.L. (2025).
The impact of 1D seismostratigraphical amplification effects on probabilistic seismic hazard maps at regional scale: the case of Central Italy. GNGTS General Assembly, 11–14 February 2025, Bologna.

Ariano, M., Fantozzi, P.L., Albarello, D. (2024).
A systematic analysis at stations of the Italian seismic network to test the role of local topographic effect. GNGTS General Assembly, 13–16 February 2024, Ferrara.

Ariano, M., Fantozzi, P.L., Albarello, D. (2024).
A systematic analysis to test the role of local topographic effect. Congresso Nazionale SGI–SIMP 2024. https://doi.org/10.3301/ABSGI.2024.02

Ariano, M., Fantozzi, P.L., Albarello, D. (2025).
NTC18 Standard: Topographical Conditions in the Siena Case Study – Application and Verification. GNGTS General Assembly, 11–14 February 2025, Bologna.

Ariano, M., Fantozzi, P.L., Albarello, D. (2025).
Realization of the database of seismostratigraphic features of seismically homogeneous microzones throughout the country. GNGTS General Assembly, 11–14 February 2025, Bologna.

Barnaba, C., Minarelli, L., Di Giulio, G., Laurenzano, G., Affatato, A., Taverna, P., Vassallo, M., Caputo, R., Cultrera, G. (2024).
One-dimensional numerical approach versus experimental quantifications of site effect parameters: the Ferrara test area. GNGTS General Assembly, 13–16 February 2024, Ferrara.

Brunelli, G., Lanzano, G., Pacor, F., Felicetta, C., Sgobba, S., PRIN SERENA WP06 WG. (2023).
Estimation of the seismic microzonation amplification factors from the GMMs between-station residuals. GNGTS General Assembly, 7–9 February 2023, Bologna.

Caielli, G., De Franco, R., Gaudiosi, I., Mendicelli, A., Mori, F., Moscatelli, M., Peronace, E., Porchia, A., Albarello, D., Catalano, S., GdL PRIN SERENA. (2022).
The commitment of the CNR IGAG for the prevention of seismic risk in the PRIN SERENA Project. IGAG DAYS 2022, Cagliari. https://www.igag.cnr.it/documents/144/IGAG-Days-abstract-book-2022.pdf

Caielli, G., De Franco, R., Gaudiosi, I., Mendicelli, A., Moscatelli, M., Norini, G., Rusconi, D., Simionato, M. (2024).
A geological–geophysical approach for the large-scale evaluation of seismic amplification in the plain area: example of the Brescia basin (Pianura Padana). GNGTS General Assembly, 13–16 February 2024, Ferrara.

Caielli, G., Rusconi, D., De Franco, R., Gaudiosi, I., Norini, G. (2025).
Reconstruction of subsoil in the Po Plain for a large-scale evaluation of seismic amplification effects. GNGTS General Assembly, 11–14 February 2025, Bologna.

Carfagna, N., Pieruccini, P., Fantozzi, P., Albarello, D. (2024).
Mapping Seismic Site Effects at Regional and National Scale – SERENA Project. Congresso Nazionale SGI–SIMP 2024. https://doi.org/10.3301/ABSGI.2024.02

Carfagna, N., Pieruccini, P., Fantozzi, P., Albarello, D. (2024).
Mapping seismostratigraphical amplification effects at regional scale from geological data. GNGTS General Assembly, 13–16 February 2024, Ferrara.

Castelbarco, T., Lanzano, G., Brunelli, G., Sgobba, S., Pacor, F., Luzi, L., Pergalani, F. (2025).
1D response analysis of seismic stations in ITACA for Seismic Microzonation purposes. GNGTS General Assembly, 11–14 February 2025, Bologna.

Cultrera, G., Barnaba, C., Gallipoli, M.R., Martini, G., Pacor, F., Brunelli, G., Cara, F., Di Giulio, G., Felicetta, C., Hailemikael, S., Lanzano, G., Lovati, S., Mercuri, A., Minarelli, L., Sgobba, S., Parolai, S., Pettenati, F.,

Laurenzano, G., Calamita, G., Gaudiosi, I., Tragni, N., Stabile, T.A., Peloso, A., Albarello, D. (2023).
Mapping seismic site effects at regional and national scale: empirical testing and calibration.
GNGTS General Assembly, 7–9 February 2023, Bologna.

Cultrera, G., Mercuri, A. (2024).
Using data from CRISP database to infer site response behaviour. GNGTS General Assembly, 13–16 February 2024, Ferrara.

D'Agostino, A., Porchia, A., Tortorici, G., Pavano, F., Ortolano, G., Cavuoto, G., Moscatelli, M., Catalano, S. (2024).
Automated tools for the reconstruction and spatialization of stratigraphic successions to support seismic site effects analysis. Congresso SGI–SIMP, Bari, 3–5 September 2024. https://doi.org/10.3301/ABSGI.2024.02

D'Agostino, A., Porchia, A., Cavuoto, G., Pavano, F., Moscatelli, M., Tortorici, G., Catalano, S. (2024).
Automated stratigraphic reconstruction and spatialization for seismic site effect analysis.
GNGTS General Assembly, 13–16 February 2024, Ferrara.

D'Agostino, A., et al. (2025).
Da carta geologica a mappa delle Zone a Stratigrafia Omogenea: un metodo automatico per la ricostruzione e spazializzazione di colonne stratigrafiche in ambiente GIS. Congresso GIT 2025.

D'Agostino, A., Porchia, A., Gaudiosi, I., Tortorici, G., Catalano, S. (2025).
Large-scale seismic site effect modelling through automated definition of the Stratigraphically Homogeneous Zones: the case of Basilicata Region. GNGTS General Assembly, 11–14 February 2025, Bologna.

Gallipoli, M.R., Calamita, G., Laurenzano, G., Taverna, P., Klin, P., Tortorici, G., Catalano, S., Barnaba, C. (2025).
1D stratigraphic modelling vs experimental seismic amplification: can a possible convergence exist? The case of Val d'Agri. GNGTS General Assembly, 11–14 February 2025, Bologna.

Gaudiosi, I., Porchia, A., Caielli, G., Albarello, D., De Franco, R., Moscatelli, M. (2023).
Amplification of ground motions incorporating uncertainty in subsurface soils throughout extensive seismic microzonation data. GNGTS General Assembly, 7–9 February 2023, Bologna.

Gaudiosi, I., Acunzo, G., Albarello, D., Moscatelli, M. (2024).
Stochastic modelling as a method for providing seismic hazard estimates of site effects over wide areas.
GNGTS General Assembly, 13–16 February 2024, Ferrara.

Hailemikael, S., Cultrera, G., Barnaba, C., Laurenzano, G., Martini, G., Peloso, A., Cara, F., Di Giulio, G., Famiani, D. (2024).
Testing synthetic site amplification maps through comparison with empirical estimates in Central Italy.
GNGTS General Assembly, 13–16 February 2024, Ferrara.

Hailemikael, S., Cultrera, G., Peloso, A., Martini, G., Barnaba, C., Laurenzano, G., Lanzano, G., Sgobba, S., Gallipoli, M.R., WP6 PRIN SERENA Working Group. (2025).
Empirical estimates of site amplification factors in Italy. GNGTS General Assembly, 11–14 February 2025, Bologna.

Mendicelli, A., Mori, F., Varone, C., Simionato, M., Moscatelli, M. (2024).
Mapping recent flood covers using machine learning techniques. GNGTS General Assembly, 13–16 February 2024, Ferrara.

Mercuri, A., Cultrera, G. (2025).
A statistical analysis on soil response at the Italian Seismic Network: the CRISP database.
GNGTS General Assembly, 11–14 February 2025, Bologna.

Monte, N., Reichenbach, P., Disperati, L., D'Addario, E., Alvioli, M., Bucci, F., Santangelo, M., Marchesini, I. (2024).
Seismic-induced landslide scenarios with physically-based models at regional scale. GNGTS General Assembly, 13–16 February 2024, Ferrara.

Monte, N., et al. (2024).
Geotechnical characterization of the lithological map of Italy. VIII Congresso AIGAA 2024, Naples, 27–29 June 2024.

Monte, N., Marchesini, I., Reichenbach, P., Alvioli, M., Bucci, F., Santangelo, M. (2024).
Scenari da frane indotte da terremoti con modelli fisicamente basati a scala regionale. XVIII Convegno Nazionale GIT–SI, 16–19 June 2024, Malnisio (PN).

Monte, N., Bucci, F., Mevoli, F.A., Reichenbach, P., Alvioli, M., Santangelo, M., Marchesini, I. (2025).

Calibration of geotechnical parameters for slope stability assessment at the regional scale. XIX Convegno Nazionale GIT, 16–18 June 2025, Milazzo (ME).

Paolucci, E., Albarello, D. (2025).
Possible measure of soil factors in the Italian seismic code. GNGTS General Assembly, 11–14 February 2025, Bologna.

Sgobba, S., Felicetta, C., Lanzano, G., Pacor, F., Bortolotti, T., Menafoglio, A. (2024).
Capturing spatial variability of empirical site amplification functions δS2S: a case study in Central Italy. GNGTS General Assembly, 13–16 February 2024, Ferrara.

Tragni, N., Laurenzano, G., Klin, P., Stabile, T.A., Gallipoli, M.R. (2024).
Site response analysis in the Agri Valley (Basilicata) using the generalized inversion technique. GNGTS General Assembly, 13–16 February 2024, Ferrara.

International Conference Proceedings

Albarello, D. (2024).
Assessing seismic site effects at regional scale: the SERENA research project. EGU General Assembly 2024, Vienna, Austria, 14–19 April 2024, EGU243611. https://doi.org/10.5194/egusphere-egu24-3611

Ariano, M., Fantozzi, P.L., Albarello, D. (2024).
A systematic analysis at stations of the Italian seismic network to test the role of local topographic effect. EGU General Assembly 2024, Vienna, Austria, 14–19 April 2024, EGU243606. https://doi.org/10.5194/egusphere-egu24-3606

Ariano, M., Fantozzi, P.L., Albarello, D. (2025).
NTC18 Standard (EC8): Topographical Conditions in the Siena Case Study – Application and Verification. GISTAM Congress 2025, Porto, Portugal, 1–3 April 2025.

Brunelli, G., Lanzano, G., Pacor, F., Felicetta, C., Sgobba, S. (2023).
Estimation of the seismic microzonation amplification factors from the GMMs betweenstation residuals. XXVIII General Assembly of the International Union of Geodesy and Geophysics (IUGG), Berlin, Germany, 2023.

Carfagna, N., Pieruccini, P., Fantozzi, P.L., Albarello, D. (2024).
Mapping seismostratigraphical amplification effects at regional scale from geological data. EGU General Assembly 2024, Vienna, Austria, 14–19 April 2024, EGU243608. https://doi.org/10.5194/egusphere-egu24-3608

Cultrera, G., Mercuri, A. (2025).
Statistical analysis on soil response of the Italian Seismic Network from the CRISP database. EGU General Assembly 2025, Vienna, Austria, 27 April–2 May 2025, EGU256773. https://doi.org/10.5194/egusphere-egu25-6773

Gaudiosi, I., Mendicelli, A., Porchia, A., Tortorici, G., D'Agostino, A., Pennica, F., Catalano, S., Albarello, D., Moscatelli, M. (2026).
Effects of surface geology in Italy: evaluation through stochastic simulations. 7th IASPEI/IAEE International Symposium on the Effects of Surface Geology on Seismic Motion, Grenoble, France, 19–21 October 2026.

Gallipoli, M.R., Calamita, G., Laurenzano, G., Taverna, P., Klin, P., Tortorici, G., Catalano, S., Barnaba, C. (2025).
How reliable are 1D models in reproducing the site seismic amplification functions? A case study in the Val d'Agri Basin, Italy. EGU General Assembly 2025, Vienna, Austria, 27 April–2 May 2025, EGU2510902. https://doi.org/10.5194/egusphere-egu25-10902

Hailemikael, S., Cultrera, G., Peloso, A., Martini, G., Barnaba, C., Laurenzano, G., Lanzano, G., Sgobba, S., Gallipoli, M.R. (2025).
Empirical estimates of site amplification factors in Italy. EGU General Assembly 2025, Vienna, Austria, 27 April–2 May 2025, EGU257487. https://doi.org/10.5194/egusphere-egu25-7487

Lanzano, G., Brunelli, G., Pacor, F., Felicetta, C., Sgobba, S. (2024).
Advantages and limitations of using GMMs residuals for the empirical siteeffects assessment: lessons learned from the analysis of the Italian recording stations. AGU Fall Meeting 2024, 10 December 2024.

Mercuri, A., Cultrera, G., Minarelli, L., Quintiliani, M., Bordoni, P., Famiani, D., Casale, P., Pischiutta, M., Ladina, C., Cara, F., Di Giulio, G., Pucillo, S., Tarabusi, G., INGV CRISP Working Group. (2024).
CRISP: a database for the site characterization of the Italian seismic network. 18th World Conference on Earthquake Engineering (WCEE2024), Milan, Italy, 30 June–5 July 2024.

Monte, N., Bucci, F., Mevoli, F.A., Santangelo, M., Reichenbach, P., Di Matteo, L., Marchesini, I. (2024).
Geotechnical Characterization of the Lithological Map of Italy. EGU General Assembly 2024, Vienna, Austria, 14–19 April 2024.

Monte, N., Bucci, F., Mevoli, F.A., Santangelo, M., Reichenbach, P., Di Matteo, L., Marchesini, I. (2025).
A geotechnical database for geohydrological modeling at regional and national scales. EGU General Assembly 2025, Vienna, Austria, 27 April–2 May 2025, EGU253720. https://doi.org/10.5194/egusphere-egu25-3720

Tragni, N., Laurenzano, G., Klin, P., Stabile, T.A., Gallipoli, M.R. (2024).
Site response at permanent stations in the High Agri Valley (Basilicata, Italy). ESC 2024, Corfu, Greece, 22–27 September 2024.